Hydrogenation of succinic acid and carbon dioxide over molybdenum carbide catalysts

Marwa Abou Hamdan

N°d'ordre NNT : 2019LYSE1065

THESE de DOCTORAT DE L'UNIVERSITE DE LYON
opérée au sein de
l'Université Claude Bernard Lyon 1

Ecole Doctorale de Chimie de l'Université de Lyon
ED 206

Spécialité de doctorat : Chimie

Soutenue publiquement le 28/05/2019, par :
Marwa Abou Hamdan

Hydrogenation of succinic acid and carbon dioxide over molybdenum carbide catalysts

---

Devant le jury composé de :

Prof. Pascal Fongarland	Professeur, UCBL1	Président du jury
Prof. Sébastien Royer	Professeur, Univ. Lille	Rapporteur
Dr. Florence Epron	Directrice de Recherche CNRS, Poitiers	Rapporteur
Dr. Laurent Delannoy	Maître de Conférences, Sorbonne Univ.	Examinateur
Dr. Catherine Pinel	Directrice de Recherche CNRS, UCBL1	Directrice de thèse
Dr. Noémie Perret	Chargée de Recherche CNRS, UCBL1	Co-directrice de thèse
Prof. Mohamad Jahjah	Enseignant, Univ. Libanaise	Invité

UNIVERSITE CLAUDE BERNARD - LYON 1

Président de l'Université	**M. le Professeur Frédéric FLEURY**
Président du Conseil Académique	M. le Professeur Hamda BEN HADID
Vice-président du Conseil d'Administration	M. le Professeur Didier REVEL
Vice-président de la Commission Formation et Vie Universitaire	M. le Professeur Philippe CHEVALIER
Vice-président de la Commission Recherche	M. Fabrice VALLÉE
Directrice Générale des Services	Mme Dominique MARCHAND

COMPOSANTES SANTE

Faculté de Médecine Lyon Est – Claude Bernard	Directeur : M. le Professeur G. RODE
Faculté de Médecine et de Maïeutique Lyon Sud – Charles Mérieux	Directeur : Mme la Professeure C. BURILLON
Faculté d'Odontologie	Directeur : M. le Professeur D. BOURGEOIS
Institut des Sciences Pharmaceutiques et Biologiques	Directeur : Mme la Professeure C. VINCIGUERRA
Institut des Sciences et Techniques de la Réadaptation	Directeur : M. X. PERROT
Département de formation et Centre de Recherche en Biologie Humaine	Directeur : Mme la Professeure A-M. SCHOTT

COMPOSANTES ET DEPARTEMENTS DE SCIENCES ET TECHNOLOGIE

Faculté des Sciences et Technologies	Directeur : M. F. DE MARCHI
Département Biologie	Directeur : M. le Professeur F. THEVENARD
Département Chimie Biochimie	Directeur : Mme C. FELIX
Département GEP	Directeur : M. Hassan HAMMOURI
Département Informatique	Directeur : M. le Professeur S. AKKOUCHE
Département Mathématiques	Directeur : M. le Professeur G. TOMANOV
Département Mécanique	Directeur : M. le Professeur H. BEN HADID
Département Physique	Directeur : M. le Professeur J-C PLENET
UFR Sciences et Techniques des Activités Physiques et Sportives	Directeur : M. Y. VANPOULLE
Observatoire des Sciences de l'Univers de Lyon	Directeur : M. B. GUIDERDONI
Polytech Lyon	Directeur : M. le Professeur E. PERRIN
Ecole Supérieure de Chimie Physique Electronique	Directeur : M. G. PIGNAULT
Institut Universitaire de Technologie de Lyon 1	Directeur : M. le Professeur C. VITON
Ecole Supérieure du Professorat et de l'Education	Directeur : M. le Professeur A. MOUGNIOTTE
Institut de Science Financière et d'Assurances	Directeur : M. N. LEBOISNE

Acknowledgments

This work was carried out at IRCELYON “Institut de Recherches sur la Catalyse et l’Environnement de Lyon”, UMR 5256 University Calude Bernard Lyon 1 - CNRS, Lyon - France within CDFA “Chimie Durable du Fondamental à l'Application” team; with co-direction from LCIO “Laboratoire de Chimie de Coordination Inorganique et Organométallique”, Lebanese University - Faculty of Sciences I, Beirut - Lebanon, and grant from CICS “Conseil Islamique Chiite Supreme”.

First of all I would like to thank Prof. Sebastein ROYER (Lille University) and Dr. Florence EPRON (CNRS Poitiers) for honoring me by accepting to review my thesis and for their very positive feedback on my work. I also warmly thank my teacher Prof. Pascale FONGARLAND (UCBL1) and Dr. Laurent DELANNOY (Sorbonne University) for accepting to participate in the evaluation of this work and for their presence in my PhD defense.

I express my sincere gratitude to my thesis supervisor Dr. Catherine PINEL and co-supervisor Dr. Noémie PERRET for their guidance and advices throughout this work, and for the time that they dedicated for this project. I also thank my co-director from Lebanon Prof. Mohamad JAHJAH for his aid that initially contributed in directing me to the PhD offer.

Special thanks to Dr. Laurent PICCOLO for his direction for the carbon dioxide hydrogenation project and for his experience and time that he offered for the work and the manuscript, many thanks too for Ruben CHECCA who took care of the technical side of this part. I also thank Dr. Michèle BESSON for her help especially in her constructive notes on the manuscript and defense presentation. Thanks also to Dr. Stephane LORIDANT for his contribution through RAMAN analysis.

I would like to sincerely thank the interns Abdallah NASSEREDDINE and Anthony DUPLAN who participated in parts of this work through their internships.

Many thanks to the administrative staff of IRCELYON and particularly Anne-Marie and Marie-Laure who helped me in all administrative procedures. I also thank the informatics service especially Véronique and Hervé who were always there to resolve all issues. This work could not have been done without the indispensable contribution of the scientific services in

IRCELYON: Yoann and Françoise for XRD, Noëlle and Pascale for ICP and BET, Mimoun for TEM and STEM, Luis and Christophe for XPS, and Chantal for µ-GC gas analysis. I also acknowledge Patrick JAME and Erik BONJOUR from ISA “Institut des Sciences Analytiques” for the carbon elemental analyses. Special thanks also go to the staff of the workshop in IRCELYON especially Mustapha, Michel, and Frederic who were always very helpful and kind.

I spent the last three years with exceptional people in the CDFA team, I thank them one by one. My gratitude and warm thanks for my colleagues and friends that I met in IRCELYON who made the work atmosphere so much pleasurable and shared with me all the special moments through this stage; huge thanks to Zahraa, Lama, Ranin, Kamila, Natalia, Sarah, Maxime, Achraf, Hanaa, and Modibo.

At the end, my greatest thanks go to my lovely family, my mom, sisters, and my husband for being always there for me and for their moral support that contributed in achieving my PhD diploma.

Résumé

Ce travail de thèse porte sur la synthèse des carbures de molybdène sur support et l'évaluation de leurs performances catalytiques pour l'hydrogénation de l'acide succinique en phase aqueuse en réacteur discontinu et l'hydrogénation du dioxyde de carbone en phase gazeuse en réacteur à flux continu. Les catalyseurs ont été préparés par la méthode de réduction - carburation, dans laquelle les paramètres ont été modifiés, ce qui a conduit à différentes propriétés structurales ce qui a affecté les comportements catalytiques. L'effet de la vitesse spatiale horaire du gaz de carburation, de la composition du gaz et de la température finale ont été étudiés. Les différents catalyseurs testés étaient actifs dans la conversion de l'acide succinique en γ-butyrolactone et, plus remarquablement, en acide butyrique. Avec des catalyseurs à base de métaux précieux, l'acide butyrique n'avait été reporté qu'en petite quantité. Les intermédiaires sont ensuite convertis en tétrahydrofurane, butanol, 1,4-butanediol et butane. La désactivation observée lors du recyclage du catalyseur a été principalement attribuée à une diminution des quantités de molybdène et de carbone carbidiques comme le suggère l'analyse XPS. Des essais préliminaires d'hydrogénation de dioxyde de carbone ont montré que ces catalyseurs se comportaient principalement comme des catalyseurs pour la réaction inverse du gaz à l'eau. De plus, des teneurs élevées en carbone entravent l'activité catalytique d'une manière opposée à l'hydrogénation de l'acide succinique. Le support semble jouer un rôle crucial dans la réactivité des catalyseurs, la conversion du dioxyde de carbone ainsi que la sélectivité en méthane et méthanol diminuent suivant l'ordre: carbure de molybdène sur support DT51 TiO_2> P25 TiO_2 ≈ ZrO_2.

Mots clés: carbure de molybdène, hydrogénation, acide succinique, phase aqueuse, dioxyde de carbone, phase gazeuse, support TiO_2.

Abstract

This work focuses on the synthesis of supported molybdenum carbides and the evaluation of their catalytic performance in the hydrogenation of succinic acid hydrogenation in aqueous phase using batch reactor and the hydrogenation of carbon dioxide in gas phase using continuous flow reactor. The catalysts were prepared by the temperature programmed reduction carburization method, where the parameters were modified leading to different catalytic properties. The effect of the gas hourly space velocity, the gas composition and the final temperature were investigated. The catalysts were active in converting succinic acid to γ-butyrolactone and more remarkably butyric acid. With precious metal based catalysts used in literature, butyric acid had only been reported in small quantities. At longer reaction times, the intermediates were then converted to tetrahydrofuran, butanol, 1,4-butanediol and butane gas. The deactivation observed while recycling the catalyst was mainly attributed to a decrease in the amounts of carbidic molybdenum and carbidic carbon. Preliminary tests in carbon dioxide hydrogenation showed that these catalysts behave mainly as reverse water gas shift catalysts. Moreover high carbon content hinders the catalytic activity in an opposite manner to the hydrogenation of succinic acid. The support seems to play a crucial role in the reactivity of the catalysts, carbon dioxide conversion as well as methane and methanol selectivity decreased in the order: molybdenum carbide supported on DT51 TiO_2 > P25 TiO_2 ≈ ZrO_2.

Keywords: Molybdenum carbide, hydrogenation, succinic acid, aqueous phase, carbon dioxide, gas phase, TiO_2 support.

Table of contents

List of abbreviations

% wt: percentage by weight

% v/v: percentage by volume

AC: activated carbon

BA: butyric acid

Bcc: body centered cubic

BDO: 1,4-butanediol

BOL: 1-butanol

CNF: carbon nanofibers

EDX: energy dispersive X-ray

EG: ethylene glycol

Fcc: face centered cubic

FT: Fischer-Tropsch

GBL: γ-butyrolactone

GCNS: graphitized carbon nanotubes

GHSV: gas hourly space velocity

GVL: γ-valerolactone

Hcp: hexagonal closed packed

HC: hydrocarbon

HCS: hollow carbon spheres

HDN: hydrodenitrogenation

HDO: hydrodeoxygenation

HDS: hydrodesulfurization

Hex: simple hexagonal

ICP: Inductively coupled plasma

LA: levulinic acid

MC: mesoporous carbon

PZC: point of zero charge

RWGS: reverse water gas shift

TEM: transmission electron microscopy

THF: tetrahydrofuran

TMC: transition metal carbides

TPRC: temperature programmed reduction carburization

SA: succinic acid

STEM: scanning transmission electron microscopy

TGA-MS: thermo-gravimetric analysis coupled with mass spectrometry

WGS: water gas shift

WHSV: weight hourly space velocity

XPS: X-ray photoelectron spectroscopy

XRD: X-ray diffraction

General introduction

The literature dealing with the formulation of catalysts with noble metal-like behavior in heterogeneous catalytic processes reveals the development and use of transition metal carbides “TMCs”. TMCs are compounds formed by the incorporation of carbon atoms into the interstitial lattices of early transition metals. They are potential substitutes for the conventional noble metal catalysts in certain reactions where their catalytic activity is comparable to that of noble metals but with unique pathways and sometimes distinct products selectivity. They are active catalysts in a wide range of reactions including: hydrodesulfurization and hydrodenitrogenation, Fischer-Tropsch synthesis, and water-gas shift. Recently, several studies showed the efficiency of molybdenum carbides for the transformation of biomass-based resources mainly through hydrodeoxygenation reactions where C-O bonds cleavage is desired without any C-C cleavage.

The fermentation of lignocellulosic biomass using bacteria produces succinic acid (SA) which is a platform molecule that can be hydrogenated to valuable products including γ-butyrolactone, 1,4-butanediol and tetrahydrofuran. These chemicals are mainly employed as solvents, food additives, intermediates for polymer synthesis and pharmaceuticals. Water is preferably chosen as solvent for this reaction since after fermentation, SA is obtained in aqueous phase. It is then necessary for the catalysts to be stable under the severe hydrothermal conditions ($T \geq 160$ °C, $P \geq 80$ bar, water) that are required for this reaction. Noble metal supported catalysts have principally been studied for the hydrogenation of SA in aqueous phase. The main limitations to the use of noble-metal catalysts are their scarcity and high prices. For an economically viable valorization of biomass derivatives, it would be interesting to replace group VIII (8 to 10) metals by less expensive and more abundant metals.

In this project, we propose the preparation of new supported molybdenum carbide catalysts for the aqueous phase hydrogenation of SA. Taking in account that the molybdenum carbide phase and molybdenum to carbon ratio can directly affect the performance of the catalysts, we optimized the catalyst synthesis conditions to prepare

the most efficient catalyst for this reaction.

Within the same frame of using sustainable resources, a significant interest is paid to the valorization of carbon dioxide (CO_2) whose emission is constantly increasing and contributes in the increase in global temperatures and climate changes due to the ''greenhouse effect''. CO_2 might be considered as a cheap C1 building block for value-added products, but its transformation is rather difficult, especially in an industrial scale. This is because a possible heterogeneous catalytic conversion is hindered by the high stability and low chemical reactivity of CO_2. One particular approach to CO_2 utilization is its hydrogenation reduction to CO, CH_4, or CH_3OH using catalysts and heat. Lately, TMCs have been proposed as catalysts for CO_2 reduction. A number of density functional theory (DFT) computational studies along with some experimental work have been reported employing TMCs for the production of carbon monoxide, methane, and methanol. Motivated by these interesting reports, we tested different supported molybdenum carbide catalysts for the hydrogenation of CO_2. The conditions of the reaction are optimized with P25 TiO_2-supported molybdenum carbide catalyst. Catalysts supported on other oxides such as DT51 TiO_2 and ZrO_2 were also evaluated.

This thesis is divided into five chapters:

Chapter 1 covers a literature review which comprises three main parts. The first part is dedicated to the description of transition metal carbides, their structure and composition, bonding and electronic properties, applications, and preparation methods. The second part focused on succinic acid building block, its production and valorization mainly via hydrogenation. It is completed by reporting a selection of the catalysts used for this reaction. The third part of this chapter is about the use of carbon dioxide as a C1 building block for the production of carbon monoxide, methane, and methanol via heterogeneously catalyzed hydrogenation reactions.

Chapter 2 includes all the materials and experimental methods used for the synthesis and characterizations of supported molybdenum carbide catalysts, catalytic tests of succinic acid hydrogenation in aqueous phase, and carbon dioxide hydrogenation in gas phase, in addition to the analytic methods used in data treatments.

Chapter 3 includes results dealing with the preparation of supported molybdenum

carbides using temperature programmed reduction carburization method. This chapter focuses on the effects of the preparation parameters such as the carburizing temperature, the carbon source, and the nature of support on some structural and textural properties of the obtained materials. The catalysts characterizations by XRD, TEM, STEM, XPS, carbon elemental analysis, and ICP are described first. Then, the catalytic results for the aqueous phase hydrogenation of succinic acid over these catalysts are discussed, addressing the effects of the catalysts preparation conditions on the catalytic behavior in this reaction.

Chapter 4 shows further optimization of the catalyst preparation conditions by changing the gas hourly space velocity during the preparation. The best performing catalyst was used for the optimization of the reaction conditions for succinic acid hydrogenation. An overview on the reaction pathway was done by conducting reactions from the intermediates. The catalyst stability and recyclability was also addressed in this chapter.

Chapter 5 covers carbon dioxide hydrogenation in gas phase using the catalysts already prepared and characterized in the previous two chapters. It includes screening of the reaction conditions, and the effects of the catalysts preparation conditions and the support on the catalytic performances.

CHAPTER 1.

Literature Review

I. Transition metal carbides (TMCs)

TMCs are alloys of carbon and transition metal atoms; they are formed by the incorporation of carbon into the lattice of the metal. These materials are also denoted as "interstitial alloys", since the carbon atoms occupy the interstitial spaces between the metal ones [1–4].

The first part of this section gives an overview of TMCs. The structure, composition, bonding and electronic properties of the TMC are briefly presented, followed by a description of the preparation of these materials. Then their diverse applications are presented. TMCs are used in many technological applications such as electronic, magnetic, and optical fields owing to their remarkable properties and interesting nature, in addition to their increasing use as catalysts [1–7]. In our work, we are specifically concerned in molybdenum carbides among TMCs, and thus specific examples will be given whenever possible.

I.1. Structure and composition of TMCs

TMCs have many crystal structures, the main ones being face centered cubic (fcc), hexagonal closed packed (hcp) or simple hexagonal (hex) (Figure 1) [8,9]. Usually, the TMC adopts a structure different from that of the parent metal. For example, pure

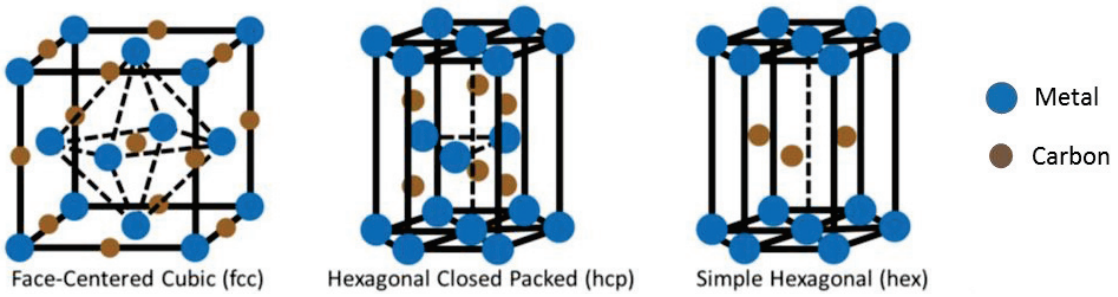

Figure 1 Common structures in TMCs [9].

molybdenum and tungsten metals are body centered cubic (bcc), while their stable carbide phases are hcp and hex, respectively [8]. A structure not adopted by carbides is the body-centered cubic (bcc), because this lattice cannot accommodate an interstitial atom.

The structure and stoichiometry of the materials emerging from different transition metals depend on geometric and electronic factors [1,3,9,10]. The geometric factor is determined experimentally. Indeed, on the left of the periodic table, the structures tend to be simple, while on the right the structures become more complicated. These trends were given by Hägg's rule, which states that the structure of the formed alloy depends on the ratio (r) of the radius of the carbon to that of the transition metal:

$r = r_{carbon}/r_{metal}$

When $r < 0.59$, the transition metals form the common structures: fcc, hcp, or hex. The early transition elements have relatively large atomic radii and the carbon atoms can occupy the interstitial sites between metal atoms. For example, in groups 4 and 5 the preferred structure is fcc (NaCl) with atomic radii between 0.132 nm (V) to 0.158 nm (Zr); whereas in group 6, hexagonal and orthorhombic structures appear (Table 1), with atomic radii ranging from 0.125 (Cr) to 0.137 (W). In our specific example of molybdenum carbide, the ratio of C to Mo is 0.566 (with atomic radii of 0.077 nm and 0.136 nm for C and Mo respectively) [10], and the stable structure is hcp (Table 1).

Table 1 Crystal structure of transition metal carbides of groups 4-6. Produced from references [9,11–15]

Group 4 (IVB)		**Group 5 (VB)**		**Group 6 (VIB)**	
TiC	fcc	VC_{1-x}	fcc	Cr_3C_2	orthorhombic
TiC_{1-x}		VC, V_2C, V_4C_3, V_6C_5, V_8C_7		Cr_7C_6, $Cr_{23}C_6$	
ZrC_{1-x}	fcc	NbC_{1-x}	fcc	Mo_2C	hcp
ZrC		NbC, Nb_2C, Nn_3C_2, Nb_4C_3		MoC_{1-x}, MoC, Mo_3C_2	
HfC_{1-x}	fcc	TaC_{1-x}	fcc	WC	hex
HfC, Hf_3C_2, Hf_6C_5		TaC,Ta_2C, Ta_3C_2, Ta_4C_3		WC_{1-x}, W_2C	

Stable carbide Other possible carbides

On the other hand, when r > 0.59, more complex structures are formed [1,3,9,10]. Toward the right in the periodic table (i.e. groups 7-10), the size of the metal atom decreases (e.g. the atomic radii of Mn and Fe are 0.112 nm and 0.124 nm respectively) [10]. Accordingly, the lattice is not able to accommodate the carbon atoms while maintaining the metal-metal interactions at the same time, and thus produces more complex structures (e.g. triclinic, tetragonal, and orthorhombic).

Even though minor exceptions exist, Hägg's rule is usually useful for predicting structures of TMCs.

Regarding the composition in TMCs, there are some common trends within the periodic table. Usually, the carbides of groups 4 and 5 transition metals present a one to one stoichiometry (i.e. MC; M stands for transition metal and C for carbon), e.g. TiC, ZrC, HfC. In group 5 (VB), M_2C stoichiometry starts to appear, e.g. V_2C, Nb_2C, and Ta_2C but it is not the most stable carbide phase. Nevertheless, this phase becomes more favorable for group 6 (VIB) elements, e.g. Mo_2C (Table 1). In addition, sub-stoichiometry such as MoC_{1-x} and WC_{1-x} can exist and the MC stoichiometry (e.g. MoC, or WC) can also be formed. While, the stoichiometry of carbides of the transition metals of group 8 to 10 (e.g. Fe, Co, and Ni) usually shifts to M_3C [6,9,11,16].

The second factor that determines crystal structures of TMCs is the electronic one. According to the Engel-Brewer theory, the structure adopted by a metal or an alloy can be predicted based on the electronic configuration, as it depends on the total number of sp electrons. Thus, as the sp electron count increases, the structure goes from bcc → hcp → fcc as observed in the series of metal Mo → Re → Pd [1,2]. The electronic properties will be further discussed in the following section.

I.2. **Bonding and electronic properties of TMCs**

TMCs have physical properties that resemble those of ceramics such as the hardness, high melting points > 3300 K, and strength > 3×10^5 MPa. At the same time, their electronic and magnetic properties are characteristic of metals such as good electrical and heat conductivity [1,7].

The unusual properties of TMCs urged theoretical chemists to study the chemical

bonding of these materials. The electronic behavior of TMCs gives the impression that their electron density has increased by alloying [2]. The bonding in these compounds is due to the interaction between the 2s and 2p orbitals of carbon with the d orbitals (t_{2g} and e_g) of the metal (Scheme 1) [1]. In the case of molybdenum, the 4d orbital of the metal is occupied by 5 electrons [17].

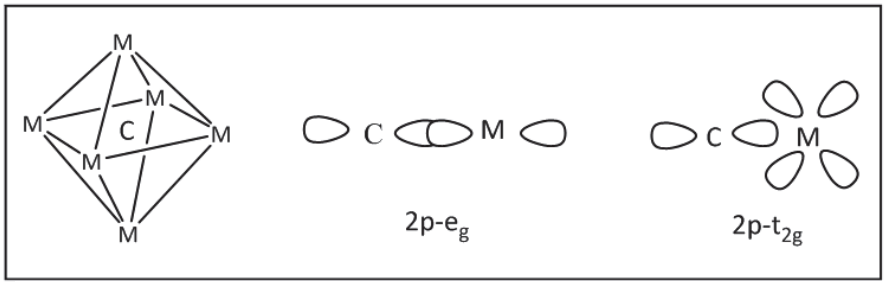

Scheme 1. Electronic structure of transition metal carbides: 2p orbital of carbon and d orbital (t_{2g} and e_g states) of the metal [1].

Theories on the type of bonding in TMCs have changed significantly over the years and are summarized by Oyama [2]. The type of bonding is not the same among different TMCs, as they can exhibit covalent, ionic and metallic bonds. For example the V-C bonds were proved to be much more ionic than the Mo-C bonds [18]. The oxidation state of Mo in a thin carbide film was determined to be around $Mo^{0.2+}$, whereas the oxidation state of V in the carbide is $V^{1.2+}$. This indicates that there is very little charge transfer between Mo and C, and that the Mo-C bonding is mainly covalent, compared to a significant indication of ionic bonding in the V-C bond [18]. The charge transfer decreases when moving from group 4 to 6 which can be due to the increase in electronegativity of the metals. Based on theoretical calculations, X-ray photoelectron spectroscopy and near edge X-ray absorption fine structure spectroscopy, the electron transfer is from the transition metal to carbon [19].

I.3. **Applications of TMCs**

Because of their great strength, hardness, and durability, TMCs have been used in applications requiring extreme conditions of temperature and pressure such as rocket nozzles, cutting tools, and snow tires [1]. Moreover, TMCs have interesting optical, electronic, and magnetic properties and have been used for optical coatings, electrical connections, diffusion barriers, and coatings for metal objects [1,9].

I.3.1. **TMC as catalysts**

In early 70s, TMCs started to attract attention as catalysts because of their high specific surface area and relatively inexpensive prices [1]. The great interest in the catalytic applications of these materials was induced after the popular report of Levy and Boudart who noted platinum-like catalytic behavior of tungsten carbide [20].

The use of TMCs as heterogeneous catalysts is common in gas phase reactions, whereas they are also reported for some fewer liquid phase catalytic applications. They are employed as bulk catalysts (e.g. Mo_2C), supported catalysts (e.g. Mo_2C/Al_2O_3), or as supports for other metals (e.g. Cu/Mo_2C). To focus specifically on the catalytic activity of the TMCs we will not include examples where they are used as supports.

TMCs are currently known for their activity in hydroprocessing reactions such as hydrodesulfurization (HDS), hydrodenitrogenation (HDN), and hydrodeoxygenation (HDO) that are used to remove sulfur, nitrogen, or oxygen from streams, such as in petroleum or biomass-derived oil. Furthermore, the catalytic activity of TMCs is also reported in water-gas shift, isomerization, and Fischer-Tropsch reactions [21–24]. They are capable of adsorbing, activating and transferring active surface hydrogen to reactant molecules [25]. In the following part, a few examples will be given for the aforementioned reactions (Table 2).

Table 2 Selected examples of reactions reported in the literature over molybdenum carbides

Entry	Catalyst	Reaction	T (°C)	P (bar)	Conversion (%)	Ref
1	10% Mo_2C/Al_2O_3	HDS of thiophene to n-butane + other C_4 alkenes	420	1	15	[26]
2	40% Mo_2C/γ -Al_2O_3-P	HDS of dibenzothiophene to biphenyl	370	31	80	[27]
3	Mo_2C	HDN of pyridine to C_4 and C_5 alkanes	380	1	50	[28]
4	5% Mo_2C/C	HDN of indole to ethylcyclohexane + ethylbenzene	350	50	100	[29]
5	10% Mo_2C/Al_2O_3	Fischer-Tropsch synthesis (C_1 - C_5 alkanes)	300	10	14	[30]
6	10% MoC_{1-x}/TiO_2	Fischer-Tropsch synthesis (olefins and paraffins)	200	1	10	[31]
7	Mo_2C	Water-gas shift	295	1	30	[24]

I.3.1.1. **Hydrotreating reactions**

Hydrotreating is a process widely used in the petroleum industry for producing high quality fuels and upgrading heavy crude oil by reducing sulfur and/or nitrogen content [32]. The reported activity of TMCs in these reactions is not new [33,34]. Some examples in the literature particularly on molybdenum carbides are listed in Table 2.

In gas phase HDS of thiophene in flow reactor (Table 2, entry 1), Mo_2C/Al_2O_3 catalyst showed superior activity (normalized per mole of molybdenum) than the conventional sulfided Mo/Al_2O_3 catalyst with the same Mo loading after 18h of reaction. The products distribution was similar for the two catalysts (37% n-butane, 26% 1-butene, 25% cis-2-butene, 10% trans-2-butene, and 2% butadiene) [26].

Oyama et al. studied $Mo_2C/\gamma\text{-}Al_2O_3$ with phosphorous additive for hydrotreating reactions in trickle-bed reactor. The authors found that the steady-state conversion and turnover rate of the carbide catalyst was higher than the reference sulfided commercial catalyst ($Ni\text{-}Mo\text{-}S/Al_2O_3$). For example, for the HDS of dibenzothiophene, $Mo_2C/\gamma\text{-}Al_2O_3\text{-}P$ catalyst exhibits a turnover rate of 1.2 $10^{-3}s^{-1}$ compared to 0.6 $10^{-3}s^{-1}$ for $Ni\text{-}Mo\text{-}S/Al_2O_3$ (Table 2, entry 2).

Xiao et al. reported the preparation of bulk Mo_2C catalyst and tested it for pyridine gas-phase HDN reaction [28]. The authors found excellent performance of the catalyst with a high selectivity to C_4 and C_5 alkanes (Table 2, entry 3). HDN of indole to ethylcyclohexane and ethylbenzene was performed over Mo_2C supported on various carbon black composites in a down flow reactor (Table 2, entry 4). The authors showed that the catalytic activity was dependent on the dispersion of the active phase, i.e. higher HDN conversion were obtained over catalysts with higher dispersion [29].

I.3.1.2. **Fischer-Tropsch synthesis**

The Fischer-Tropsch (FT) reaction which involves the conversion of CO and H_2 into hydrocarbons and alcohols is performed usually using Fe and/or Co based catalysts. Early transition metal carbides, in particular Mo and W carbides, have been reported to be active for this reaction. However products selectivity remains a major challenge where molybdenum carbide catalyst mainly gives methane and light alkanes [32].

Khodakov et al. tested 10% Mo_2C/Al_2O_3 catalyst for FT synthesis in a fixed-bed reactor at 300°C and 10 bar (Table 2, entry 5). The authors stated that the catalyst was relatively stable and the catalytic performance remained unchanged during 40 h of reaction. The products were mainly methane, light paraffins and carbon dioxide. This study also showed the effect of catalyst promotion with potassium which resulted in lower FT reaction rate but higher selectivity to light olefins and C_{5+} hydrocarbons [30].

Adesina et al. investigated the catalytic properties of Mo_2C catalysts supported on various semiconductor oxides for FT synthesis. They concluded that reaction rates follow the order MoC_{1-x}/TiO_2 (Table 2, entry 6) > MoC_{1-x}/SiO_2 > MoC_{1-x}/ZrO_2 > MoC_{1-x}/Al_2O_3. Molybdenum carbide formation rates (during syntheses) followed the same trend. Moreover, methane selectivity decreased in the order MoC_{1-x}/ZrO_2 > MoC_{1-x}/SiO_2 > MoC_{1-x}/Al_2O_3 > MoC_{1-x}/TiO_2 in agreement with the chain growth probability trend, estimated from Anderson-Schulz-Flory equation. Thus, MoC_{1-x}/TiO_2 was the optimal catalyst in this study [31].

I.3.1.3. **Water-gas shift reaction**

The water-gas shift (WGS) reaction is an industrially important reaction for the production of H_2 at the expense of CO, given by the equation: $CO + H_2O \leftrightarrow CO_2 + H_2$.

The WGS is exothermic reaction; the research regarding the use of carbides for this process has focused primarily on the low temperature WGS [32]. Patt et al. were among the first to report the WGS activity of Mo_2C (Table 2, entry 7). The catalytic rates were comparable to those for $Cu/Zn/Al_2O_3$ (the industrial catalyst) on a weight basis under identical conditions. These authors reported that there was no evidence of methanation activity for both catalysts under the conditions employed. In addition, the carbide catalyst was stable after 48 h of reaction [24].

I.3.1.4. **Biomass-related reactions over TMC catalysts**

- **Hydrodeoxygenation**

Recently, molybdenum carbides have received more interest for their application in the transformation of biomass-based resources. Biomass must undergo several transformations in order to be converted into biofuels and fine chemicals. The biomass

derivatives obtained through hydrolysis contain a large amount of oxygen, i.e. a high O/C ratio. Accordingly, hydrodeoxygenation (HDO) is a significant reaction and should be performed via a catalyst which is able to selectively cleave C-O bonds without any C-C cleavage [6]. TMCs have been reported to be highly selective in the HDO of vegetable oils derived from biomass. Some examples reported in the literature are listed in Table 3.

Zheng et al. were in the first to report the conversion of renewable vegetable oils (such as, soybean, rapeseed, olive and sunflower oil) into diesel like hydrocarbon mixtures on molybdenum carbide catalysts with high activity and selectivity [35]. They showed that Mo_2C/AC catalyst achieved the highest yield of hydrocarbon with olive oil (88%), and the catalyst was found to be active and stable over 16 runs (Table 3, entry 1).

The same group assessed the use of cellulose-derived carbon materials as supports for Mo_2C. The catalysts were tested for hydrodeoxygenation of maize oil [36]. The authors showed that graphitized carbon nanosphere supported catalyst gave high conversion and hydrocarbon yield (91% and 88% respectively), which were 21% and 31% higher than the conversion and yield of the un-graphitized carbon nanosphere supported catalyst (Table 3, entry 2).

Bitter et al. compared the performance of molybdenum and tungsten carbides supported on carbon nanofibers for the hydrodeoxygenation of oleic acid, present in vegetable oils [37]. Both catalysts showed good activity, but Mo_2C/CNF catalyst was found to be more active and more stable than W_2C/CNF. The catalysts also exhibited different products selectivity where Mo_2C/CNF catalyst was selective to paraffin (Table 3, entry 3), and W_2C/CNF was more selective to olefin.

Albeit the very good results reported for the conversion of vegetable oils over carbide catalysts, the concern lies in the competition between “first generation biofuels” and food crops. Therefore more attention is directed towards waste oil or non-edible lignocellulosic resources “second generation feedstocks” [6].

Table 3 Examples of reactions reported in the literature for biomass valorization over TMCs

Entry	Catalyst	Reaction	Conditions			Results		Ref
			T (°C)	P (bar)	Solvent	Conversion (%)	Yield (%)	
1	20% Mo_2C/AC[a]	HDO of olive oil to C_{16}-C_{18} alkanes	280	15	hexane	94	88	[35]
2	20% Mo_2C/GCNS[b]	HDO of maize oil to C_{18} alkanes	260	25	hexane	91	88	[36]
3	7.5% Mo_2C/CNF[c]	HDO of oleic acid to paraffin	350	50	dodecane	100	80	[37]
4	10% Mo_2C/CNF	HDO of guaiacol to phenol, cyclohexane, benzene, anisole	300	32	n-decane	67	33[d]	[38]
5	14% MoC_x/HCS[e]	HDO of phenol to benzene	350	80	n-octane	87	85	[39]
6	30% WC_x/MC[f]	Conversion of cellulose to ethylene glycol	245	60	water	100	73	[40]
7	20% Mo_2C/CNF	Hydrogenation of levulinic acid to γ-valerolactone	200	30	water	99	90	[41]

[a] Activated carbon, [b] Graphitized carbon nanospheres, [c] Carbon nanofibers, [d] Total yield of HDO products, [e] Hollow carbon spheres, [f] Mesoporous carbon.

Origin: Vegetable oils Origin: Lignin Origin: Cellulose

Hydrodeoxygenation of guaiacol, a model molecule resulting from lignin depolymerization, was performed on molybdenum carbide supported on carbon nanofibers catalyst [38]. Mo_2C/CNF catalyst achieved a guaiacol conversion of 67% with HDO yield of 33% (Table 3, entry 4). The rest of the products were those of demethylation/methyl substitution reactions of guaiacol and products.

García et al. studied the HDO of phenol over Mo_2C supported on hollow carbon spheres [39]. A high selectivity to benzene was obtained with high phenol conversion (Table 3, entry 5). The authors deduced from the experimental and computational investigations that direct deoxygenation route which leads to benzene was preferred over the hydrogenation route that leads to cyclohexane. They referred this preference to direct deoxygenation to the affinity of phenol to adsorb on Mo_2C surface. They also examined the effect of water during the HDO reaction. Phenol and water were in competition for the Mo adsorption sites. When the water partial pressure increased, the Mo active sites were covered by water, thus hindering the access of phenol to the Mo surface atoms. Deactivation of the catalyst resulted from the formation of MoO_2.

- **Hydrogenation**

Cellulose can serve as a sustainable feedstock for fuels, chemicals and polymers that are currently produced from petroleum [6]. Zhang et al. reported the conversion of cellulose to ethylene glycol (EG: a monomer for the large scale manufacture of polyethylene teraphtalate) over tungsten carbide catalyst supported on mesoporous carbon. Full conversion of cellulose was achieved with 73% yield of EG (Table 3, entry 6). The authors explained that the 3D interconnected mesoporous structure favored high dispersion and accessibility of active components of WC_x, thus the conversion of cellulose to EG is facilitated [40].

Another attractive approach lies in the transformation of cellulose into levulinic acid (LA) by acid-catalyzed hydrolysis [6]. LA is a C5 keto-acid classified as potential platform chemical in the biorefinery notion. Teixeira da Silva et al. studied the hydrogenation of LA over molybdenum carbide based catalysts [41]. Molybdenum carbide supported on carbon nanotubes achieved 99 % conversion and 90% selectivity to γ-valerolactone using a continuous-flow reactor (Table 3, entry 7). They showed that in a turnover frequency

basis, the values were similar to those obtained for a ruthenium catalyst evaluated under the same conditions.

I.3.1.5. Stability of TMC catalysts

Albeit the aforementioned examples that reported good stability for TMC catalysts throughout the catalytic reactions, this is not the case in many other reports. The main causes of deactivation in literature are the oxidation of the transition metal species and carbon deposition on the catalyst.

Mortensen et al. [42] studied the stability of Mo_2C/ZrO_2 catalyst for HDO of phenol and 1-octanol as a simplified bio-oil model system. The conversion of 1-octanol was higher than phenol. In the stability tests, the conversion of 1-octanol decreased throughout the 76 h experiment from 70% initial conversion to 37% at the end. The authors believed that the cause behind this deactivation was the water produced as by-product from the deoxygenation reaction. They drew out this conclusion by elucidating the deactivation mechanism, where water was co-fed with 1-octanol solution. A rapid deactivation of the catalyst occurred and the conversion of 1-octanol decreased from 64% to 11% within the first 12 h. This was accompanied with the detection of traces of CO_2 and CH_4 in the gas phase, which the authors considered a possible indication of the oxidation of Mo_2C.

Lee et al. [43] also observed pronounced deactivation of Mo_2C for HDO of furfural at 150 °C and 1 bar in a plug-flow reactor. They found that the deactivation was partly because of carbon deposition, but oxidation of the catalyst could not be excluded.

Claridge et al. [44] observed that molybdenum carbide deactivated in reforming of methane due to the formation of MoO_2 and that the level of deactivation increased with the strength of the oxidizing agent as: $O_2 > H_2O \approx CO_2$.

I.3.2. The origin of analogy between TMCs and noble metal catalysts

In the 5th raw of the periodic table, the crystal structures of the elements from group 6, 8 and 10 evolve from bcc (Mo) to hcp (Ru) and fcc (Pd), which is the same trend found in the series Mo, Mo_2C, Mo_2N (Table 4). In fact, carbon sp electrons increase the apparent electron-to-atom ratio, producing relatively Pt-like electronic structure. After

confirmation that the electron transfer is from the metal to carbon, it was shown that the formation of the carbide may modify the nature of the d-band of the parent metal. In order to accommodate the carbon atoms, the host metallic lattice may have to expand, thus leading to an increase of the metal-metal bond distance, which in turn causes contraction of the metal d-band. This contraction gives greater density of states near the Fermi level, and thus gives rise to catalytic properties that are different from those of the parent metals but similar to those of group 8–10 noble metals [11,45,46].

Table 4 Analogy in structure progression of elements from group 6, 8 and 10 with molybdenum carbides and nitrides

Group 6 (VIB)		**Group 8 (VIII)**		**Group 10 (VIII)**	
Mo	bcc	Ru	hcp	Pd	fcc
Parent metal		**Carbide**		**Nitride**	
Mo	bcc	Mo_2C	hcp	Mo_2N	fcc

The properties of interstitial alloys are directly linked to their way of preparation. Indeed, the parameters affecting the size, morphology, and crystal structure of the resulting compounds have to be controlled. Therefore the next section will focus on the methods of preparation of metal carbides, and more specifically, supported carbides, that we are interested in within this work. Again, whenever it is suitable, the examples will be given on molybdenum carbides.

I.4. **Preparation of TMCs**

Several methods have been developed for the preparation of carbides according to the targeted use of the material. The methods that use quite elevated temperatures (1225-2026 °C) for the preparation of carbides produce materials with very low surface area. These methods are convenient for applications that require the strength and hardness properties of the carbides. However, when the materials are prepared for catalysis purposes, these methods are not useful as the surface area is a critical parameter for this application. Herein we distinguish between the methods of preparation of low surface area carbides and methods of preparation of high surface area carbides which is desired for TMCs employed in catalytic applications. The former methods will be presented briefly

as they are of little interest for our discussion.

We are interested in supported carbides however the carburization processes for TMCs reported in literature are mainly focused on the bulk material. Therefore the methods of preparation of bulk TMCs are presented first in this part, for the sake of clarity, followed by the supported ones.

I.4.1. Methods producing low surface area carbides

I.4.1.1. Direct reaction of the transition metal and carbon (solid-solid)

TMCs can be prepared by mixing the metallic powder (M) with solid carbon (C) under H_2 or vacuum at elevated temperatures (1225-2026 °C).

The thermodynamic of this reaction shows that carbide formation is favored at lower temperatures, but high temperatures are used to overcome solid-state diffusion limitations [1,2].

I.4.1.2. Reaction of metal oxide and carbon (solid-solid)

A metal precursor is mixed with carbon and heated at high temperatures (1225-2026 °C) as with the pure metals [1,2]. Direct transformation of metal oxides to carbides is economically beneficial since the oxide does not have to be reduced to the metal in a preliminary step.

I.4.1.3. Reaction of metal containing compounds with hydrocarbon gas (solid-gas or vapor-gas)

Another way to produce TMCs is the decomposition of metal compounds or metal halide vapors by reacting them with gaseous hydrocarbons under high temperature (1126-2626 °C) [1,2].

I.4.2. Method producing high surface area carbides: Temperature-programmed reaction

This method includes the reaction of metal precursor with carbon-containing reactive gas (CO, hydrocarbons, or a mixture of hydrocarbon and hydrogen) [1,2,4]. Generally, the carburization of a solid with a gas is preferred over reaction with solid carbon because

solid-solid reactions require high temperatures to avoid diffusion limitations.

Temperature-programmed reduction-carburization (TPRC) is a TMCs preparation method developed by the group of Boudart [4,47,48] which is classified within the methods that involve the solid-gas interaction. In this process, a metal precursor or supported metal precursor powder is placed under a reductive-carburizing gas flow, while raising the temperature slowly in a uniform heating ramp until reaching the maximum temperature needed. Ammonium heptamolybdate tetrahydrate or molybdenum trioxide are usually used as precursor. By monitoring changes in the exit gas composition it is possible to determine the different synthesis steps and investigate the reaction intermediates. Through this method of synthesis it is possible to bypass the metallic state that is susceptible to sintering because the synthesis involves the simultaneous reduction and carburization of the transition metal oxide to carbide resulting in products with high specific surface areas [4,47–49].

Aside from hydrocarbons, other sources of carbon can be used. For example Ren et al. used glucose as a carbon source to prepare Mo_2C-Ni/ZrO_2 by the so called glucose-assisted incipient wetness impregnation with subsequent reduction carburization. In this case the reduction carburization process was conducted under H_2/N_2 [50].

Moreover, when the support itself is carbon, it is used as a carbon source for the carburization of the metal oxide via carbothermal hydrogen reduction method [6] e.g. Mo_2C/AC [51]. However, in this work we focus only on TPRC with hydrocarbons as carbon source, and thus the provided examples cover only this process.

Specific example: Preparation of molybdenum carbides by TPRC

As we are specifically concerned in molybdenum carbides in this work, a few examples of their preparation by TPRC method are detailed below.

As mentioned in section I.1, molybdenum carbide systems consist of different phases, most of which have two compositions, MoC and Mo_2C, which may co-exist [52]; and the main crystallographic phases are the hexagonal, cubic, and orthorhombic molybdenum carbide phases [53].

An example of preparing bulk hcp Mo_2C by TPRC of MoO_3 using 20% v/v CH_4/H_2 gas is given by Boudart [47]. Figure 2 shows that the transformation occurs in two stages. In the first stage, water is formed at T ≈ 610 °C where the precursor MoO_3 is reduced to MoO_2 (confirmed by the analysis of the intermediate products). In the second stage of transformation, more water is produced accompanied by methane consumption at T ≈ 665 °C. Therefore, it is concluded that reduction and carburization occur simultaneously, where oxygen atoms diffuse from the bulk to the surface as carbidic carbon inserts in opposite direction. The resulting product is Mo_2C of surface area around 60 m^2/g. When pure H_2 is used, MoO_3 is reduced to MoO_2 which in turn is reduced to metallic molybdenum. The surface area of metallic Mo is below 3 m^2/g, so the metallic stage should be bypassed during the preparation to obtain a metal carbide with high surface area [47].

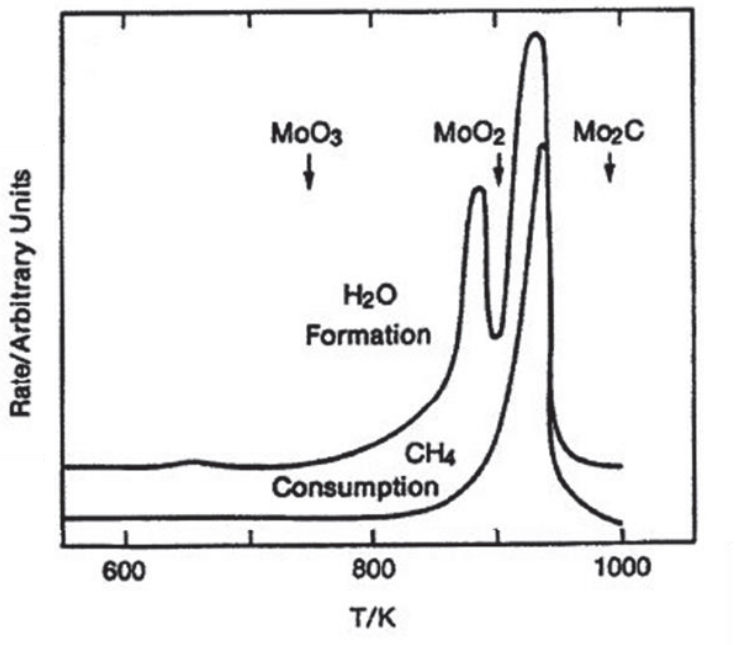

Figure 2 TPR profiles of carburization and reduction of MoO_3 [49].

The transformation route of molybdenum trioxide to molybdenum carbide seems to differ depending on several parameters. For instance, in the example of the preparation of hcp Mo_2C with 20% CH_4/H_2 discussed above the transformation goes through $MoO_3 \rightarrow MoO_2 \rightarrow Mo_2C$ [45,47], however others claim the formation of an intermediate fcc phase MoO_xC_y i.e. $MoO_3 \rightarrow MoO_2 \rightarrow MoO_xC_y \rightarrow Mo_2C$ [54]. On the other hand, for the preparation of fcc MoC_{1-x} the transformation route has been reported to be: $MoO_3 \rightarrow MoO_2 + MoO_xH_y \rightarrow MoC_{1-x}$ [55], or also $MoO_3 \rightarrow MoO_2 \rightarrow MoC_{1-x}$ [56].

I.4.2.1. **Effects of carburization conditions**

A challenging aspect in the preparation of molybdenum carbides -as for other TMCs- is controlling their crystallographic structure and morphology. The TPRC process is sensitive to many parameters that make the choice of the preparation conditions critical. The success of a synthesis can be highly sensitive to the gas composition (i.e. % v/v HC/H_2), the nature of the carbon source, heating rate, maximum carburization temperature, and holding time. Table 5 includes examples on the preparation of bulk and supported molybdenum carbides. Some information on the preparation is not mentioned in the table for simplicity purposes, they can be found in details in the corresponding references.

Table 5 Examples of preparations of molybdenum carbides reported in the literature

Entry	Precursor	Reactive gas % v/v (HC/H_2)	Heating rate (°C/min)	T_{max} (°C)	Holding time (h)	Molybdenum carbide phase	Size (nm)	Ref.
1	$(NH_4)_6Mo_7O_{24}{\cdot}4H_2O$	20% CH_4/H_2	1	630	5	hcp	9	[45]
2	$(NH_4)_6Mo_7O_{24}{\cdot}4H_2O$	20% CH_4/H_2	1	700	5	hcp	12	[45]
3	$(NH_4)_6Mo_7O_{24}{\cdot}4H_2O$	20% CH_4/H_2	1	800	5	hcp	16	[45]
4	MoO_3	20% CH_4/H_2	1	700	2	hcp	7	[54]
5	MoO_3	20% CH_4/H_2	1	750	1	hcp	5	[57]
6	MoO_3	20% CH_4/H_2	10	700	3	hcp	-	[58]
7	$(NH_4)_6Mo_7O_{24}{\cdot}4H_2O$	80% CH_4/H_2	1	700	5	hcp + fcc	7	[45]
8	MoO_3	10% C_2H_6/H_2	1	630	1	hcp + fcc	3	[57]
9	$MoO_3.nH_2O$	20% C_2H_6/H_2	10	720	-	fcc	2	[56]
10	MoO_3	10% C_2H_6/H_2	1	700	2	hcp	6	[54]
11	MoO_3	5% C_4H_{10}/H_2	1	550	1	fcc	1	[57]
12	$(NH_4)_6Mo_7O_{24}{\cdot}4H_2O$	20% CH_4/H_2	10	700	3	fcc	-	[58]
13	$(NH_4)_6Mo_7O_{24}{\cdot}4H_2O$	20% C_3H_8/H_2	5	700	2	fcc + hcp	9	[31]

14	$(NH_4)_6Mo_7O_{24}{\cdot}4H_2O$	20% CH_4/H_2	2.5	650	2	hcp	3	[41]
15	$(NH_4)_6Mo_7O_{24}{\cdot}4H_2O$	20% CH_4/H_2	5	700	2	fcc	5	[59]
16	$(NH_4)_6Mo_7O_{24}{\cdot}4H_2O$	20% C_3H_8/H_2	5	700	2	fcc + hcp	3	[31]
17	$(NH_4)_6Mo_7O_{24}{\cdot}4H_2O$	20% C_3H_8/H_2	5	700	2	fcc + hcp	14	[31]
18	$(NH_4)_6Mo_7O_{24}{\cdot}4H_2O$	20% CH_4/H_2	0.5	550	4	hcp	-	[42]
19	$(NH_4)_6Mo_7O_{24}{\cdot}4H_2O$	20% C_3H_8/H_2	5	700	2	fcc + hcp	14	[31]
20	$(NH_4)_6Mo_7O_{24}{\cdot}4H_2O$	20% CH_4/H_2	5 then 1	650	3	hcp	43	[60]

Unsupported | Supported on carbon nanotubes | Supported on ZrO_2

Supported on Al_2O_3 | Supported on SiO_2 | Supported on TiO_2

a) Bulk molybdenum carbides

The preparation of bulk molybdenum carbides has been largely studied and some of the keys parameters are discussed hereafter.

Upon conducting the carburization using 20% v/v CH_4/H_2 reactive mixture, the hexagonal hcp phase is usually obtained regardless of the other parameters of carburization as shown in entries 1 to 6 in Table 5 [45,54,57].

Increasing the carburization temperature (from 630 to 800°C) generates larger molybdenum carbide particles as shown in entries 1, 2, and 3 [45]. Similarly, holding the maximum temperature for longer time causes an increase in the crystallite size (entries 2 and 4) [45,54].

Increasing the concentration of methane itself from 20% (entry 2) to 80% (entry 7) within the reactive gas mixture caused a change of crystallographic phase, from pure hcp to a mixture of hcp and fcc molybdenum carbide. But at the same time, this also increases the deposition of excess carbon on the surface [45].

Increasing the chain length of the hydrocarbon from CH_4 (entry 5) to C_2H_6 (entry 8) and C_4H_{10} (entry 11) lowers the temperatures required for the complete formation of carbide from 750 °C to 630 °C and 550 °C, respectively. Accordingly, the size of molybdenum carbides carburized at lower temperature is smaller [57].

Carburization with C_2H_6/H_2 generates a mixture of fcc and hcp phases at low concentration of hydrocarbon (10 % v/v, entry 8) [57], while pure cubic phase is obtained at 20 % v/v (entry 9) [56]. Carburization using C_4H_{10} produces fcc cubic molybdenum carbide phase (entry 11) [45,54,57,61,62].

In summary, the reports dealing with the effects of carburizing agent on the structure of bulk TMCs show that the type and concentration of the carbon source affect the crystallographic structure and the carburization degree of the material [45,54,57,61,62]. On the other hand, carburizing at higher temperatures and longer time produces molybdenum carbide particles with larger crystallite size [28,45,54,57,61,63,64]. Despite that, the effects of the preparation conditions may overlap as TPRC synthesis method is sensitive to all the aforementioned parameters.

b) Supported molybdenum carbides

Concerning the supported molybdenum carbides, less data are available in literature on the effects of preparation conditions on the properties of the material.

Ammonium heptamolybdate tetrahydrate is usually used as precursor. A calcination step (heating under air) can be done before the TPRC to generate molybdenum trioxide, or TPRC can be conducted directly, the decomposition of the precursor salts occurs then during the thermal treatment.

A study on the preparation of bulk and supported molybdenum carbide showed that when employing the same carburization conditions (20% v/v CH_4/H_2 at 700 °C), the unsupported molybdenum carbide exhibits hcp structure (Table 5 entry 6) whereas the alumina-supported molybdenum carbide has an fcc structure (entry 12) [58]. Accordingly, it is not possible to predict the molybdenum carbide phase when new supported materials and new synthesized conditions are used.

Molybdenum carbide supported on carbon nanotubes was prepared using 20% CH_4/H_2. The hcp phase was obtained at 650 °C in a report (entry 14) [41]; whereas fcc phase was obtained at 700 °C in another report (entry 15) [59]. The final temperature of carburization seems to affect the crystallographic phase. This confirms the sensitivity of the preparation of these materials. It is important to control the parameters during the synthesis in order to ensure reproducibility and accuracy in producing the desired phase.

A report on the preparation of supported molybdenum carbides using 20% v/v C_3H_8/H_2 at 700 °C showed that a mixture of fcc and hcp molybdenum carbide phases was obtained on all the oxide supports: Al_2O_3 (entry 13), SiO_2 (entry 16), ZrO_2 (entry 17), and TiO_2 (entry 19) [31]. They concluded in this study that TiO_2-supported molybdenum oxide performed maximum carburization reaction rate among other oxides. Aside from the aforementioned report, another study reported the formation of large crystallites (~ 25 nm) of hexagonal Mo_2C on anatase TiO_2 using 20% v/v CH_4/H_2 at 650 °C (entry 20) [60].

Mo_2C/ZrO_2 with hcp structure was synthesized using 20% v/v CH_4/H_2 at 550°C (entry 18). The authors observed MoO_2 as an intermediate during the transformation [42].

In the case of supported material, TPRC is preceded by the deposition of the precursor on the support (i.e. preparation of the supported metal precursor); this step is discussed

in the following part.

I.4.3. **Preparation of the supported metal precursor**

There are two main steps in the preparation of supported catalysts: the first one consists on the deposition of the precursor of the metal on the support, and the second one is the activation step (transformation of the material into the required active state of the metal). The activation may include calcination at specific temperatures under air to remove any moisture that may stay after the first step, and decompose the precursor salts. More importantly, activation generally comprises reduction of the metal oxide to the required reduced state (e.g. the zero charged metallic state), or reduction-carburization as in the case of TMCs.

As a matter of fact, most metal catalysts of industrial interest are supported. Indeed, the support may play a fundamental role in the activity and stability of catalysts. Moreover the nature of the support can affect the acidity and basicity of the catalyst, and hence the catalytic response. Using supports allows to reduce the amount of the metal used, and can provide high dispersion for the active phase on the surface [65]. Properties of supported catalysts depend on many factors such as the metal precursor, the nature of the support, and the preparation procedure.

I.4.3.1. **The metal precursor**

When choosing the metal precursor, some factors should be taken into account. For example the solubility of the precursor in the solvent chosen for the preparation**,** the counter ions that can easily be decomposed to volatile products or act as poisons (e.g. Cl), the possible interactions with the chosen support, in addition to other considerations such as availability and prices.

As already mentioned, in the case of molybdenum carbides, the two common molybdenum precursors usually used in the preparation are: ammonium heptamolybdate tetrahydrate ($(NH_4)_6Mo_7O_{24}.4H_2O$), and molybdenum trioxide (MoO_3).

I.4.3.2. **The nature of the support**

The most common supports used industrially for supporting catalysts include alumina, silica, titania, zirconia, magnesia, zinc oxide, zeolites, and carbons [66]. Some of these supports are used in our work for the preparation of supported molybdenum carbides, and thus will be described below. The supports and some of their properties are listed in Table 6.

Table 6 Supports used in this work with the corresponding surface area and PZC [67].

Support	**Phase**	**Surface area (m^2/g)**	**PZC**
TiO_2	Anatase (DT51)	92	5.9
	75% Anatase/25% Rutile (P25)	55	6.3
	Rutile*	10	6
ZrO_2	Monoclinic + tetragonal	129	7

***Not used in this work but mentioned for clarity**

- Titanium dioxide: Titania is largely used as supports in heterogeneous catalysis. One of the most important applications of TiO_2 (anatase) in industrial catalysts is as support for vanadia-tungsta (V_2O_5-WO_3/TiO_2) and vanadia-molybdena (V_2O_5-MoO_3/TiO_2) that are used for the selective catalytic reduction of NO_x to N_2 [66,68].

  There are many forms of titania, such as the tetragonal anatase and rutile forms, the orthorhombic brookite, and the monoclinic TiO_2 (B). Anatase and rutile forms are the most common ones. Rutile structure is the thermodynamically stable phase, but it is reported to be less useful in catalysis than anatase due to its low surface area [66]. Anatase phase transforms to rutile at temperature ≈ 500-1000 °C [69]. This phase transition usually limits the stability of catalysts supported on anatase in reactions that require high temperatures. However, this transition is strongly affected by the species deposed on pure anatase. For example, vanadium and copper oxides tend to favor the transition from anatase to rutile, whereas silicate and molybdate stabilize it, allowing to use anatase supported catalysts at high temperature [66].

  Commercial titania supports may present in pure forms such as anatase or rutile,

or as a mixture of anatase and rutile (e.g. P25 ≈ 75% anatase, 25% rutile) [70]. Titanium oxides are ionic with medium-high Lewis acidity, significant basicity, and weak Brønsted acidity [66].

- Zirconium dioxide: There are three structures of zirconia; each one is thermodynamically stable according to the temperature range. At ambient temperature, the form is monoclinic zirconia, at temperatures around 1100°C, the conversion from a monoclinic to a tetragonal structure is observed, followed by another transformation at about 2300°C from tetragonal to cubic [71]. Zirconia is also ionic and possesses characteristics similar to titania: medium Lewis acidity, significant surface basicity and very low Brønsted acidity [66].

  Zirconium oxide is reported to be a promising support for high temperature catalytic applications such as methane catalytic partial oxidation and catalytic combustion [72]. However its use for industrial catalysts is hindered by the cost and instability due to phase transformation.

I.4.3.3. **Preparation procedure**

To prepare supported interstitial alloys many ways of synthesis can be used. The choice of the preparation method depends on the nature of support and the desired material phase. The most common method used to achieve deposition of the active component precursor on a support is impregnation.

Impregnation is divided in two main ways [73,74]:

- Incipient wetness (also called dry impregnation, or capillary impregnation): The volume of the solution containing the precursor is equal to the pore volume of the support, so that at the end of the operation no excess solution remains outside of the pores [7,71]. Water is usually the solvent for inorganic salt precursors because of their high solubility in it.
- Diffusion impregnation (which is the classical wet impregnation): The volume of the precursor solution is in excess. The precursor salt migrates progressively from the solution into the heart of the grains of the support.

The impregnation method is chosen according to the catalyst case. Incipient wetness

impregnation is advantageous as no water is wasted during the preparation. Moreover, it is faster, and the loss of active precursor can be prevented fairly easily. However, when high loadings are required, incipient wetness impregnation is more difficult. The solubility of the precursor has to be sufficiently high to allow dissolving the required amount of the active component or its precursor in a volume of liquid equal to the pore volume of the support [7,65]. Consequently multiple impregnations are required to achieve the desired loading of the active component [21], and thus wet impregnation can be advantageous in this case. As we will be working with 10-12% w/w loading of molybdenum, the second method will be used.

The main factors which affect the interaction of the species in solution with the support are [7,65]:

- The pH of the solution
- The nature of the metal complex in solution, which depends on the pH and concentration of the metal in solution (e.g. Figure 3)[75,76].

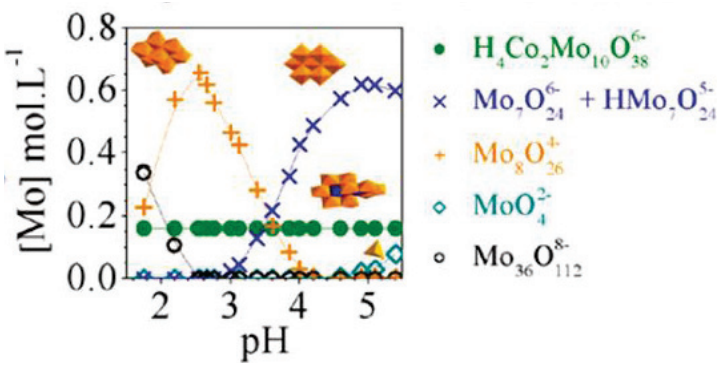

Figure 3 Variation of molybdate species as function of molybdenum concentration and pH [75].

- The point of zero charge of the support (PZC, pH at which the surface of the material has a net zero charge) [67,77]. The surface of oxide support is usually covered with hydroxyl groups, at the contact with water (during the impregnation step), these groups can behave as Brønsted acids or bases

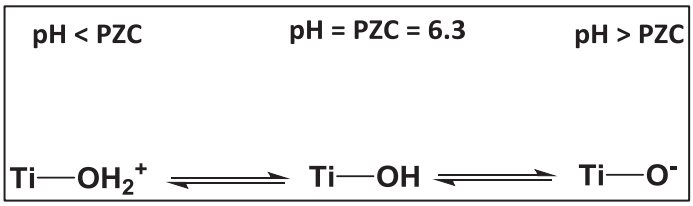

Scheme 2 Variation of surface of titanium oxide as function of pH of the solution

(according to the pH range) by exchanging a proton with the liquid solution, which gives them the ability to interact with many types of metal precursors [71].

Scheme 2 is an example of TiO_2 (P25) which is used in our work, the PZC is around 6.3 [40]. Under the PZC (when pH < 6.3) the surface will be positively charged, while it will be negatively charged above the PZC (pH > 6.3).

After preparing the supported metal precursor, the material is transformed into TMCs using TPRC method which is detailed in the previous part (Section I.4.2).

I.4.4. **Characterization techniques for TMCs catalysts**

The most significant characterizations that are necessary for the metal carbides are those that give information about the success of the carburization process.

The metal and carbon contents are usually obtained by inductively coupled plasma (ICP) and carbon elemental analysis, respectively.

X-ray diffraction (XRD) analysis is usually used to confirm the absence of the metal oxide species and the presence of the metal carbide phases; it also indicates the crystallographic structure of these phases [45,78]. While this task is easily done for bulk carbides, it becomes more complicated for the supported ones. Indeed, in many cases - according to the nature of the support and the percentage of the metal used and the size of the particles- it might not be possible to observe the peaks attributed to the carbide phase due to an overlap with the peaks of the support or high dispersion, as reported for Mo_2C/Al_2O_3 [58,79] and Mo_2C/TiO_2 [60]. Accordingly, other characterizations are indispensable especially in the case of supported metal carbides.

X-ray photoelectron spectroscopy (XPS) is an effective way of analysis for TMCs where the oxidation states of the metal and the surface chemical composition provide evidence about the reduction of the metal oxide precursor and the presence of carbidic carbon. This analysis is even more efficient if performed on non-passivated material where the state of the reduced metal can be clearly identified in the absence of the oxide layer on the surface [78,80].

Transmission electron microscopy (TEM) and scanning transmission electron microscopy (STEM) are also common analyses performed on these materials to have

information on the particles sizes, dispersion, and the phase of the metal carbide [81].

Further characterizations are in common with other catalytic materials such as BET surface area measurement, CO chemisorption, theromogravimetric analysis, TPD, Raman spectroscopy and others.

II. Succinic acid building block: production and valorization

The worldwide concerns about the sustainable production of fuels and chemicals, combined with the diminishing fossil resources, urged the development of environmentally friendly processes for the production of valuable chemicals based on renewable raw materials. The best path to accomplish this goal is to develop biorefinery where carbohydrates, oil, lignin, and other materials are extracted from biomass and converted to fuel, power, heat, and value-added chemicals [82,83].

A report by the Department of Energy of the United States in 2004 classified the top value added chemicals from biomass. The report included a list of twelve compounds that should constitute a basis for the transition from oil components to renewable resources. The topmost building block in this list is succinic acid along with the 1,4-diacids [84]. Succinic acid (SA) is a broadly investigated C4-dicarboxylic acid.

In this part, a quick review of the production routes of SA is presented. More importantly, the valorization strategies of SA -principally its hydrogenation- are discussed. The later part includes a review of the catalysts used in the literature for SA hydrogenation reaction.

II.1. Production of SA

SA market was relatively small in the past, where the annual world production in 1990 was around 17,000 metric tons. Traditional applications of SA include food additives, pharmaceutical intermediates, detergents, and cosmetics [85]. A review of the literature dealing with SA production shows two sources: petrochemical, and renewable resources via fermentation [85–89].

The potential of converting succinic acid to a variety of industrial chemicals that have

very large markets, along with the diminishing oil supplies and increasing oil prices led to a greater attention to the production of succinic acid from renewable feedstocks [82,84,85]. The production of SA has increased significantly in the last few years, as

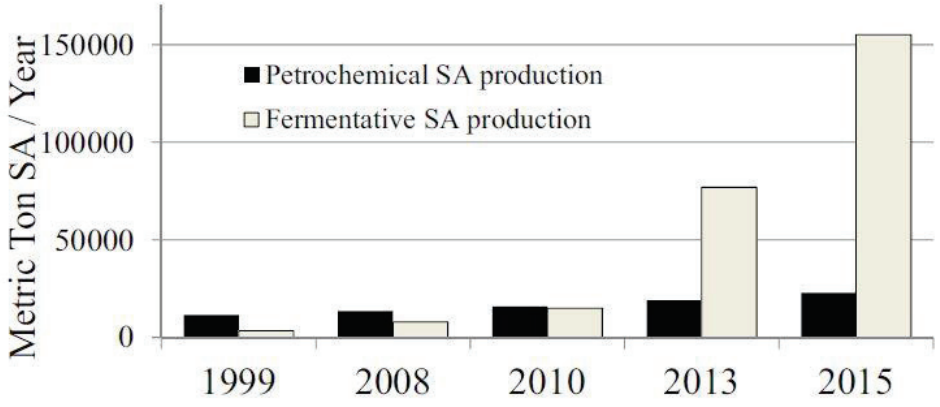

Figure 4 Evolution of the worldwide succinic acid production: petrochemical versus fermentative routes [86].

shown in Figure 4. This is due to an increase of its production by fermentative pathway compared to a nearly stable production from petrochemical route [86].

II.1.1. **Production of SA via petrochemical route**

The catalytic hydrogenation of the fossil-based maleic anhydride used to be the conventional industrial route for SA production. The two-step process (Scheme 3 Petrochemical route for succinic acid production from maleic anhydride) takes place in liquid phase at temperature in the range 120-180 °C under 5 to 40 bar of H_2, and using Ni or Pd based catalyst [86]. The obtained succinic anhydride is hydrolyzed in hot water to obtain succinic acid which is then separated by crystallization, filtering, and drying.

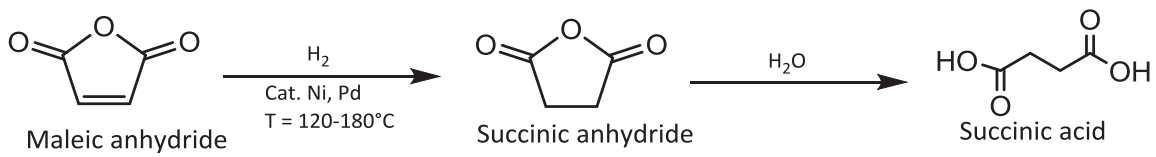

Scheme 3 Petrochemical route for succinic acid production from maleic anhydride [86].

II.1.2. **Production of SA by fermentation of sugars**

Succinic acid can be produced from renewable resources by fermentation of the abundant sugars in plant biomass (i.e., glucose, fructose, arabinose, and xylose). Glucose

is the most commonly used substrate for work related to industrially-relevant fermentations [90]. The fermentation is done using different strains of bacteria such as *Anaerobiospirillum succiniciproducens*, *Actinobacillus succigogenes, Mannheimia succiniciproducens* and genetically engineered *Escherichia coli* [85–88,90–92].

$$7\ C_6H_{12}O_6 + 6\ CO_2 \longrightarrow 12\ C_4H_6O_4 + 6\ H_2O \qquad \text{Equation 1}$$

Glucose — Succinic acid

Theoretically, ≈ 1.71 mol succinate can be produced per mol of glucose (plus CO_2) (Equation 1).

Plants for the commercial production of bio-SA emerged recently. There are four main companies: Reverdia (2012- Italy), PTTGC Innovation America (2005- United States), Succinity (2014- Spain), and BioAmber (2015- Canada). The latter two companies are not running currently. BioAmber had a demonstration unit in France for about five years before their opening in Canada and they were the first to market bio-SA with significant quantities [89]. However, in May 2018 they declared bankrupt due to the lack of investors to scale up. A few months later, in October 2018, it was supposed to be taken by Visolis and LCY Biotechnology-Taiwan [93].

It has been estimated that the global SA market would steadily grow at a compound annual growth rate around 27% and reach 768 million tons in 2025 at $2.3/kg [85] mainly due to the growth of Bio-SA as aforementioned. Interestingly, the cost of production of bio-based SA (BioAmber) is lower than that of the petrochemical one when the oil price is above $30 per barrel [89].

II.2. **Valorization of succinic acid**

With diminishing petroleum resources, increasing energy prices, and environmental concerns, the development of biorefinery processes is indispensable. As already discussed, SA is one of the promising platform molecules to replace the petrochemical C4 platforms. On one hand, a significant part of SA market is for the production of bio-based polymers such as polybutylene succinate [87]. On the other hand, it can be a precursor for a wide variety of chemical products and fuels (Scheme 4).

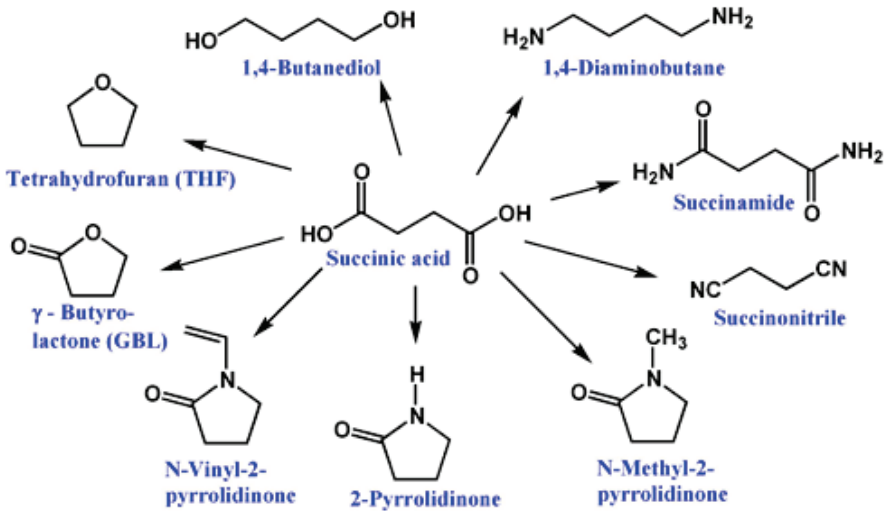

Scheme 4 Succinic acid valorization to various chemicals [90].

SA can be converted catalytically through three routes:

- Hydrogenation
- Reductive amination
- Esterification

In this project, we are mainly interested in the hydrogenation of SA that will be developed in the following part.

II.2.1. **Catalytic hydrogenation of SA**

The catalytic hydrogenation of SA is the most investigated conversion route so far. SA can be hydrogenated to valuable products as shown in Scheme 5.

In the literature [87,94–96], the main target products from SA hydrogenation are:

- γ-butyrolactone (GBL): used as an intermediate for the production of other chemicals and polymer synthesis, and as a solvent.
- 1,4-butanediol (BDO): mainly used as intermediate for polymer synthesis.
- Tetrahydrofuran (THF): used as solvent, as well as an intermediate for polymer synthesis.

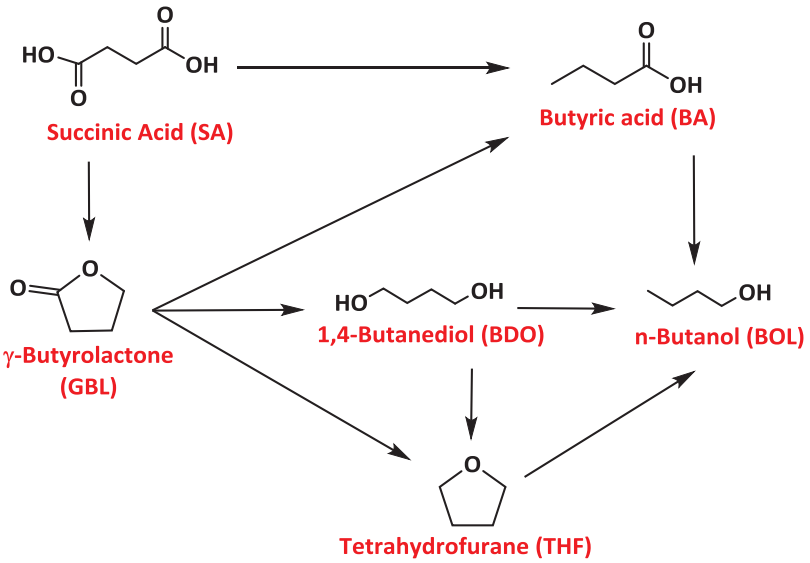

Scheme 5 General reaction route for succinic acid hydrogenation [96,98,110].

Other products may be formed such as butanol, butyric acid, propionic acid, and acetic acid.

It is expected that by 2020, one-third of SA produced will be used for the production of GBL, BDO, and THF [87]. These products are usually prepared by hydrogenation of maleic acid in organic solvents using heterogeneous metal catalysts.

The hydrogenation of carboxylic acid is a hard reaction that requires vigorous conditions [97], thus high temperature and pressure are common conditions among the literature on this reaction. In the following part, the hydrogenation in organic solvents will be presented briefly, and a more detailed discussion will be given on the aqueous phase hydrogenation process.

II.2.1.1. **Hydrogenation of SA in organic phase**

1,4-dioxane is the most common organic solvent used as reaction medium for the hydrogenation of SA and its derivatives. Table 7 shows some of the work reported in the literature on SA hydrogenation in dioxane. This is a two steps reaction: the first one is the formation of GBL, which is then converted to BDO and THF. Over hydrogenation leads mainly to butanol.

Table 7 Succinic acid hydrogenation in dioxane

Entry	Catalyst	T (°C)	P (bar)	Products selectivity[a] (%)	Ref.
1[b]	1%Ru-Co	250	103	GBL (80), BDO (11) + THF, propanol	[98]
2[c]	1%Pd-0.5%Sn/SiO_2	240	50	GBL (75)	[99]
3	1%Pd/γ-AlOOH	240	60	GBL (94)	[100]
4	0.3Re-0.3Ru[d]/MC[e]	200	80	BDO (71), GBL (18), THF (11)	[101]
5	Ru-C	240	80	THF (46), GBL (20) + BA, propionic acid	[102]

[a]: At 93-100 % conversion, [b]: 15/1 dioxane/water solvent, [c]: Succinic anhydride substrate, [d]: molar ratio, [e]: mesoporous carbon.

Most studies focus on hydrogenation of SA to GBL over precious metals such as Ru-Co (entry 1), Pd-Sn/SiO_2 (entry 2), and Pd/ γ-AlOOH catalysts (entry 3). All these catalysts were active in this reaction (93-100% conversion) and selective to GBL (75-94%) [98–100,103]. Others focus on the formation of BDO or THF. For example the reaction over Re-Ru/mesoporous carbon produces BDO with 71% selectivity, and the catalyst was found to be stable and reusable under the employed conditions (entry 4) [101]. Ru-C catalyst is also capable of converting SA to THF at higher temperature, and the yield of THF increased (up to 46%) with decreasing Ru particle size. The catalyst was stable and reusable for this reaction (entry 5) [102].

These reports are limited to organic solvent which means that they are useful in the case of the hydrogenation of readily purified SA. Nevertheless, among the challenges of the industrial production of SA from renewable resources is the cost of purification, since the fermentation process generates diluted aqueous solutions of the product. Additional efforts on the integration of bio-SA production process include the direct catalytic conversion of SA in the aqueous fermentation broth to produce valuable products without the need to isolate pure SA. The process costs can be then reduced significantly [87]. For these reasons, recent researches focus on the development of the process in aqueous phase. Furthermore, this enables the use of an abundant and non-toxic solvent that is a greener alternative to organic solvents, and thus lowers the environmental impact of the process.

II.2.1.2. **Aqueous phase hydrogenation of succinic acid**

As aforementioned, for an economically and environmentally viable valorization of bio-SA, aqueous medium is required. Thus, the catalysts should be active for this reaction and stable under hydrothermal conditions.

a) Catalysts employed for the hydrogenation of SA in aqueous phase

Various heterogeneous catalysts have been examined for the hydrogenation of SA in aqueous medium. The most active catalysts so far are those containing group 8-10 metals (monometallic, bimetallic, or trimetallic) supported either on carbon or on oxides. Moreover the catalytic activity for SA hydrogenation increases with metal dispersion, as shown for Pd/TiO_2 catalysts [104]. The choice of the metal is crucial as the activity and selectivity to the products varies according to the metal used. Many combinations have been studied in the literature; the most significant results are summarized in Table 8.

Table 8 Succinic acid hydrogenation in aqueous phase

Entry	Catalyst	T (°C)	P (bar)	Products selectivity[a] (%)			Ref.
				GBL	BDO	THF	
1	2.1%Pd/TiO_2	160	150	94			[105]
2	0.2%Pd/ZrO_2	200	100	95[b]			[106]
3	2.5%$Pd/5\%ZrO_2/C$	225	170	92			[107]
4	3.4%Re-2.2%Pd/TiO_2	160	150	-	83		[105]
5	4%Re-2%Pd/C	160	150		62		[108]
6	3%Pd-5%FeO_x/C	200	50	10	70	10	[109]
7	Ru-Sn/AC	180	100	-	82		[110]
8	2%Pd-3.4%Re/C	240	150	10	4	70	[111]

[a] at full conversion except in entry 2. [b] at 63% conversion.

Besson et al. evaluated monometallic and bimetallic catalysts in a series of publications on the aqueous-phase hydrogenation of SA [105,108,112,113]. The monometallic 2.1 wt. % Pd/TiO_2 catalyst leads selectively to GBL (94%) (Entry 1); whereas after addition of Re, the bimetallic catalyst 3.4%Re-2.2%Pd/TiO_2 was able to hydrogenate GBL selectively to

BDO (83%) (Entry 4).

Liang et al. reported the aqueous-phase hydrogenation of SA to GBL and THF using Pd/C, Re/C, and bimetallic Pd-Re/C catalysts with different Re/Pd ratios. The bimetallic catalysts exhibited superior activity to the monometallic ones. Pd/C catalyst was selective to GBL (96% at 10 h) and had limited activity for its further hydrogenation to THF. Whereas Re/C catalyst exhibited high selectivity to GBL at first (90% at 2 h), but then it was capable of converting GBL to THF (42% GBL and 39% THF at 10 h). For the bimetallic catalysts, it was found that the addition of a small amount of Re could enhance the hydrogenation activity and improve the yield of GBL in the order: Pd/C < PdRe0.3/C = PdRe0.6/C < PdRe1.1/C. The yield of THF could be increased up to 70% with higher amount of Re (Table 8, entry 8) [111].

It seems that the monometallic catalysts gave high selectivity to GBL, while the formation of THF and BDO was more significant over the bimetallic catalysts.

As previously mentioned, the conditions used in literature for performing this reaction are always harsh. For example, 170 bar and 225 °C were needed to accomplish this reaction over 2.5%Pd/5%ZrO_2/C that gives GBL in high selectivity (92%) (entry 3) [107]. Moreover a high metal loading such as 3.4%Re-2.2%Pd/TiO_2 was used to generate high selectivity (83%) of BDO (entry 4) [105].

An evolution in this reaction can be observed upon comparing the process throughout the years. Optimization of the process includes attempts towards a) using milder conditions, b) reducing the loading of the metals, and c) enhancing the stability of the catalysts under hydrothermal conditions.

Some reports reveal the attempts in using relatively milder conditions for this reaction, though high temperature and pressure are still used. Minh et al. used 4wt%Re-2wt%Pd catalyst supported on carbon at 180 °C and 150 bar. SA was fully converted after 22h with a BDO selectivity of 44%, but with important carbon loss (24%). Full conversion under milder conditions (at 160 °C, entry 5) was also reached but longer reaction time was required such that after 51 h, 62% of BDO was obtained and the carbon loss was lower (15%) [108].

Liu et al., also reported the use of FeO_x to promote Pd/C catalysts using lower H_2 pressure (50 bar H_2, 200°C, for 20 h). The final product was BDO, with 70% yield (entry 6) [109]. However, the stability of the catalysts was not satisfying in the present hydrothermal conditions due to the growth in the size of Pd particles and leaching of Fe.

In a study by Qi et al., different loadings of Pd/ZrO_2 catalysts were tested for SA hydrogenation reaction. They reported interesting results where they proved the activity and stability of 0.2%wt Pd/ZrO_2 catalyst. The catalyst gave GBL with 95% selectivity at 63 % conversion (entry 2). However, the full conversion was obtained over 1% wt. Pd/ZrO_2 catalyst with 85% selectivity to GBL [106].

The stability of heterogeneous catalysts is a challenging issue under the harsh conditions needed for the hydrogenation of SA. Many factors can lead to a decrease of the activity of the catalyst such as: leaching of the active metal, sintering of the metal particles, oxidation of the catalyst in water solvent, in addition to deposition/formation of coke.

In the case of noble metals the leaching of active metal species is one cause of deactivation, though, a resistance to leaching was found in the case of bimetallic catalysts such as the example of Re-Ru/MC catalyst reported by Kang et al. This was attributed to the strong interaction between Re–Ru metals that suppresses leaching of metal species [101].

Beckham et al., obtained 82% of BDO at 180 °C and 100 bar over Ru-Sn/AC in batch reactor (entry 7) [110]. They reported that leaching of metal from the stainless steel reactor occurred when they performed SA hydrogenation reaction in continuous reactor. They then coated the reactor tube with silica by chemical vapor deposition (CVD) to form an inert barrier to the aqueous acid feed and stable catalyst activity was observed for 84 h.

b) Reaction pathway

The reaction pathway for the hydrogenation of SA is presented in Scheme 5. GBL is formed as intermediate through hydrogenation and dehydration of SA [113]. Dehydration reactions are usually favored on acid sites while hydrogenation is favored on metal sites. BDO is formed by further ring opening and hydrogenation of GBL. This

might be due to the simultaneous activation of both oxygen atoms of GBL, as it has been proposed over Re-Pd/TiO_2 [113]. THF can be formed by dehydration of BDO in the presence of acid catalysts or from dehydration-hydrogenation of GBL [114,115].

The direct hydrogenation of the carbonyl group of GBL is more likely in water. BOL, n-propanol, BA and propionic acid can be formed as further by-products. It was proposed that BA and propionic acid are formed from SA or GBL, while BOL and propanol are formed by hydrogenation of BDO or the monoacids (Scheme 5) [115]. BOL is usually obtained from further hydrogenolysis of BDO, favored by acid sites [116]. It can generate n-propanol by C-C bond cleavage [111], e.g. over Re [115]. In a series of publications, Liang and co-workers [111,115,117] investigated the reaction pathway of the aqueous hydrogenation of SA over Pd/C, Re/C, Ru/C, Re-Ru/C and Pd-Re/C, at 240 °C and under 80 bar H_2. Starting from GBL, high selectivity towards THF was observed over Re/C, while a mixture of BDO and THF was obtained over Re-Ru/C. Starting from BA, 100% selectivity towards BOL was observed, over all the catalysts. The conversion of BDO generated mainly THF over Re/C, while propanol was also formed in the presence of Ru based catalyst. The conversion of THF was negligible.

II.2.1.3. **Promising hydrogenation of biomass derivatives by non-noble catalysts**

Despite the good activity and selectivity observed in the aforementioned reports, noble metals are scarce and there are growing concerns about future supply, availability and increasing price, in particular for metals such as Ru, Pd, Pt and Re.

For an economically viable valorization of biomass derivatives, it would be interesting to replace group 8 to 10 metals. To the best of our knowledge, there is no reported work on the hydrogenation of succinic acid with a catalyst that does not contain any precious metal.

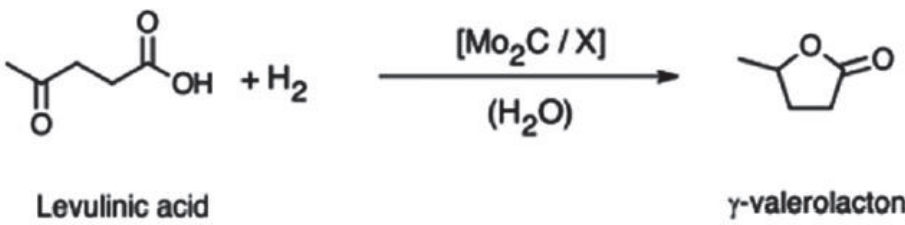

Scheme 6 Reaction pathway for LA hydrogenation to GVL. X: activated carbon or carbon nanotubes [41].

Nevertheless, as we mentioned in part I.3.1.4., Teixeira da Silva et al., used molybdenum carbide based catalysts for the hydrogenation of levulinic acid (Scheme 6) that is classified among the platform molecules along with succinic acid [41,118].

Although this reaction includes the hydrogenation of keto group which is easier than the carboxylic hydrogenation, these results make the use of transition metal carbides promising for the hydrogenation of succinic acid. This is the focus of Chapters 3 and 4 in our work.

III. Carbon dioxide as C1-building block

In the past century, the emission of carbon dioxide (CO_2) has been constantly increasing and contributing to the increase in global temperatures and climate changes due to the ‘‘greenhouse effect’’ [119,120]. Reducing CO_2 is a wide task; mainly, there are three possible strategies for this aim:

- Reduction of the amount of CO_2 produced: this requires switching from fossil fuels energy sources to renewable energy.
- Storage of CO_2: involves the development of new technologies for capturing CO_2 which is now considered an applicable process.
- Valorization of CO_2: using it in promising application areas, or converting it to industrially useful molecules.

In this work we are interested in converting CO_2 to valuable chemicals, as it is considered to be more attractive than storage if economically viable processes are developed [121]. Indeed, fulfilling the world’s growing energy demand and switching to a sustainable supply of raw materials are two of the major challenges nowadays. The catalytic transformation of carbon dioxide (CO_2) as a C1 building block is one of the promising routes which has been investigated by chemists for a long time [122–124]. However there is still a continuing requirement to develop new processes based on the CO_2 molecule. Indeed, the use of CO_2 as a chemical feedstock in current industrial processes is still limited to synthesis of urea and its derivatives, carbonates, salicylic acid, and in the production of methanol from natural gas or coal [119,123]. This limitation is mainly due to the thermodynamic stability of CO_2 [119].

III.1. Thermodynamical considerations for CO_2 conversion

Carbon dioxide molecule is linear, centro-symmetric, and has two polar bonds between the electrophilic carbon and the nucleophilic oxygen atoms [121]. Due to the stability of CO_2, a large amount of energy is necessary for its transformation. Research has proved that CO_2 reduction can be performed via photocatalysis, electrocatalysis, thermo catalysis, or combined approaches such as photo-electrocatalysis or photo-thermo catalysis [121,125–127].

When focusing on the use of CO_2 as a C1-building block, three major challenges can be pointed out on the way to industrial implementation (Scheme 7) [127]:

- Identifying industrially relevant target molecules and directing technological developments towards the promising application areas.
- Developing new catalysts: highly efficient catalysts are required due to the thermodynamic stability and low reactivity of the CO_2 molecule.
- Addressing energetic limitations: when using CO_2 as C1-building block in the chemical industry, a high-energy reactant can be used to overcome the high energy barriers and drive the chemical reactions towards low energy products.

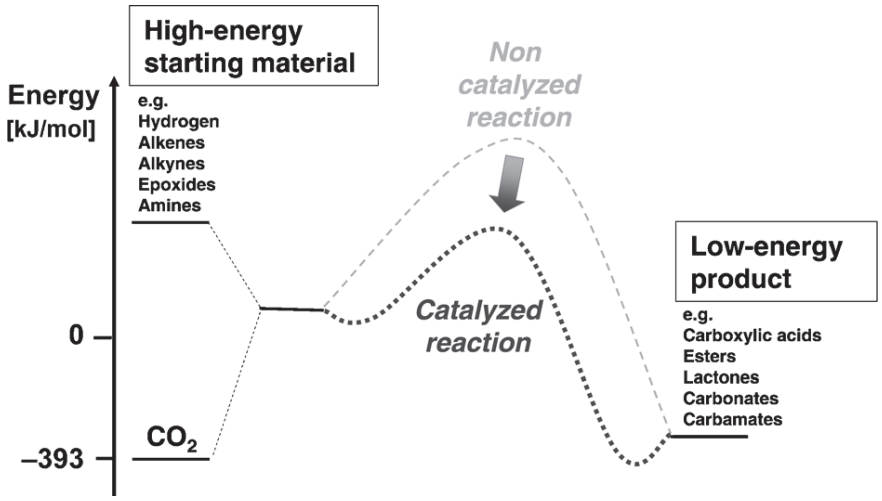

Scheme 7 simplified general schematic illustration of the energy balance of CO_2 transformation with energy-rich reactants [127].

Hydrogen is a high energy material that can be used for CO_2 transformation [120]. Evidently, the activation of CO_2 can only be done using catalysts and requires in many cases some additional energy source. The catalytic hydrogenation of CO_2 can be done

over homogeneous or heterogeneous catalysts. Heterogeneous catalysts dominate the industrial processes because of their advantages in the separation and recyclability and their applicability in flow reaction systems [121].

In view of that, we focus on the development of novel heterogeneous catalysts for the catalytic hydrogenation of CO_2 to C1 chemicals

III.2. Hydrogenation of CO_2 to C1 chemicals

With the employment of carbon capture technologies, CO_2 is considered an economically attractive renewable resource, available in huge quantities at acceptable purity, and a cheap C1 building block. By using a small fraction of this huge stream as raw material for chemical synthetic applications, waste CO_2 might turn into a valuable feedstock [122].

The hydrogenation of CO_2 generates products which can be used as raw materials, energy storage media, intermediates in many chemical industries or upgraded to fuels [119,120].

The target products currently investigated in the literature include carbon monoxide, methane, methanol, ethanol and higher alcohols, hydrocarbons, dimethyl ether, formic acid and formamides (Scheme 8).

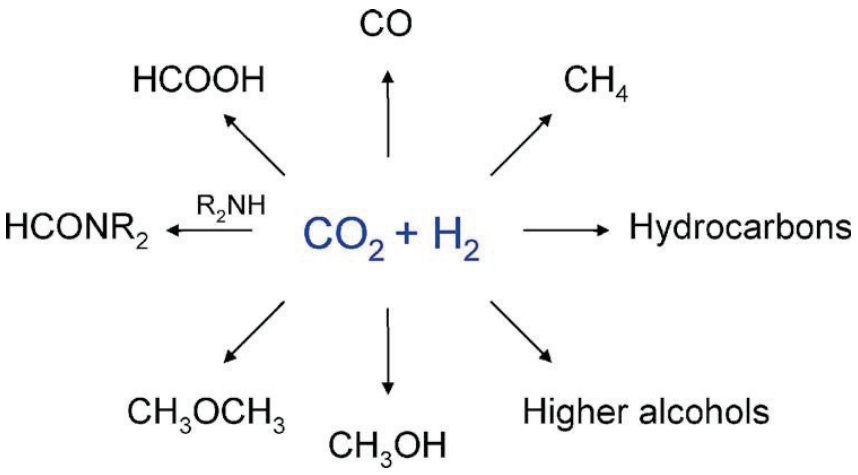

Scheme 8 Possible products obtained from CO_2 hydrogenation [119]

The scale up of CO_2 hydrogenation to industrial levels still lacks satisfactory catalysts (with desirable cost, activity, selectivity, stability, reusability, and handling), efficient and economic reactor design, and the availability of hydrogen [119].

In this part, some reactions according to our interest will be developed in more details. However the literature dealing with the hydrogenation of CO_2 is really abundant and only a couple of results will be presented and discussed.

III.2.1. **Synthesis of carbon monoxide (CO):**

Catalytic conversion of CO_2 to CO via reverse water-gas shift (RWGS) reaction is one of the most promising processes for CO_2 conversion.

Due to the importance of this reaction, the design and characterization of RWGS catalysts have attracted considerable attention [128]. CO is a valuable precursor molecule that can be used for methanol synthesis and for the production of longer-chain hydrocarbons via the Fischer-Tropsch process [129,130].

RWGS reaction is an endothermic reaction, and thus high temperature would facilitate the formation of CO (200–600°C) (Equation 2) [124].

$$CO_2 + H_2 \rightleftharpoons CO + H_2O \qquad \Delta H_{25°C} = 41.2 \text{ kJ/mol} \qquad \text{Equation 2}$$

Copper-based catalysts are among the most popular catalytic systems for WGS reaction, and thus may be also applied to the reverse reaction (RWGS) [119]. Liu et al. developed a series of bimetallic Cu-Ni/γ-Al_2O_3 catalysts for CO_2 hydrogenation. As shown in Table 9 (entry 1), the reaction under atmospheric pressure and 500 °C produced CO with 75% selectivity at 23% conversion. They found that the ratio of Cu/Ni has a significant effect on conversion and selectivity. Cu favored CO formation, while Ni was active for CH_4 production [131].

On the other hand, Wang et al. showed that when Ni is supported on ceria, it was a very active catalyst (42% conversion) and fully selective to CO at 600 °C and atmospheric pressure (entry 2) [132].

Table 9 Examples of results reported in the literature for CO_2 hydrogenation to CO

Entry	Catalyst	T (°C)	P (bar)	CO_2 Conversion (%)	CO selectivity (%)	Ref.
1	Cu-Ni/ γ-Al_2O_3	500	1	23	75	[131]
2	Ni/CeO_2	600	1	42	99.6	[132]
3	Pd/SiO_2	450	1	40.8	89	[133]
4	Pt/SiO_2	280	1	2.0	100	[134]
5	Fe/TiO_2	270	20	2.6	73	[135]
6	Mo/γ-Al_2O_3	600	1	34.2	97	[136]

Besides, various metals such as Fe, Mo, as well as precious metals such as Pt and Pd were reported to be also active towards the production of CO as shown in Table 9. Usually these metals are supported on oxides, and their activity and selectivity were found to be influenced by the metal dispersion, the nature of the oxide support, and obviously the nature of the metal itself.

III.2.2. **Methanation reaction**

Catalytic hydrogenation of CO_2 to methane is an important catalytic process for CO_2 valorization [137]. Generally, methane is available from natural gas; however, the attempts for reducing the use of fossil energy resources gave more attention to its production from sustainable resources [124]. Furthermore, methanation of CO_2 has gained increasing attention through the "power to gas" approach used for energy storage. Throughout this concept, the intermittent renewable energies such as wind and solar radiation are used to power water electrocatalysis, generating H_2. The reaction of the produced H_2 with effluent CO_2 can be subsequently done and the produced methane itself can be stored in classical natural gas infrastructures and be used on demand [138,139].

$$CO_2 + 4H_2 \rightleftharpoons CH_4 + 2H_2O \qquad \Delta H_{25°C} = -252.9 \text{ kJ/mol} \qquad \text{Equation 3}$$

Methanation reaction is an exothermic process (Equation 3). Nickel catalysts supported on oxides are the most widely studied materials for this reaction (Sabatier reaction); though, one of major problems with Ni-based catalysts is the deactivation due to carbon deposition and sintering of nickel [137]. Alternatively, noble metals (e.g. Ru, Pd, or Rh) supported on various oxides (e.g., SiO_2, TiO_2, Al_2O_3, and CeO_2) are considered stable and more efficient for methanation than nickel (Table 10); nevertheless they are more expensive.

Table 10 Some of the catalysts reported in the literature for CO_2 hydrogenation to CH_4

Entry	Catalyst	T (°C)	P (bar)	CO_2 Conversion (%)	CH_4 selectivity (%)	Ref.
1	Ni/SiO_2	450	1	36.8	81.8	[133]
2	Ni/Al_2O_3	250	1	39	97	[140]
3	Ni/CeO_2	450	1	80	100	[141]
4	$Rh/\gamma\text{-}Al_2O_3$	200	1	98	100	[142]
5	$Ru/CeO_2/Al_2O_3$	250	1	20	100	[143]
6	$Pd\text{-}Mg/SiO_2$	450	1	59.2	95.3	[133]
7	Rh/TiO_2	270	20	7.9	72.7	[135]

III.2.3. **Synthesis of methanol (CH_3OH)**

For several years, a great interest has been brought to the synthesis of methanol from the catalytic conversion of CO_2. Methanol is a common solvent that can replace fuels and serve as a raw material in chemical industries [134].

Today, most of the methanol produced is synthesized from syngas, i.e. through CO hydrogenation [144]. An alternative feedstock is CO_2, where methanol can be produced either via CO_2 conversion to CO (RWGS) and subsequent hydrogenation of CO, or by the direct hydrogenation of CO_2 [119,120,145].

$$CO_2 + 3H_2 \rightleftharpoons CH_3OH + H_2O \quad \Delta H_{25°C} = -49.5\ kJ/mol \qquad \text{Equation 4}$$

Conversion of CO_2 to methanol is an exothermic reversible reaction and involves decreasing in the number of moles of products with respect to reactants (Equation 4). According to Le Chatelier principle, decreasing the reaction temperature and increasing the pressure fight against exothermicity and decreasing number of moles respectively, and thus favor the synthesis of methanol [120].

$Cu/ZnO/Al_2O_3$ is currently the commercial catalyst for methanol production from $H_2/CO/CO_2$ [146–148]. Through this process, it is estimated that several million tons of CO_2 are converted into methanol each year [124,149]. However, relatively harsh reaction conditions (220-300°C and 50-100 bar) are used [146,148]. Therefore, the methanol production from CO_2 by direct hydrogenation under mild reaction conditions is still a challenge for researchers and industries.

Aside from the commercial catalyst, continuous work is done to find an active and selective catalyst stable and efficient under milder conditions. The results of selected works on the hydrogenation of CO_2 to methanol are reported in Table 11.

Cu/ZnO remains the most efficient combination. Cu/ZnO interface sites are supposed to be the catalytically active ones, where the synergy between Cu and ZnO was attributed to the formation of CuZn alloy which undergoes surface oxidation during methanol synthesis reaction creating a catalytically active Cu/ZnO interface [129]. Accordingly, this combination is abundant in the literature for methanol synthesis studies (e.g. entries 1,2, and 3 of Table 11) [150–152].

Pd-based catalysts have shown high selectivity for the hydrogenation of CO_2 to methanol. For example, at 250°C and 30 bar, Pd/ZnO supported on carbon nanotubes (CNT) catalyzed methanol formation with 99.6% selectivity at 6.3% conversion of CO_2 (entry 4) [153]. Pd supported on Ga_2O_3 plate (entry 5) also reveals remarkable activity (17.2% conversion) and selectivity to methanol (51.6%) at 50 bar and at 250 °C [154].

Lalev et al. compared two Pd/ZnO catalysts prepared in two different ways and lead to enormous change in the selectivity toward the products. The authors showed that the catalyst prepared by via sol immobilization (entry 6) was selective to methanol (60%) and they referred that to the formation of PdZn alloy nanoparticles with controlled particle size. However, the catalyst prepared via impregnation possessed only metallic Pd

nanoparticles that favored the formation of CO (99%) [155].

Table 11 Some of the catalysts reported for CO_2 hydrogenation to methanol in the literature

Entry	Catalyst	T (°C)	P (bar)	CO_2 Conversion (%)	CH_3OH selectivity (%)	Ref.
1	Cu/ZnO	240	30	16.5	78.2	[150]
2	$Cu/ZnO/ZrO_2$	220	80	21	68	[151]
3	$Cu/ZnO/ZrO_2/Al_2O_3$	230	30	23.2	60.3	[152]
4	Pd/ZnO/CNTs	250	30	6.3	99.6	[153]
5	Pd/Ga_2O_3	250	50	17.3	51.6	[154]
6	Pd/ZnO	250	20	10.7	60	[155]

III.3. **Carbide catalysts for CO_2 hydrogenation**

Recently, TMCs have attracted attention as promising catalysts for the conversion of CO_2 into CO, methanol, methane and other hydrocarbons [56,80,156–163]. They were used as a catalyst alone or as a support for metal nanoparticles.

In a series of publications, Illas and coworkers reported computational and experimental studies that prove the ability of molybdenum carbides to uptake and activate CO_2 [80,156,158,161,162,164–166].

The theoretical calculations showed the high activity of molybdenum carbide surfaces in CO_2 activation, which surpasses that of other transition metal carbide surfaces such as TiC(001) [165].

Combined computational and experimental work showed that the major products of the hydrogenation of CO_2 at 5 bar and 227°C on Mo terminated β-Mo_2C(001) surface were CO, CH_4, and CH_3OH in addition to traces of C_2H_6, CH_3OCH_3, and C_2H_5OH. Mo terminated β-Mo_2C(001) surface partially dissociated CO_2 at low temperature, and the CO produced also can decompose if the temperature is increased, leading to decreased CO and methanol selectivity in favor to methane. On the other hand, a C-terminated β-Mo_2C(001) surface was not strong for CO_2 decomposition, and the ratio CO/CH_4 in the

products significantly increases. δ-MoC(001) possessed similar reactivity to the C-terminated β-Mo_2C(001), RWGS was the main reaction and only CO and CH_3OH were produced [164].

These results show that the metal to carbon ratio is a key parameter to be taken in consideration when evaluating the catalytic performance of TMC catalysts in this reaction.

Rodriguez et al. reported a comparison between cubic MoC_{1-x} and hexagonal Mo_2C catalysts in CO_2 hydrogenation at 250 °C and 20 bar. They showed that Mo_2C had higher activity and selectivity for the methanation reaction (37% at 17% conversion) (Table 12, entry 2); whereas MoC_{1-x} was less active but more selective to CO (51 % at 11% conversion) and methanol (Table 12 entry 1) [56]. The addition of Cu - known to be active in CO_2 hydrogenation and to ameliorate the selectivity to methanol (cf Table 11) - to the Mo_2C system increased CO_2 conversion and increased the amount of methanol (31% at 21% conversion) while decreasing the amount of methane (Table 12 entry 3) [161].

The group of Illas also reported that the hexagonal Mo_2C was an efficient and selective catalyst for CO_2 conversion to CO through the reverse water-gas shift reaction at 400°C and atmospheric pressure. A selectivity superior to 99% towards CO at 16% conversion was obtained (Table 12 entry 4) [162].

Table 12 Molybdenum carbide catalysts reported for CO_2 hydrogenation

Entry	Catalyst	T (°C)	P (bar)	CO_2 Conversion (%)	Products selectivity (%)			Ref.
					CO	CH_3OH	CH_4	
1	MoC_{1-x}	250	20	11	51	23	16	[56]
2	Mo_2C	250	20	17	34	12	37	[56]
3	5% Cu/Mo_2C	250	20	21	38	31	20	[161]
4	Mo_2C	400	1	16	99	-	-	[162]

In the above mentioned studies, the carbides were unsupported, or served themselves as supports for metal particles. In this thesis, we have prepared molybdenum carbide

catalysts supported on two types of TiO_2 and ZrO_2, and evaluated them for the hydrogenation of CO_2 in gas-phase.

IV. **Conclusion**

The literature review shows that molybdenum carbides have catalytic properties similar to noble metal based catalysts. They were mainly used in gas phase reactions, and their use in liquid phase reactions related to biomass is recent. Lately, they started to gain attention to be used for CO_2 hydrogenation.

To the best of our knowledge there is no reported work for the use of molybdenum carbide catalysts in the hydrogenation of succinic acid in aqueous phase, nor oxide-supported molybdenum carbide catalysts for CO_2 hydrogenation in gas phase.

In our work we are interested in synthesizing new catalysts based on molybdenum carbides supported mainly on TiO_2 (P25), and other supports TiO_2 (DT51), and ZrO_2 for comparison purposes. The effects of the synthesis conditions are evaluated by changing the carburizing gas nature (CH_4 or C_2H_6), the percentage of the hydrocarbon in the reaction mixture i.e. % v/v HC/H_2 (5%, 10%, 20% and 40%), the maximum carburizing temperature (600 °C, 700 °C and 800 °C), and the gas space velocity during preparation. The success of the carburization is verified by the analysis techniques XRD, XPS, TEM, ICP, and carbon elemental analysis.

The supported molybdenum carbide catalysts were tested for aqueous phase hydrogenation of succinic acid, and gas phase CO_2 hydrogenation.

The experimental part is presented in Chapter 2. This section includes the description of the equipments, methods and the characterization techniques used to conduct the work.

Chapter 3 shows the synthesis and characterization of a series of supported molybdenum carbide catalysts. The effects of the synthesis conditions are assessed on molybdenum carbide supported on P25 TiO_2 by changing the carburizing gas nature, the percentage of the hydrocarbon in the reaction mixture i.e. % v/v HC/H_2, and the maximum carburizing temperature. TiO_2 (P25), TiO_2 (DT51) and ZrO_2 are evaluated as supports for the catalyst. The influence of the different preparation parameters on the

catalytic response in the hydrogenation of succinic acid in aqueous phase at 240°C and 150 bar are presented.

Chapter 4 includes the optimizations of succinic acid hydrogenation reaction conditions (temperature and pressure) using molybdenum carbide catalyst supported on P25 TiO_2. Further optimization in the preparation parameters of the catalyst (such as the gas hourly space velocity during preparation) is conducted. The stability and reusability of the catalyst are also discussed in this chapter.

The results of testing the molybdenum carbide catalysts for CO_2 hydrogenation reaction in gas phase are presented in Chapter 5. The conditions of the reaction (temperature, pressure, reactants flow, and catalyst loadings) are optimized with P25 TiO_2-supported molybdenum carbide catalyst. The other catalysts based on molybdenum carbide supported on TiO_2 (DT51), and ZrO_2 are also evaluated.

CHAPTER 2.

Experimental Part

I. Preparation of the catalysts

I.1. Materials used for the preparation of the catalysts

All materials used for catalysts preparation are listed in Table 13, they were used as received without any further purification.

Table 13 The materials used in the preparation of the catalysts.

	Compound	Chemical formula	Supplier
Precursor	Ammonium molybdate tetrahydrate (99.98 %)	$(NH_4)_6Mo_7O_{24}.4H_2O$	Sigma Aldrich
Supports	Titanium dioxide P25	TiO_2	Degussa-Evonik
	Titanium dioxide DT51	TiO_2	Cristal
	Zirconium dioxide	ZrO_2	MEL Chemicals
Gases	Methane (99.93 %)	CH_4	Air Liquide France Industrie
	Ethane (99.95 %)	C_2H_6	
	Hydrogen (99.99 %)	H_2	
	Oxygen (00.99 %)/Nitrogen (99.00 %)	1% v/v O_2/N_2	
	Argon (99.99 %)	Ar	

I.2. Preparation of the supported molybdenum oxide by impregnation

The first step is classical wet impregnation. In a 250 mL round bottom flask, the desired amount of $(NH_4)_6Mo_7O_{24}.4H_2O$ precursor was mixed with the support in 60 mL of ultra-pure water. For example, in order to prepare 10% w/w MoC/TiO_2, 1 g of the precursor

and 5 g of the support are used. The suspension was then stirred at 700 rpm for 2 h at room temperature. After that, water was evaporated in a rotavap at 80 °C and 300 mbar, and the solid was dried overnight in an oven at 80 °C under N_2.

In case of preparation of MoO_3/TiO_2, the powder obtained after the above process was calcined under air at 600 °C with 0.5 °C/min heating rate.

I.3. Preparation of molybdenum carbide by temperature programmed reduction-carburization

For the second step, the dried solid was crushed to fine powder and placed in a quartz cell (Scheme 9). The cell was introduced into an oven and connected to a regulator where the heating ramp, maximum temperature, and holding time are defined. The temperature was continuously monitored using a thermocouple inserted in a thermowell close to the catalyst bed.

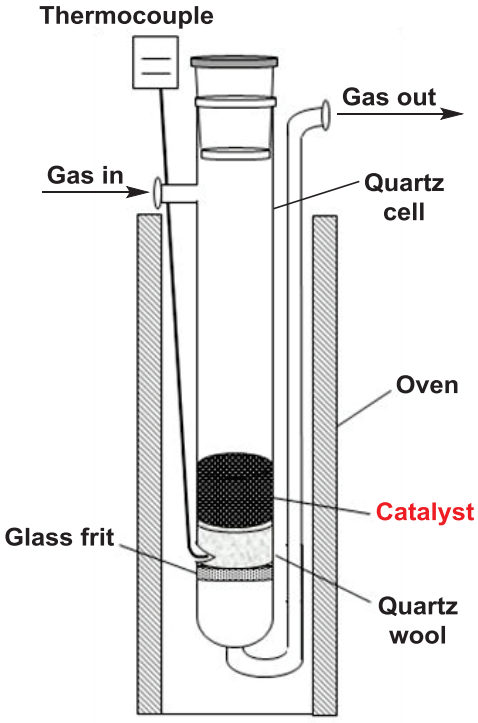

Scheme 9. The set-up used for the reduction-carburization process

A reductive-carburizing gas stream (C_2H_6/H_2 or CH_4/H_2 with different concentrations of hydrocarbon ranging from 5% to 40%) was employed while raising the temperature at 0.5 °C/min till reaching the chosen maximum temperature, which was held constant for 2 h at the maximum point. Then the catalyst was cooled down to room temperature under argon, and finally passivated for 4 h under 1% v/v O_2/N_2 (Scheme 10).

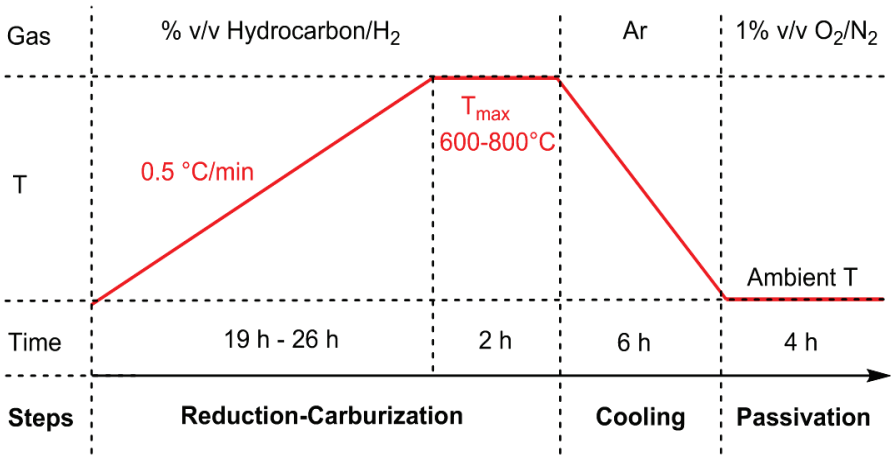

Scheme 10. Second step of the catalyst preparation

The gas hourly space velocity (GHSV) of the reactive gas stream was varied in the range of 1527-7636 h^{-1}. It is defined by the quotient of the entering reactive gas "volumetric flow rate" (60 mL/min was maintained for all the experiments) divided by the catalyst bed volume in the reactor (varied between 1.1 mL and 5.5 mL):

$$\mathrm{GHSV}(\mathrm{h}^{-1}) = \frac{\text{gas flow rate (mL/h)}}{\text{catalyst bed volume (mL)}}$$

II. Characterization of the catalysts

II.1. Elemental analysis

II.1.1. Elemental analysis of molybdenum: Inductively coupled plasma-optical emission spectroscopy (ICP-OES)

The elemental analysis includes identification and quantification of elements in a sample even at trace level. ICP-OES is an analytical technique used for the detection of chemical elements. It is a type of emission spectroscopy that uses the inductively coupled plasma to generate excited atoms and ions, which in turn emit electromagnetic radiation at wavelengths characteristic of a specific element. The intensity of the emission of the thermally excited species is detected and quantified with an optical emission spectrometer. The intensity measurements are converted to elemental concentration by comparison with calibration of standards.

The apparatus was ACTIVA instrument (HORIBA Jobin Yvon). It was used to measure the

concentration of Mo element within the supported molybdenum carbide catalysts, and to detect any presence of the Mo metal in the final solution after the catalytic test, and thus evaluate the possibility of leaching of Mo from the catalyst into the reaction solution.

Prior to the analysis of the catalysts, the samples were mineralized by fusion with lithium tetraborate in Pt-Au crucibles at 1100 °C, and then recovered with 20% HCl. In the case of solution analysis, the remaining solution after the reaction was evaporated in a quartz crucible on a hot plate and then in an oven at 600 °C, recovered with H_2SO_4 + HNO_3, and then analyzed.

II.1.2. **Elemental analysis of carbon and oxygen**

Carbon elemental analysis was conducted via a LECO micro-analyzer SC144. Around 15 mg of the sample was weighed in a tin capsule. After folding the capsule (looking like wrapped tin foil), a specific amount of iron was placed in a ceramic crucible, followed by the sample, and finally tungsten of amount twice that of iron. The sample was transferred into the reactor chamber and the total combustion was done at elevated temperature (1050-1350°C) under the oxygen flow in the horizontal furnace. Carbon is converted to carbon dioxide and quantified by thermal conductivity detector.

Prior to the analysis, three blank analyses were done (empty tin capsules). Then two commercial samples of Mo_2C with known carbon content (5.89%) were measured as reference for the accuracy of the analysis. After that, the samples with unknown amount of carbon were analyzed by batches of 8. Finally, the 2 references were analyzed once again.

The estimation of the uncertainties was done by analyzing references. The estimated error was based on the differences between the theoretical and experimental values obtained for references over the all range for each element. For carbon content between 1 and 30 weight percent, the measurement error is < 0.3%.

Oxygen analysis was done with EMGA 620 W analyzer (HORIBA Jobin Yvon). The system uses fusion in a helium pulse furnace to extract oxygen. The sample falls into a graphite crucible heated to a high temperature between 2500 °C and 2800 °C. Oxygen is converted into carbon monoxide by combining with the carbon of the crucible. CO is measured by a non-dispersive infrared cell, then oxidized to CO_2 and trapped.

II.2. **BET surface area (S)**

The specific surface area of the catalysts were measured based on the principle of physical adsorption of nitrogen gas on the surface of the solid (Brunauer-Emmett-Teller theory). The volume of gas (nitrogen) adsorbed on the surface of the particles is measured at the boiling point of nitrogen (-196 °C). The volume of the adsorbed N_2 gas monolayer V_m can be calculated by plotting $\frac{P}{V_{ads}(P_0-P)} = f\left(\frac{P}{P_0}\right)$ using the BET equation:

$$\frac{P}{V_{ads}(P_0 - P)} = \frac{C-1}{V_m.C} \times \left(\frac{P}{P_0}\right) + \frac{1}{V_m.C}$$

Where:

- P is the pressure at equilibrium
- P_0 is the saturation pressure of adsorbate at the temperature of adsorption
- C is BET constant
- V_{ads} is the volume adsorbed at -196 °C
- V_m is the volume of adsorbed monolayer

The linear relationship of this equation is maintained only in the range of $0.05 < \frac{P}{P_0} < 0.35$. The value of the slope ($\frac{C-1}{V_m.C}$) and the y-intercept ($\frac{1}{V_m.C}$) of the line are used to calculate the monolayer adsorbed gas quantity V_m and the BET constant C. Then, the total surface area of the catalyst is deduced by using the following equation:

$$S = \frac{V_m}{V} \times N_A \times \alpha$$

Where:

- S is the BET surface area (m^2/g)
- V_m is the volume of adsorbed monolayer obtained from the plot (m^3/g)
- V is the molar volume of nitrogen (m^3/mol)
- N_A is Avogadro's number (6.022×10^{23} mol^{-1})
- α is the area occupied by nitrogen molecule (16.2×10^{-20} m^2)

Before the analysis, the catalysts were desorbed at 150 °C for 3 h under ultra-high vacuum (10^{-4} mbar). Then the measurement was done using ASAP 2020 Micromeritics apparatus.

II.3. **X-ray diffraction (XRD)**

X-ray diffraction is primarily used for phase identification of a crystalline material and can provide information on unit cell dimensions. The equipment consists of three basic elements: an X-ray tube, a sample holder, and an X-ray detector. X-rays are generated by a cathode ray tube, filtered to produce monochromatic radiation, and directed towards the sample. The interaction of the incident rays with the sample produces constructive interference and diffracted rays that are collected by the detector. The detector in turns converts them into a series of intensity peaks that form the diffractogram as a function of the angle 2θ if Bragg's law is satisfied as follows:

$$n\lambda = 2d \sin\theta$$

Where:

- n is the order of diffraction line
- λ is the wavelength of the incident beam (Å)
- d is the inter-planar lattice spacing (Å)
- θ is the diffraction angle (degree)

The PXRD patterns of the catalysts were recorded at a detector step of 2 seconds in a measuring range 2θ = 20-80° using a Bruker D8A25 X-ray diffractometer and a CuKα radiation source (λ = 1.54184 Å).

Phase identification, phase quantity, lattice parameters, and mean crystallite sizes of error ± 2 nm (d = 4/3 * LVol-IB; with LVol-IB the volume averaged column height) were obtained by performing Rietveld refinement using Topas 5 software.

The concept of Rietveld refinement method is based on simulating the measured diffractogram of the sample by a crystallographic model pattern, then adjusting the parameters of this model so that the simulated diffractogram is as close as possible to the measured diffractogram. Hence, this method of analysis is only possible when all the phases present in the sample are already known and predicted. The crystal structures reference cards used were taken from the Inorganic Crystal Structure Database (ICSD) and International Center for Diffraction Data (ICDD) as shown in Table 14.

Table 14. The compounds analyzed by Rietveld refinement and their database codes

Compound formula	Crystal system	Space group	Reference code
MoC	Cubic	Fm-3m	618309
MoC	Hexagonal	P63/mmc	156478
MoC	Orthorhombic	Pbcn	1527881
MoO_xC_y	Cubic	Fm-3m	00-017-0104
MoO_3	Monoclinic	P121/m1	80577
MoO_3	Orthorhombic	Pnma	180590
MoO_2	Monoclinic	P121/c1	23722
Mo	Cubic	Im-3m	173131
TiO_2	Anatase, tetragonal	I41/amdz	193269
TiO_2	Rutile, tetragonal	P42/mnm	04-006-1919
Ti_5O_9	Triclinic	P1 (1)	04-007-0523
Ti_4O_7	Triclinic	P1 (2)	04-007-0437
ZrO_2	Tetragonal	P42/nmcz	85322
ZrO_2	Monoclinic	P121/c1	57157

The difference (in the peak width and intensity) is shown under the diffractograms. It is obtained by subtracting the simulated diffractogram from the measured one, so that a

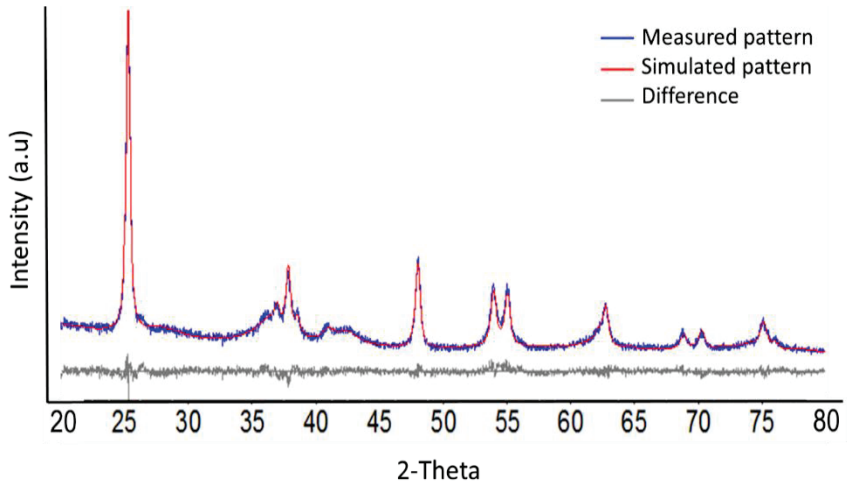

Figure 5. Example of Rietveld refinement of MoC/TiO_2

straight difference curve (only noise) gives evidence about the accuracy of the fitting (e.g. Figure 5).

II.4. Environmental transmission electron microscopy (E-TEM), scanning transmission electron microscopy (STEM), and energy dispersive X-ray (EDX)

Transmission electron microscopy is a technique of analysis that provides morphologic, compositional, and crystallographic information of samples. A beam of energetic electrons is transmitted through an ultra-thin sample. The electrons interact with the sample. The beam then passes through multiple electromagnetic lenses, down the column, and makes contact with the screen where the electrons are converted to light to form a high-resolution, black and white image. The lighter areas of the image represent the places where a greater number of electrons were able to pass through the sample, and the darker areas reflect the dense areas of the sample. These differences provide information on the structure, texture, size, and shape of the material.

In regular TEM, air needs to be pumped out of the chamber to create vacuum space where electrons are able to move. However for E-TEM it is possible to perform the analysis under dynamic temperature conditions (up to 1300 °C) and partial pressure (up to 20 mbar) of gas according to the desired in situ conditions.

Scanning transmission electron microscopy (STEM) operation mode is similar to that of TEM. This technique scans a very finely focused beam of electrons across the sample in a raster pattern. Interactions between the beam electrons and sample atoms generate a serial signal stream, which is correlated with beam position to build a virtual image. Its primary advantage over TEM is enabling the use of other signals that cannot be spatially correlated in TEM, including secondary electrons, scattered beam electrons, characteristic X-rays, and electron energy loss.

TEM and STEM images were obtained using Environmental Transmission Electron Microscope: FTI TITAN E-TEM instrument operated at 80-300 kV, equipped with a X-MAX SDD EDX detector from Oxford-Instrument and a Tridiem ERs GIF from Gatan. It is also equipped with a mass spectrometer and a plasma cleaner. The microscope was used in the regular mode under vacuum. Because of its very high resolution, it permits the detection of elements that are not visible by traditional microscopy. The samples were

prepared by dispersing the solid in ethanol and then depositing them onto carbon-coated copper grids.

An energy dispersive X-ray (EDX) systems connected to TEM instrument was also used. The imaging capability of the microscope identifies the specimen of interest, and the data generated by EDX analysis consist of spectra showing peaks corresponding to the elements and thus verifying the true composition and homogeneity of the analyzed sample.

II.5. **X-ray photoelectron spectroscopy (XPS)**

XPS is a surface-sensitive spectroscopic technique that measures the elemental composition, chemical state, and electronic state of the elements that exist within a material. XPS spectra are obtained by irradiating a material with a beam of X-rays while simultaneously measuring the kinetic energy and number of electrons that escape from the top 0 to 10 nm of the material being analyzed. The kinetic energy of the electron depends upon the photon energy and the binding energy of the electron:

$$KE = h\nu - BE$$

Where:

- KE is the kinetic energy of the ejected electron
- $h\nu$ is the photon energy
- BE is the binding energy which is the energy required to separate the electron from the surface

The XPS spectrum is obtained by plotting the number of photoelectrons emitted as a function of their binding energy.

The surface chemical composition and oxidation states of Mo in catalyst samples were analyzed using a commercial XPS instrument (AXIS Ultra DLD KRATOS) with monochromatized AlKα source (hν = 1486.6 eV). The binding energies (± 0.5 eV) were referred to the C1s line set at BE = 284.6 eV. Peaks decompositions, fittings and quantitative determinations were performed using the Casa XPS and Igor Pro software.

For the analyses of the non-passivated samples that should not be exposed to air, the sample was transferred directly after synthesis to a glovebox equipped with an output

connection dedicated for the XPS handle. The sample was prepared inside the glovebox and then placed in the XPS chamber. There was no contact with oxygen as the samples stayed under argon.

II.6. **Raman spectroscopy**

Raman analysis is a vibrational spectroscopic technique used to provide information on molecular vibrations and crystal structures. This technique uses a laser light source to irradiate the sample, and generates an infinitesimal amount of Raman scattered light. The electromagnetic radiation from the illuminated spot is collected with a lens and sent through a monochromator. Elastic scattered radiation at the wavelength corresponding to the laser line is filtered out while the rest of the collected light is dispersed onto a detector.

Raman spectrum is expressed in a form of intensity of scattered light versus wavenumber (the reciprocal of wavelength, called Raman shift). In order to convert spectral wavelength to wavenumbers of shift in the Raman spectrum, the following formula can be used:

$$\Delta\omega = \left(\frac{1}{\lambda_0} - \frac{1}{\lambda_1}\right)$$

Where:

- $\Delta\omega$: is the Raman shift (The above equation multiplied by 10^7 gives $\Delta\omega$ in cm^{-1})
- λ_0: is the excitation wavelength (nm)
- λ_1: is the Raman spectrum wavelength (nm)

The Raman spectra were recorded at room temperature using a LabRam HR (Jobin Yvon–Horiba) spectrometer equipped with a CCD detector cooled at -76 °C. Measurements were carried out under microscope with a 50x objective that focuses the laser beam on the sample surface and collects the scattered light. The exciting line at 514.53 nm of a Ar+ laser was used with a power limited at 100 µW. It was previously checked that the samples laser heating was negligible with such power. A 300 grooves/mm grating was used to disperse light, leading to band position accuracy within 4 cm^{-1}.

II.7. **Thermogravimetric Analysis coupled with Mass Spectrometry (TGA-MS)**

Thermogravimetric analysis measures the weight loss of a sample over time as the temperature changes under a chosen gas stream. It provides information about physical and chemical phenomena such as desorption, phase transitions, and thermal decomposition as well as solid-gas reactions. Coupling a mass spectrometer to a TGA allows the evolved gases to be analyzed and identified giving additional valuable information about the behavior of the sample under the chosen conditions.

In this work, TGA-MS was done under 50 mL/min flow of 3% v/v H_2/Ar at 5 °C/min up to 650 °C. The mass spectrum of the evolved gas was recorded as a function of temperature, the signals observed were m/z = 17 and 18 corresponding to the formation of water.

III. **Catalytic testing**

All materials used for the hydrogenation reactions are listed in Table 15, they were used as received without any further purification.

Table 15. The materials used for the catalytic tests

	Compound	Chemical formula	Supplier	Purity (%)
Substrates	Succinic acid	$C_4H_6O_4$	Sigma Aldrich	99
	Levulinic acid	$C_5H_8O_3$	Sigma Aldrich	98
Products	γ-butyrolactone	$C_4H_6O_2$	Sigma Aldrich	99
	Butyric acid	$C_4H_8O_2$	Sigma Aldrich	99
	Tetrahydrofuran	C_4H_8O	Carlo Erba	99.5
	1,4-Butanediol	$C_4H_{10}O_2$	Sigma Aldrich	99
	1-Butanol	$C_4H_{10}O$	Carlo Erba	99.5
	Butyl butyrate	$C_8H_{16}O_2$	Sigma Aldrich	98
	γ-valerolactone	$C_5H_8O_2$	Sigma Aldrich	99
Solvents	1,4-Dioxane	$C_4H_8O_2$	Carlo Erba	99.8
	Ethanol	C_2H_6O	Carlo Erba	99.9

	Methanol	CH_4O	Sigma Aldrich	99.9
	Ultrapure water	H_2O	ELGA	18.2 MΩ.cm

III.1. Aqueous phase hydrogenation of SA

III.1.1. Reaction procedure

The aqueous phase hydrogenation experiments were performed using a 300 mL high-pressure batch (Parr 4560) Hastelloy autoclave (Scheme 11) equipped with:

- A stainless steel counter-blade
- A 0-200 bar pressure gauge
- A 200 bar safety rupture disc
- A thermocouple probe sites inside a thermowell in the reactor
- A tube dipping in the reactor with a valve in order to take samples from the liquid solution. A 8 µm Hastelloy filter is connected to its end to allow the sampling while keeping the catalyst behind
- A magnetically driven impeller agitator

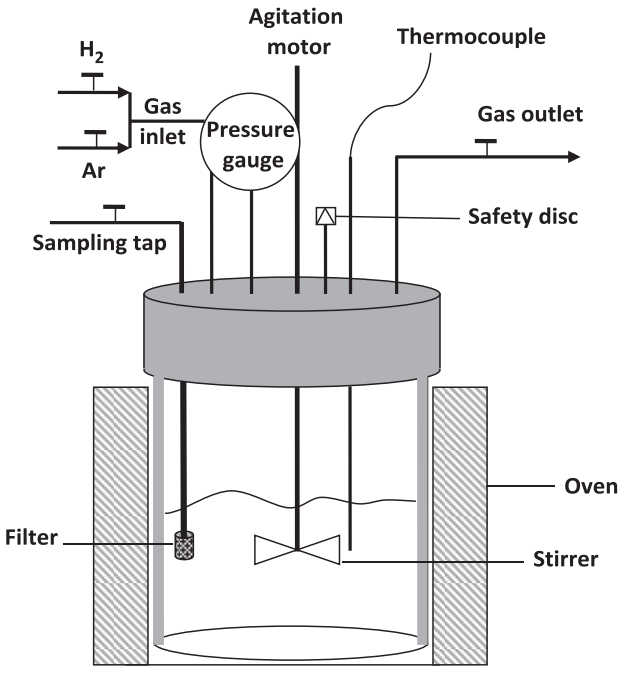

Scheme 11 The batch reactor setup.

- An electrical heating oven
- A regulator where the desired temperature and agitation speed are controlled

A 100 mL aqueous solution of succinic acid "SA" (0.12-0.14 M; pH = 2.3) was prepared using ~1.5 g of SA powder in 100 mL of distilled water. The solution was placed in an ultra-sonic bath at 40°C for 20 min to ensure the solubilization of SA.

The prepared solution was transferred into the reactor, and 0.6 g of the catalyst was added to it. After sealing, the autoclave was purged three times with argon to insure the elimination of oxygen from inside. The solution was stirred at 900 rpm while heating up to the desired reaction temperature (160-240 °C), this point was taken as t_0 of the reaction. After heating, the pressure increases to ~10-20 bar depending on the used temperature, then H_2 gas was added until reaching the target pressure (90-150 bar). The reactions were conducted for 22-48 hours, and liquid samples were collected periodically every 2 hours during the day in order to follow the evolution of the reaction.

III.1.2. **Analyses of the liquid products**

III.1.2.1. **Gas chromatography (GC)**

Analysis of the reaction products in the liquid samples was performed using a GC Agilent Technologies 6890N with a flame ionization detector employing a VF-WAXms column (30 m × 0.25 mm × 0.25 µm) with helium as a carrier gas. The temperature ramp is 1 hour long as shown in Scheme 12.

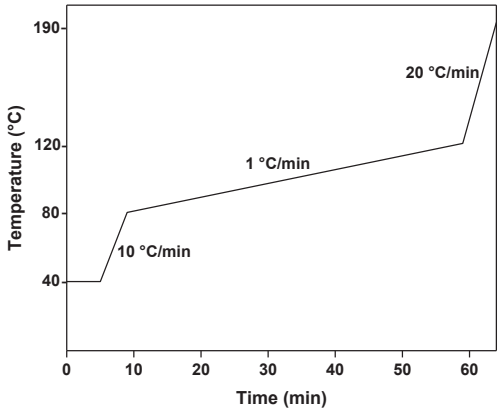

Scheme 12 GC method ramp.

The GC shows a very good separation of the potential products formed during the reaction (γ-butyrolactone, butyric acid, butanol, tetrahydrofuran, 1,4-butanediol), but it does not detect SA (Figure 6).

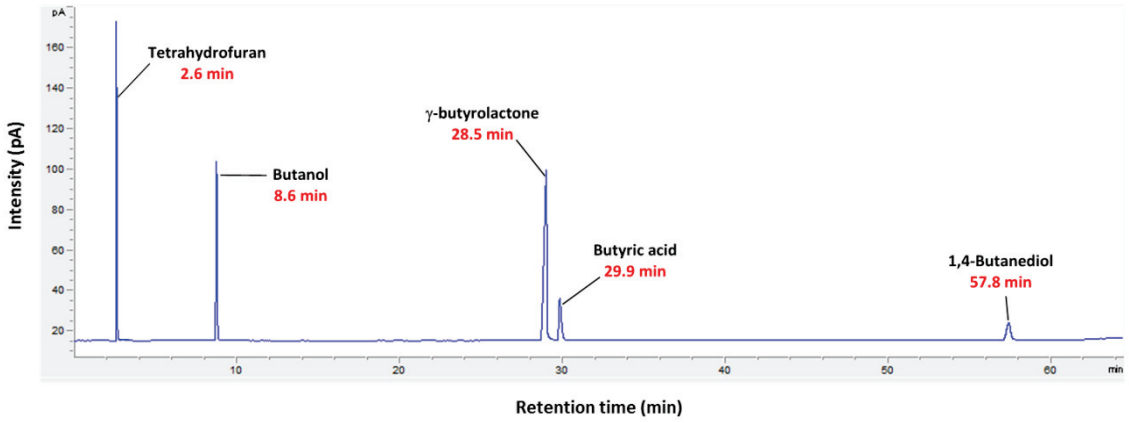

Figure 6 Products separated by GC and their retention times.

III.1.2.2. **HPLC**

The concentration of SA was monitored using a Shimadzu LC 20A HPLC connected to a refractive index detector (RID-10A). The separation was achieved (Figure 7) using ICSep Coregel 107H column (7.8 × 300 mm) heated at 40 °C in a column oven (CTO-10ASvp). A solution of H_2SO_4 (0.001 mol/L) in ultra-pure water was used as the mobile phase at a flow rate of 0.5 mL/min. At this flow rate the pressure of the column is 53 bar. The water used for preparing the eluent was degassed prior to use, and a degasser (Degassex DG-4400 from Phenomenex) was also connected to the HPLC to ensure the elimination of any gas bubbles.

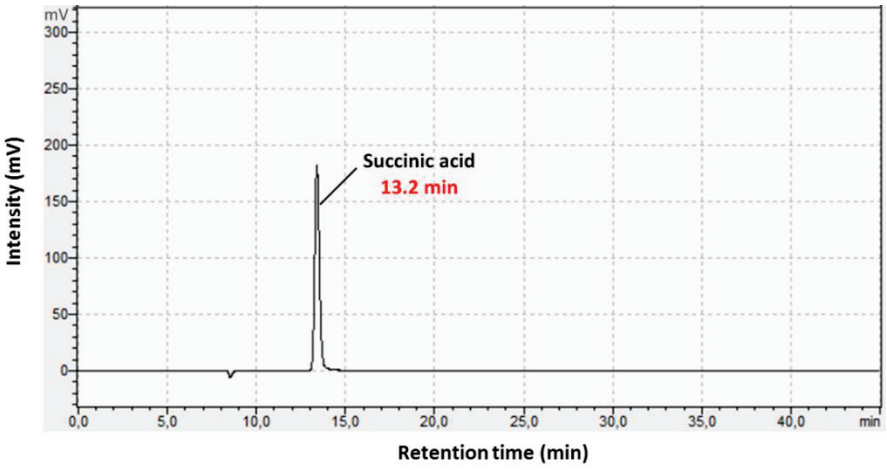

Figure 7 Example of HPLC chromatogram showing Succinic acid and its retention time.

III.1.2.3. **TOC**

The total organic carbon (TOC) in solution was measured by using a Shimadzu TOC-VCSH analyzer. It was used to check the carbon balance in the liquid phase and the possible formation of gaseous products. The TOC measurements were also compared to the total amount of carbon quantified by HPLC and GC to verify if the quantification by HPLC and GC is complete.

Operation mode: TOC is determined by measuring total carbon (NPOC: Non-purgeable organic carbon) after removal of the inorganic carbon in the sample. The sample is first acidified with hydrochloric acid (HCl 37%), and the inorganic carbon is removed by purging with a purified gas. The sample is then injected into a catalytic reactor which oxidizes totally organic compounds (NPOC) into CO_2. The oxidation is carried out at 720 °C over Pt/Al_2O_3 catalyst with clean air. The formed CO_2 passes through a water trap and then it is sent to the infrared detector that measures the CO_2 concentration. Prior each set of analysis, two blank injections (water) and a standard solution of nicotinic acid (0.1 g/L) were used for the calibration of the device.

Expression of the results: The used TOC method measures the carbon in the range 0-500 ppm.

TOC is calculated based on the expression:

$$\mathrm{TOC} = (\mathrm{nC_{SA}} * \mathrm{M_C} * [\mathrm{SA}]_t) + \sum_i \mathrm{nC_i} * \mathrm{M_C} * [\mathrm{P_i}]_t$$

Where:

- nC is the number of carbon atoms in the substance (e.g. $\mathrm{nC_{SA}} = 4$)
- $[\mathrm{SA}]_t$ is the concentration of SA at time t
- $\mathrm{M_C}$ is the molar mass of carbon (12 g/mol)

Then for initial concentration of 0.128 M of SA, the TOC at t_0 is given by:

$$TOC_{t0} = 4 * 12 * 0.128$$
$$= 6.144\ \mathrm{g/L}$$
$$= 6144\ mg/L$$

Therefore, the analyzed samples should be diluted such that the results fall in the range

of 0-500 ppm to be analyzable according to the method used. For our concentration the samples were diluted 70 times with ultra-pure water and then analyzed.

III.1.3. **Calculation of SA conversion, products yield, and carbon balance**

- SA concentration (%) and conversion (%) are based on initial concentration of SA ($[SA]_0$) and defined by:

$$\text{SA concentration } (\%) = \frac{[SA]_t}{[SA]_0} \times 100 \quad \text{and} \quad \text{SA conversion } (\%) = \frac{[SA]_0 - [SA]_t}{[SA]_0} \times 100$$

Where $[SA]_t$ refers to the concentration of SA at time *t*.

- Selectivity and yield of a product *i* are given by:

$$\text{Selectivity } (\%) = \frac{[P_i]_t}{[SA]_0 - [SA]_t} \times 100 \quad \text{and} \quad \text{Product yield } (\%) = \frac{[P_i]_t}{[SA]_0} \times 100$$

Where $[P_i]_t$ refers to the concentration of the product *i* at time *t*.

- The carbon balance (CB) in the liquid phase is given by:

$$\text{CB } (\%) = \frac{4*[SA]_t + \sum_i n_i*[P_i]_t}{4*[SA]_0} \times 100$$

Where n_i refers to the number of carbon of the product *i.*

- The initial reaction rate was calculated based on the slope of the linear curve (up to 6-8h), at low conversion (< 40%).

$$V_0(\text{mmol}_{\text{Substrate}}\ g_{Mo}^{-1}\ h^{-1}) = \frac{\text{mmole of reactant}}{\text{mass of Mo} \times \text{time}}$$

Repeated reactions delivered conversion and products yield reproducible within ± 3%. Therefore the selectivity is given with an error of ± 3% and the reaction rate with an uncertainty of 1.0 $mmol_{SA}\ g_{Mo}^{-1}\ h^{-1}$. Carbon balance and TOC values are given with a precision of 8%.

III.1.4. **Analysis of gas products**

After some reactions, the gases were collected by disconnecting the gas outlet, attaching a 0.6 Liter gas bag with push lock valve (Tedlar bags from SUPELCO), and depressurizing some of the pressure to fill in the bag. The gases were qualitatively analyzed using a micro-GC SRA with MS Agilent 5975 detector. Three columns were used:

Alumina (10 m × 3 µm) at 90 °C for C_3–C_4 hydrocarbons, Poraplot U (8 m × 30 µm) for C_2–C_3 compounds and CO_2, and MolSieve 5A (10 m × 12 µm) for H_2, CO, and CH_4.

III.1.5. Catalyst recovery

After finishing the reaction, the solution with the catalyst inside was filtered, washed with distilled water (under air), and dried in an oven at 80 °C.

For the catalyst recovered under nitrogen, the experiments were performed using a 100 mL (Parr 4598) Hastelloy reactor. The small reactor was disconnected from all gas and water lines and transferred while still closed into a glove bag (Aldrich AtmosBag). This bag is an inflatable polyethylene glove box alternative. The filtration setup was also placed inside the bag, and two ports were used for nitrogen gas input and purging output which were sealed after filling with nitrogen. An additional hole was also used for the vacuum line of filtration (Figure 8).

Figure 8 Catalyst recovery under nitrogen.

III.2. CO_2 hydrogenation

III.2.1. General reaction

The evaluation of the catalysts in the hydrogenation of CO_2 was carried out in a fixed-bed flow reactor (Scheme 13). A mass of 0.4-0.8 g of the catalyst was placed in a tubular Pyrex glass reactor of 1.3 cm diameter, comprising a glass frit which keeps the catalyst

while allowing the gas to pass through. This glass tube was inserted into a steel reactor allowing the system to withstand the pressure (< 50 bar). The set was then inserted into a tubular oven connected to a temperature controller. The system was purged with the reaction mixture $H_2/CO_2/N_2$ and then kept exposed to this flow till a total pressure of 30 bar at which heating was started. The reaction was kept for 3 hours, after which the system was cooled back to room temperature.

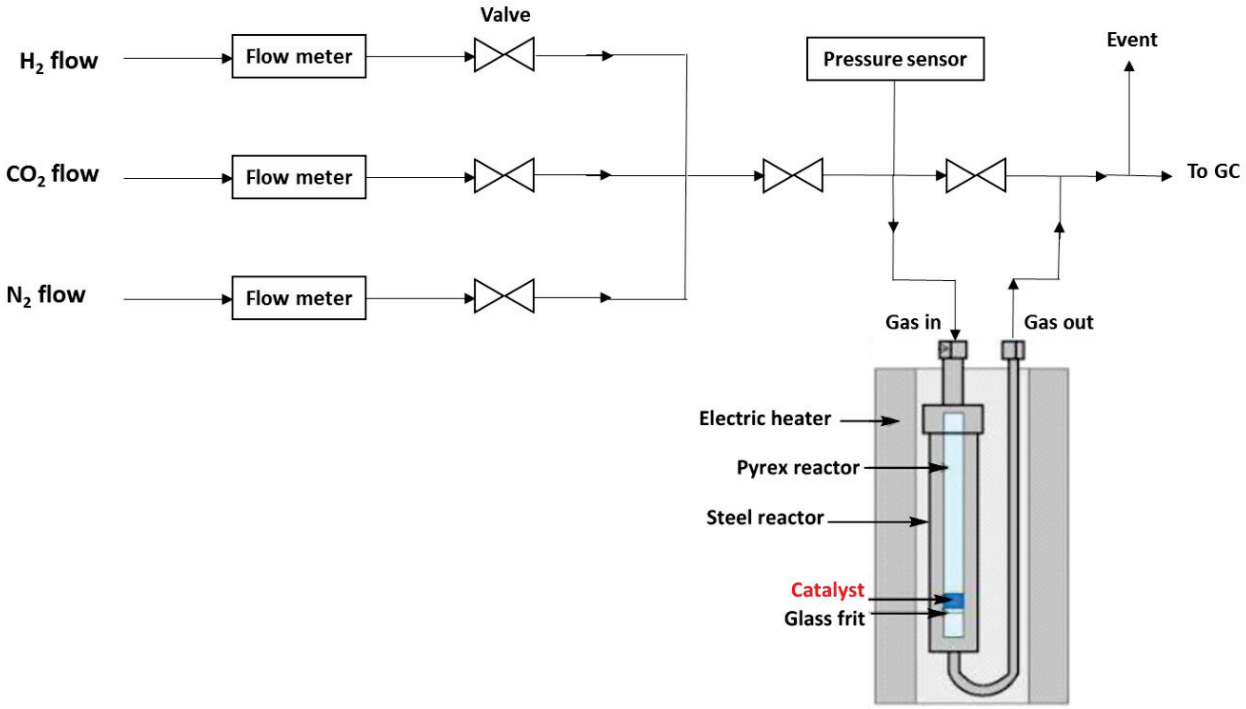

Scheme 13 Set up of the reactor used for CO_2 hydrogenation.

III.2.2. **Products analysis**

The reaction system was connected to SRA Instruments gas chromatograph (µ-GC) where samples were taken automatically every 3 minutes during the reaction. Four columns were set up in the µ-GC: MolSieve 5A for H_2, O_2/Ar, N_2, CO, and CH_4; Poraplot U for C2–C3 compounds and CO_2; Alumina for C4-C6 compounds; and Stabilwax for oxygenates (e.g. CH_3OH).

III.2.2.1. **Calculation of CO_2 conversion and products yield and selectivity**

The data obtained through µ-GC allows determining the conversion of CO_2 and products selectivity.

The conversion of CO_2 is given by:

$$CO_2\ conversion\ (\%) = \frac{F(CO_2)_{in} - F(CO_2)_{out}}{F(CO_2)_{in}} \times 100$$

Where:

- $F(CO_2)_{in}$ is the flow of CO_2 in the feed entering in the reactor
- $F(CO_2)_{out}$ is the flow of effluent CO_2.

The selectivities of products are given by:

$$Selectivity\ P\ (\%) = \frac{F(P)_{out}}{F(CO_2)_{in} - F(CO_2)_{out}} \times 100$$

Where:

- $F(P)_{out}$ is the flow rate of the product in the effluent gas.

CHAPTER 3.

Synthesis of supported molybdenum carbides for succinic acid hydrogenation

During the preparation of supported molybdenum carbides, many parameters should be taken into consideration, especially during the temperature programmed reduction carburization (TPRC) process (cf Chapter 1). This chapter sheds light on some of the effects of the conditions of TPRC, mainly the nature of hydrocarbon used in the reactive gas mixture (CH_4 or C_2H_6), the concentration of the carburizing gas (i.e. % v/v hydrocarbon/H_2) and the maximum carburization temperature. The effect of the nature of the support (P25 TiO_2, DT51 TiO_2, and ZrO_2) versus bulk catalyst is also investigated.

I. Synthesis of supported molybdenum carbides by temperature programmed reduction carburization

The catalysts were prepared in two main steps. The first one is the impregnation where the molybdenum species are deposited on the support. The second step is the TPRC where reduction and carburization of the supported molybdenum oxide takes place at the same time.

The two common molybdenum precursors used in the literature for the preparation of molybdenum carbides are molybdenum trioxide and ammonium heptamolybdate tetrahydrate. The former one is usually used for the synthesis of bulk carbide while the latter one is used for the supported material [31,41,58–60]. This is mainly due to the solubility limitations of molybdenum trioxide in water (0.49 g / 100 mL at 28 °C), compared to ammonium heptamolybdate tetrahydrate (65 g / 100 mL). Moreover, the price of molybdenum trioxide (99.97 % trace metals basis) is 389 € for 25 g (corresponding to 17 g of Mo) which is more than 3 times higher than the price of

ammonium heptamolybdate tetrahydrate (99.98 % trace metals basis) 206 € for 50 g (corresponding to 27 g of Mo) “Sigma-Aldrich, France”.

Hence, the supported molybdenum materials in our work were prepared by impregnation of ammonium heptamolybdate tetrahydrate on the support, in water at room temperature. Water was then removed by rotary evaporator in order to insure the total deposition of molybdenum species (cf Chapter 2). The molybdenum percentage was determined by ICP analysis and it corresponds to the nominal loading (around 10% wt. Mo). The impregnation of ammonium heptamolybdate tetrahydrate on P25 TiO_2 in water occurs at pH = 5.3 which is slightly lower than the PZC of TiO_2 P25 (pH_{PZC} = 6.3) [67]. The predominant species in solution at this pH should be $Mo_7O_{24}^{6-}$ [75,76]. The support must bear a slight positive charge which should favor the interaction with the anionic species. However when preliminary syntheses were done using filtration instead of rotary evaporation, a large amount of molybdenum was in the filtrate, and the final loading ranged between 2.2 and 6.6 % depending on the difference in washings, instead of the desired 10 %. Thus, for all the catalysts, water was removed using the rotavap, and this impregnation procedure was used for all the supported catalysts in this thesis.

I.1. **Effects of reduction-carburization parameters**

In order to study the effects of several parameters on the characteristics of the prepared material and its catalytic performance, we modified one parameter at a time, while fixing the others. Eleven catalysts were prepared with different conditions of reduction-carburization to figure out their effects. Large batches (ca. 10 g) of supported molybdenum oxide were prepared, and, when possible, each carburization parameter was evaluated using the same batch of starting material. Table 16 lists the catalysts with the parameters employed during their preparation by TPRC and the corresponding notations. The carbon source in the reactive mixture was either methane or ethane. The concentration of hydrocarbon in hydrogen was varied from 5 % to 40 % v/v in the case of methane, and from 5 % to 20 % v/v in the case of ethane. Then the hydrocarbons concentration was fixed at 20 % v/v and the carburization was conducted at either 600 °C, 700°C or 800 °C. In this chapter, the GHSV employed during the reduction-carburization is fixed at 1091 h^{-1}, the ramp of temperature is always at 0.5

°C/min, and in this first section, the support P25 TiO_2 is used for all the syntheses.

The given catalysts notations are denoted as follows: **MoC_{VN-T}/S**, where:

- MoC refers to molybdenum carbide; the stoichiometry is not specified for the sake of clarity
- V is the volumetric percentage of hydrocarbon in hydrogen.
- N is the first letter corresponding to the nature of hydrocarbon (E for ethane and M for methane)
- T is the final carburization temperature that was held for 2 h
- S refers to the type of the support (P25 TiO_2, DT51TiO_2, ZrO_2)

Thus, for a catalyst MoC supported on P25 TiO_2 and prepared under 5% v/v CH_4/H_2 at 700°C, the notation is: **$MoC_{5M-700}/P25TiO_2$**.

Table 16 List of the catalysts with the corresponding preparation conditions

Catalyst	Support	hydrocarbon	%[a]	T (°C)
$MoC_{5M-700}/P25TiO_2$	P25 TiO_2	Methane	5	700
$MoC_{10M-700}/P25TiO_2$	P25 TiO_2	Methane	10	700
$MoC_{20M-700}/P25TiO_2$	P25 TiO_2	Methane	20	700
$MoC_{40M-700}/P25TiO_2$	P25 TiO_2	Methane	40	700
$MoC_{20M-600}/P25TiO_2$	P25 TiO_2	Methane	20	600
$MoC_{20M-800}/P25TiO_2$	P25 TiO_2	Methane	20	800
$MoC_{5E-700}/P25TiO_2$	P25 TiO_2	Ethane	5	700
$MoC_{10E-700}/P25TiO_2$	P25 TiO_2	Ethane	10	700
$MoC_{20E-700}/P25TiO_2$	P25 TiO_2	Ethane	20	700
$MoC_{20E-600}/P25TiO_2$	P25 TiO_2	Ethane	20	600
$MoC_{20E-800}/P25TiO_2$	P25 TiO_2	Ethane	20	800

[a] % v/v Hydrocarbon/H_2

I.1.1. Methane as carbon source

I.1.1.1. The percentage of methane in the reactive gas mixture

To study the effect of the percentage of hydrocarbon in the reactive mixture, four catalysts with 5%, 10%, 20%, and 40% v/v of CH_4/H_2 were prepared (Table 16). The maximum carburization temperature was kept the same for the three catalysts (700°C).

ICP analysis confirmed the presence of the complete amount of molybdenum impregnated (~10%) in the 4 catalysts (Table 17). The theoretical percentage of carbon if stoichiometry is respected for 10% w/w MoC/TiO_2 and 10%w/w $MoC_{0.5}/TiO_2$ are 1.2% and 0.6% respectively. The carbon weight percentages determined by carbon elemental analysis for the catalysts synthesized with 5-20 % of methane are close to each other (range from 0.4 to 0.8%) which indicates either incomplete carburization or a stoichiometry (x) around 0.5 for MoC_x. Whereas the catalyst synthesized with 40% of methane "$MoC_{40M\text{-}700}/P25TiO_2$" exhibits the highest carbon content (1.2%, Table 17). This amount is equal to the theoretical carbon percentage for MoC, yet it cannot guarantee the full carburization as it includes all types of carbon (including graphite), not only the carbidic one.

Table 17 characterizations of catalysts prepared by different methane concentrations.

Catalyst	% Mo[a]	% C[a]	% A/R[b]	Crystallite size[c] (nm)	a[d] (Å)
$MoC_{5M\text{-}700}/P25TiO_2$	9.7	0.4	50	2	4.224
$MoC_{10M\text{-}700}/P25TiO_2$	9.3	0.8	67	3	4.227
$MoC_{20M\text{-}700}/P25TiO_2$	9.5	0.6	72	3	4.256
$MoC_{40M\text{-}700}/P25TiO_2$	9.4	1.2	75	2	4.259

[a] Weight percentage; [b] Anatase/Rutile composition (% Anatase); [c] of fcc MoC ,determined by XRD ; [d] lattice parameter for fcc MoC.

The literature on supported molybdenum carbides obtained by carburization with 20% v/v CH_4/H_2 shows the production of either hexagonal or cubic molybdenum carbide. Li et al. prepared hexagonal molybdenum carbide supported on anatase TiO_2 via a series of temperature-programmed processes where the temperature was raised to 400 °C at a rate of 5 °C/min, then from 400 °C to 650 °C at a rate of 1 °C/min where

it was kept for 3h [60]. The produced supported hexagonal molybdenum carbides were large particles of 43 nm size. Mai et al. also prepared hexagonal molybdenum carbide supported on carbon nanotubes with 20% v/v CH_4/H_2 at 2.5 °C/min till 650°C [41]. The authors mentioned that their results contradict with those of Frank et al. who obtained cubic molybdenum carbide supported on carbon nanotubes when employing 20% v/v CH_4/H_2 at 5 °C/min till 700 °C [59]. Accordingly, in our case, it was not possible to predict the final molybdenum carbide crystallographic phase depending on the literature available on supported molybdenum carbides.

XRD analysis provides information about the crystallographic structure of the material and the crystallite size. Analyses of the four catalysts prepared with different methane concentrations were done, the diffractograms are shown in Figure 9. The diffractogram of P25 TiO_2 is added for comparison.

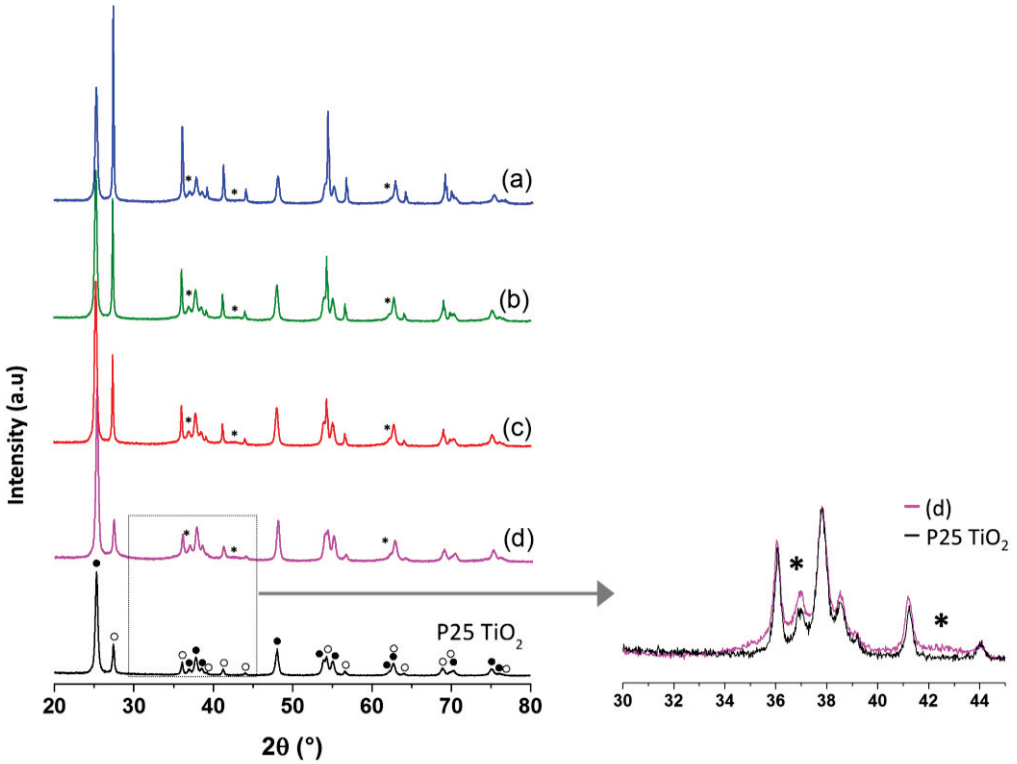

Figure 9 XRD diffraction patterns of the support P25 TiO_2 and the catalysts: a) $MoC_{5M\text{-}700}/P25TiO_2$, b) $MoC_{10M\text{-}700}/P25TiO_2$, c) $MoC_{20M\text{-}700}/P25TiO_2$, and d) $MoC_{40M\text{-}700}/P25TiO_2$. Peaks associated with ● Anatase, ○ Rutile, * Fcc MoC phase.

Basically, the peaks corresponding to MoC overlapped with the ones of the support where mainly the peaks corresponding to TiO_2 anatase and rutile phases are observed. Rietveld refinement was conducted using Topas 5 software in order to help us with the

identification of the different crystalline phases, even those corresponding to molybdenum carbide. In the four catalysts, the predominant MoC phase is the face centered cubic structure, with broad peaks at 2θ = 36.4°, 42.2° and 61.3° that can be associated with the planes (111), (002), and (022), respectively. The only peak corresponding to molybdenum carbide which does not overlap with the support is the one at 42.2°. The enlarged diffractogram of $MoC_{40M\text{-}700}/P25TiO_2$ and the support, when superposed with the same baseline, shows the small augmentation due to the presence of the cubic MoC on the support at 36.4 ° and 42.2°. Neither the hexagonal Mo_2C with significant peaks at 2θ = 34.4°, 37.9°, 39.4°, and 52.2°, nor the oxycarbide MoO_xC_y with peaks at 2θ = 37.1°, 44.1°, and 62.9° do appear in the 4 catalysts. The crystallite size of MoC was estimated around 2-3 nm.

MoO_2 was reported as an intermediate phase during the synthesis of cubic MoC_{1-x} with 20% C_2H_6/H_2 and 720°C from $MoO_3.nH_2O$ [56]. The authors of this study showed through in situ XRD experiments that the synthesis of the cubic MoC proceeds first by reduction by hydrogen of MoO_3 to MoO_2 through Mo_4O_{11}. MoO_2 appears from 530 °C, and ethane reacts in the last step where the transition from MoO_2 to MoC_{1-x} occurs at 680 °C. Accordingly, the presence of MoO_2 would be therefore an indication of incomplete carburization. However its absence could not be completely excluded in our case as the two main peaks of MoO_2 are at 2θ = 26.03° and 37.02° which are under those of TiO_2 support. It is worth noting that under pure H_2, MoO_3 is reduced to MoO_2 at 590 °C, and MoO_2 is reduced to Mo metal (2θ = 40.6°) at 700°C [56].

Mo metal has Im-3m structure, with a lattice parameter a ≈ 3.14 nm. After incorporation of the carbon, the lattice parameter increases. MoC_x with Fm-3m structure exhibits lattice parameters in the range of 4.155 nm for $MoC_{0.5}$ to 4.281 nm for MoC. The lattice parameters determined for the four catalysts (Table 17) are within the range reported for MoC_x ($0.5 \leq x \leq 1$). Moreover they increased with increasing hydrocarbon content.

In the $MoC_{40M\text{-}700}/P25TiO_2$, the composition anatase/rutile was the same as for the support P25 (75%/25%). However for catalysts $MoC_{5M\text{-}700}/P25TiO_2$, $MoC_{10M\text{-}700}/P25TiO_2$ and $MoC_{20M\text{-}700}/P25TiO_2$ the ratio of anatase to rutile changed as clearly seen by comparing the most intense rutile peaks (at 27.4°, 36.0° and 54.2°) of Figure 9-a,b,c

with those of Figure 9-d. As mentioned in section I.4.1.2 in Chapter 1, anatase TiO_2 is known to convert to rutile at temperature above 500°C [69]. However in the presence of molybdate, the anatase phase is stabilized allowing its use at higher temperatures [66,167]. This was confirmed when conducting the carburization on the bare P25 TiO_2. XRD analysis for the carburized support (Figure 10) shows complete absence of the peaks of anatase phase, indicating a total transformation to rutile under the carburization conditions. Therefore the presence of the Mo species at the surface stabilizes the anatase phase during the gas treatment at high temperature (700 °C). Moreover, the presence of carbon on the surface also seems to stabilize the anatase phase. Indeed, the catalyst with the highest carbon content conserves the nominal percentage of anatase [168,169], and the catalyst with lower carbon content underwent the most significant phase change.

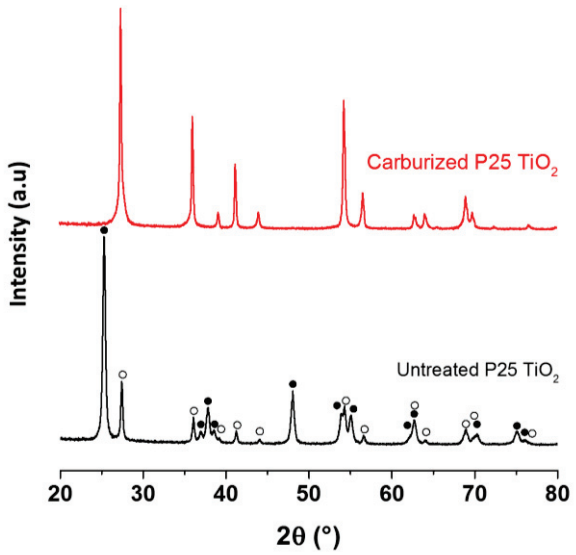

Figure 10 XRD diffraction patterns of the untreated support P25 TiO_2 and the one carburized at 700 °C with 20% v/v C_2H_6/H_2 Peaks associated with ● Anatase, ○ Rutile.

In order to confirm the crystallographic structure of MoC, STEM and TEM analysis were conducted on one sample: $MoC_{20M\text{-}700}/P25TiO_2$. The STEM pictures are shown in Figure 11. Although it was hard to see clearly the particles on the STEM images even with higher zoom, the Mo EDX mapping showed the presence of very small Mo particles that are well dispersed on the TiO_2 support.

As revealed by STEM, TEM pictures also showed the presence of small molybdenum

carbide particles (< 5 nm) but the size distribution was not done because not all the particles had rounded or homogeneous shapes. An example of electron diffraction and EDX associated with the corresponding TEM picture for $MoC_{20M\text{-}700}/P25TiO_2$ is shown in Figure 12. The EDX of the scanned spot confirms the presence of Mo at the zoomed spot. The structure and crystal system were deduced by comparing the experimental lattice parameters with the theoretical values associated with different MoC_x systems ($0.5 < x < 1$). The results show closest match with MoC of cubic crystal system with Fm-3m space group and a = 4.281 Å (Table 18). It is however worth noting that a number of cards exist for Fm-3m MoC_x ($0.68 \leq x \leq 1$) with similar lattice parameters (4.266 Å ≤ a ≤ 4.312 Å). So it was not possible to conclude on the stoichiometry of MoC_x by TEM analysis.

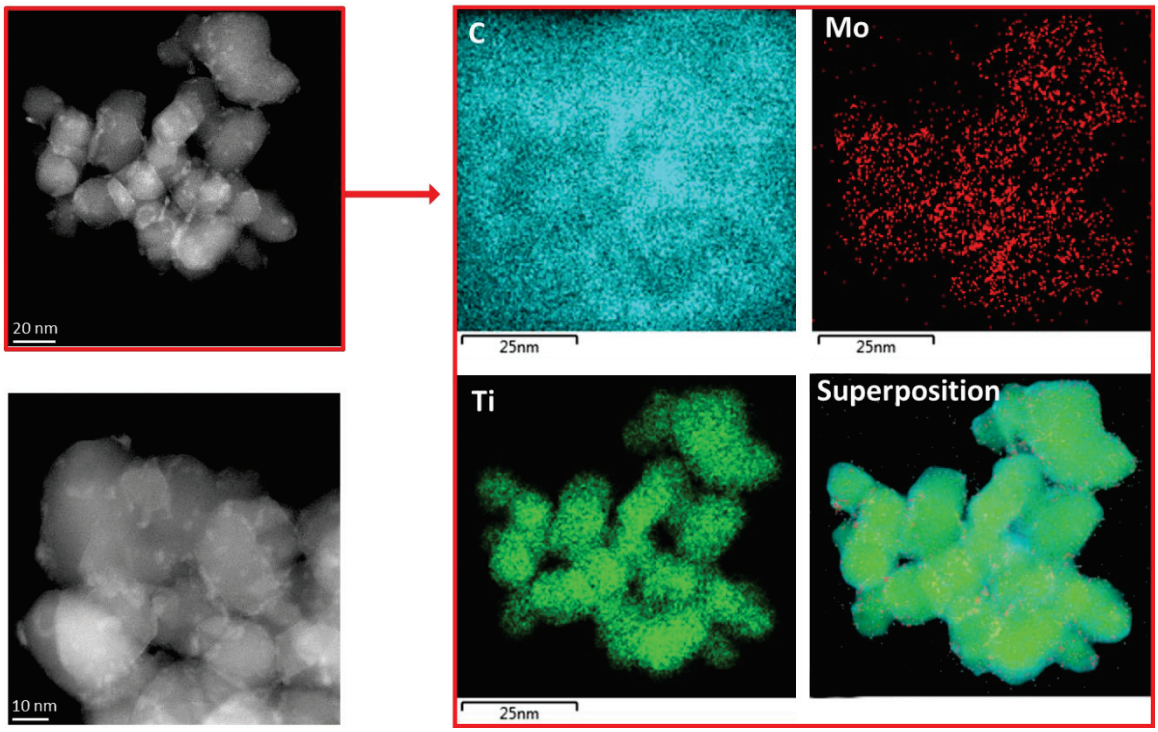

Figure 11 STEM images of $MoC_{20M\text{-}700}/P25TiO_2$ catalyst with the corresponding EDX mapping for C, Mo, and Ti.

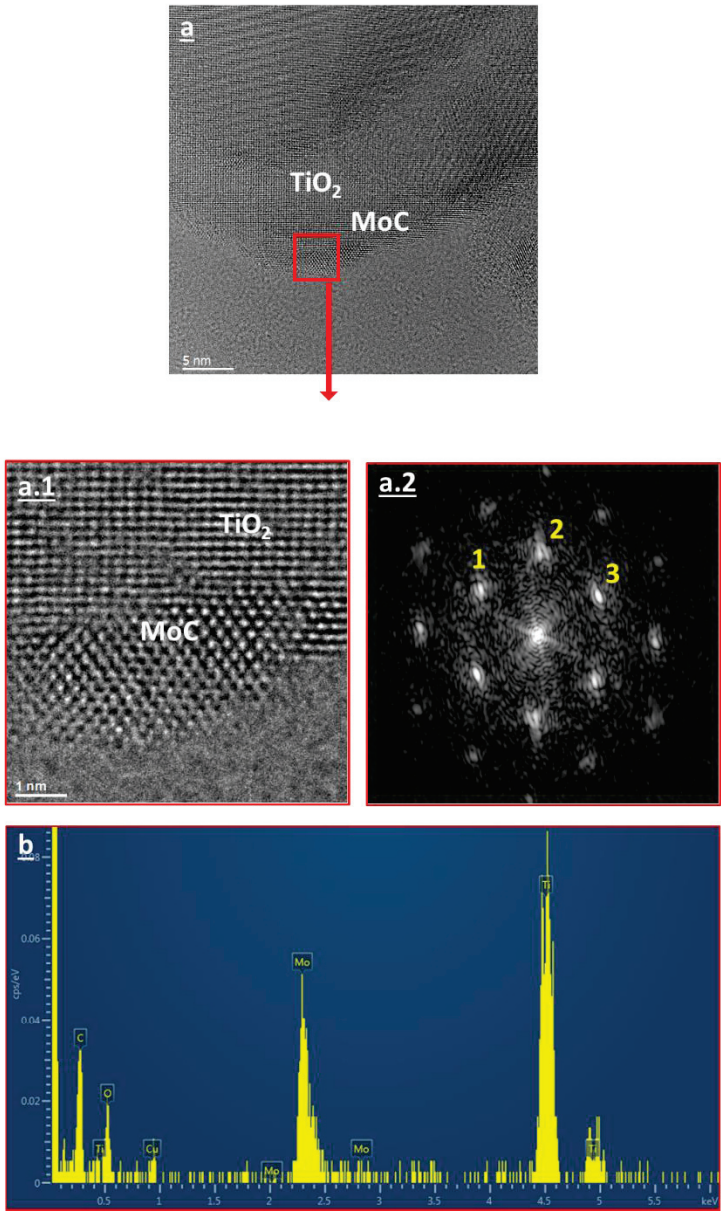

Figure 12 Representative TEM image (a, a1), electron diffraction (a.2), and EDX (b) of catalyst $MoC_{20M\text{-}700}/P25TiO_2$.

Table 18 Example of lattice parameters of $MoC_{20M\text{-}700}/P25TiO_2$, obtained from TEM analysis (Spots shown in Figure 12-a.2).

Spot	h k l	α (°)		d (nm)	
		Exp.	Theo.*	Exp.	Theo.*
1	1 1 -1	0.00	0.00	0.247	0.247
2	2 0 0	54.99	54.74	0.209	0.214
3	1 -1 1	110.94	109.47	0.246	0.247

* Theoretical values corresponding to cubic MoC, reference ICSD 197178

In order to gain more information about the Mo and C states in the catalysts, XPS analysis was done on two catalysts: $MoC_{10M\text{-}700}/P25TiO_2$ and $MoC_{40M\text{-}700}/P25TiO_2$. The Mo 3d and C 1s spectra are presented in Figure 13. The chemical states of the catalyst components and their relative abundance are compiled in Table 19.

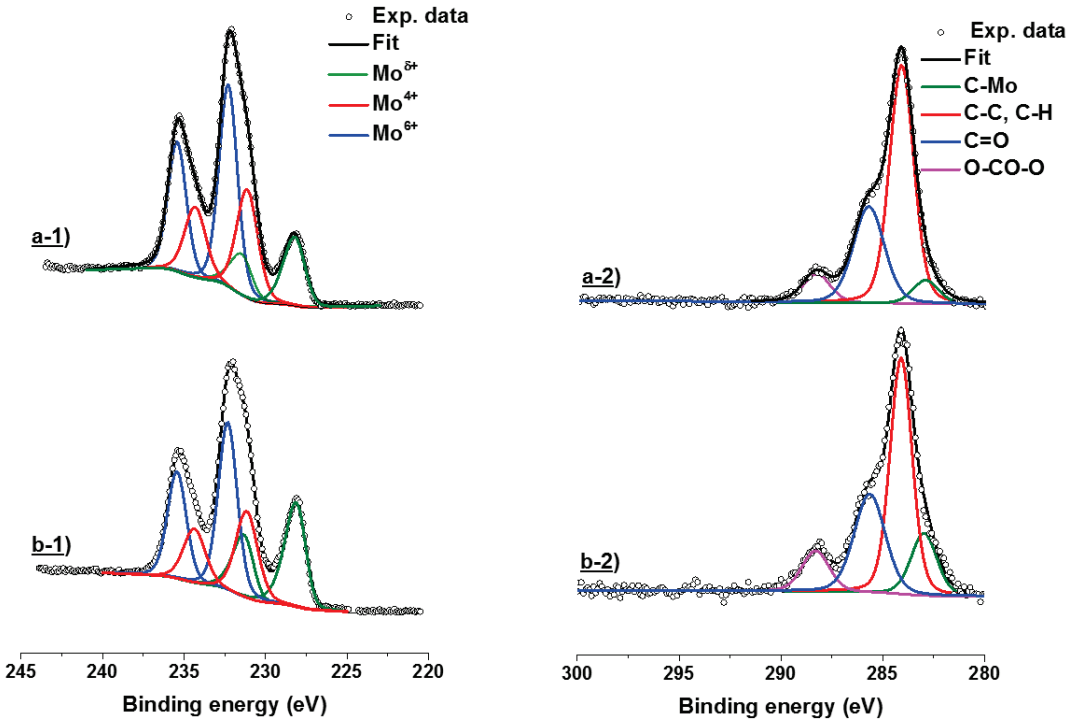

Figure 13 XPS spectra of catalysts a) $MoC_{10M\text{-}700}/P25TiO_2$ and b) $MoC_{40M\text{-}700}/P25TiO_2$ over 1) Mo 3d and 2) C 1s.

Table 19 XPS analysis: atomic concentration of Mo and C, and the abundance of Mo and C species in catalysts $MoC_{10M\text{-}700}/P25TiO_2$ and $MoC_{40M\text{-}700}/P25TiO_2$.

	Atomic concentration %		**Mo species %**			**C species %**	
Catalyst	Mo	C	$Mo^{\delta+}$	Mo^{4+}	Mo^{6+}	Carbide	Graphite
$MoC_{10M\text{-}700}/P25TiO_2$	4.7	16.1	20	31	49	6	64
$MoC_{40M\text{-}700}/P25TiO_2$	3.9	13.7	30	26	44	15	58

The Mo 3d spectra exhibit two peaks at BE = 228.2 eV and 231.4 eV which correspond to Mo $3d_{5/2}$ and Mo $3d_{3/2}$ peaks of $Mo^{\delta+}$ ($\delta < 1$). The former value is within the range 227.6 - 228.9 eV which is attributed to carbidic Mo (Mo next to carbon) in the literature [170,171]. In addition, peaks assigned to Mo^{4+} (BE = 231.1 eV and 234.3 eV) and Mo^{6+} (BE = 232.2 eV and 235.4 eV) were also observed [172,173]. These can be mainly referred to the passivation layer that is present on the surface of the catalysts. The facts

that the catalysts are passivated, and that XPS is a surface analysis, alter the possibility of quantifying the oxide species that can be associated with incomplete carburization. However, it is possible to compare the catalysts between each other as they are both passivated. By comparing the Mo species, catalyst $MoC_{10M\text{-}700}/P25TiO_2$ possesses higher amount of molybdenum oxide species (i.e. Mo^{4+} and Mo^{6+}) and lower amount of molybdenum carbide (i.e. $Mo^{\delta+}$) than catalyst $MoC_{40M\text{-}700}/P25TiO_2$ (Table 19).

The C 1s spectra Figure 13-b exhibit a peak at BE = 282.9 eV which corresponds to the carbon in the carbidic form [171]. The broad peak at BE = 284.1 eV along with the peak at 288.3 eV refer to graphitic carbon. The additional peak at 285.7 eV can be attributed to carbon in C-O or C=O groups [171,174]. The carbon species show higher carbide content in catalyst $MoC_{40M\text{-}700}/P25TiO_2$ compared to higher graphite content in $MoC_{10M\text{-}700}/P25TiO_2$ (Table 19).

In summary, the TEM and XRD results showed the presence of cubic molybdenum carbide particles on the surface of TiO_2. The carbon content, the lattice parameters and the XPS results suggest that the degree of carburization increases with the hydrocarbon percentage.

I.1.1.2. **Effect of the maximum carburization temperature**

To study the effect of the carburization temperature, two other samples were prepared at 600 °C and 800 °C with 20% v/v of CH_4/H_2 and compared to $MoC_{20M\text{-}700}/P25TiO_2$.

Table 20 Characterizations of catalysts prepared at different carburizing temperatures.

Catalyst	% Mo[a]	% C[a]	% A/R[b]	Crystallite size[c] (nm)	a[d] (Å)
$MoC_{20M\text{-}600}/P25TiO_2$	9.7	0.3	75	n.a.	n.a.
$MoC_{20M\text{-}700}/P25TiO_2$	9.5	0.6	72	3	4.256
$MoC_{20M\text{-}800}/P25TiO_2$	10.0	0.6	n.a.	n.a.	n.a.

[a] Weight percentage; [b] Anatase/Rutile composition (% Anatase); [c] of fcc MoC ,determined by XRD ; [d] lattice parameter for fcc MoC; n.a.: not available.

ICP analysis of the 3 solids confirms the presence of the total amount of molybdenum (ca. 10% w/w) in the three catalysts. Carbon elemental analysis shows very low content

of 0.3 % in the catalyst $MoC_{20M\text{-}600}/P25TiO_2$ prepared at low temperature (Table 20). The two other catalysts have the same carbon content (0.6 %) which is again less than the theoretical content for MoC and close to the one for $MoC_{0.5}$.

Figure 14 presents the XRD results for the three catalysts. For catalyst $MoC_{20M\text{-}600}/P25TiO_2$ it was difficult to see the molybdenum carbide phases (Figure 14-a) probably due to the very low amount of this phase; hence crystallite size and lattice parameters could not be determined. It was possible to see through Rietveld refinement a small peak at 26.03° referring to MoO_2 phase which emphasizes the incomplete carburization. This temperature seems not efficient to prepare molybdenum carbide with 20% v/v CH_4/H_2.

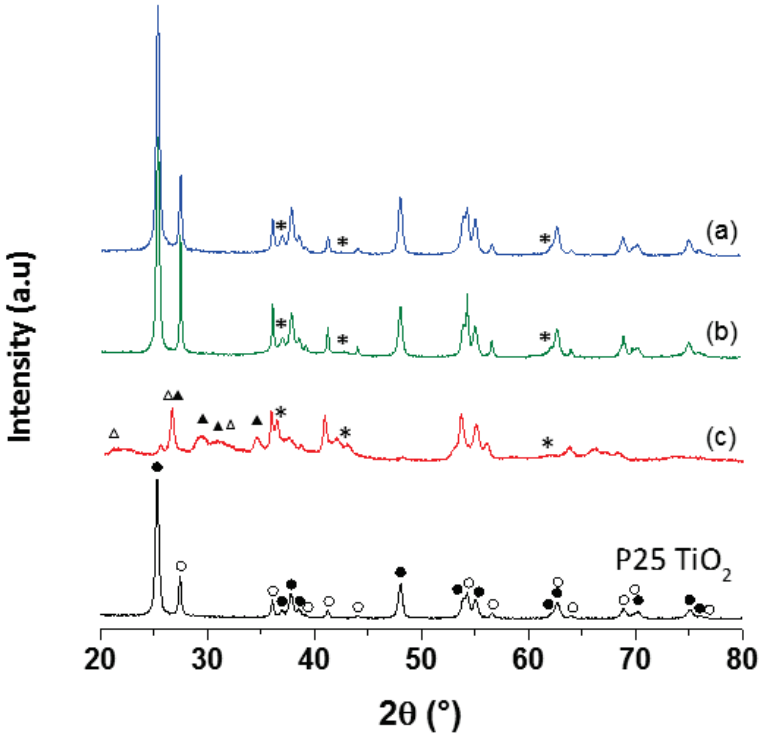

Figure 14 XRD diffraction patterns of the support P25 TiO_2 and the catalysts: a) $MoC_{20M\text{-}600}/P25TiO_2$, b) $MoC_{20M\text{-}700}/P25TiO_2$, and c) $MoC_{20M\text{-}800}/P25TiO_2$. Peaks associated with ● Anatase TiO_2, ○ Rutile TiO_2, ▲ Ti_5O_9, △ Ti_4O_7 * Cubic MoC phase.

At 700°C, as already observed, cubic MoC is formed (Figure 14-b). In catalyst $MoC_{20M\text{-}800}/P25TiO_2$ the rutile phase and most of the anatase phase of TiO_2 were transformed. It has been reported that rutile TiO_2 can be reduced and carburized under a CH_4-H_2 gas mixture at high temperature following the sequence: $TiO_2 \rightarrow Ti_5O_9 \rightarrow Ti_4O_7 \rightarrow Ti_3O_5 \rightarrow Ti_2O_3 \rightarrow TiO_xC_y$. The reported TPR profile suggests that at 800 °C, only Ti_5O_9 should be formed [168]. As expected, no peaks associated with Ti_3O_5, Ti_2O_3, or TiO_xC_y could be

observed in the XRD pattern of catalyst $MoC_{20M\text{-}800}/P25TiO_2$ as it was prepared at 800 °C. However the peaks at 26.4°, 29.0° and 30.7° can be attributed to Ti_5O_9. A smaller amount of Ti_4O_7 can also be observed at 20.7°, 26.3°, and 31.7°. Due to the difficulty of identification, the lattice parameter and crystallite size of MoC could not be determined for this sample. This was accompanied with a decrease in the surface area from 50 m^2/g ($MoC_{20M\text{-}700}/P25TiO_2$) to 28 m^2/g ($MoC_{20M\text{-}800}/P25TiO_2$).

These results show that 600°C is not efficient temperature for full carburization of molybdenum oxides in our conditions, and that 800°C is too high as the support is altered. To summarize, when using methane as carburizing agent, it seems that 700°C and high concentration of methane (20% or 40%) are the best preparation conditions for the formation of MoC/TiO_2.

I.1.2. Ethane as carbon source

As the carburization with methane was not always efficient, it was replaced by ethane as it is reported that increasing the chain length of the hydrocarbon allows the transformation from oxide to carbide to occur at lower temperature [54,57]. The same parameters studied with methane are studied with ethane.

I.1.2.1. The percentage of ethane in the reactive gas mixture

Three catalysts were prepared using ethane as carburizing agent with three different concentrations (Table 21). The percentages 5, 10, and 20 % v/v C_2H_6/H_2 were used so that a comparison can be done with 10, 20, and 40 % v/v CH_4/H_2 using equivalent carbon weight composition.

Table 21 characterizations of catalysts prepared with different ethane concentrations.

Catalyst	% Mo[a]	% C[a]	% A/R[b]	Crystallite size[c] (nm)	a[d] (Å)
$MoC_{5E\text{-}700}/P25TiO_2$	9.6	0.8	55	3	4.234
$MoC_{10E\text{-}700}/P25TiO_2$	9.6	0.8	71	3	4.246
$MoC_{20E\text{-}700}/P25TiO_2$	9.4	1.2	74	3	4.270

[a] Weight percentage; [b] Anatase/Rutile composition (% Anatase); [c] For fcc MoC, determined by XRD ; [d] lattice parameter for fcc MoC.

Figure 15 presents the XRD results obtained for the three catalysts. The crystallite size, lattice parameters, and percentages of the Anatase/Rutile phases are shown in Table 21. XRD analysis shows that the average molybdenum carbide crystallite are < 4 nm. As before, anatase started to convert to rutile when using a reductive-carburizing flow with low concentration of ethane. The A/R composition varied from 74%/26% for $MoC_{20E\text{-}700}/P25TiO_2$ to 55%/45% for $MoC_{5E\text{-}700}/P25TiO_2$ (Table 21). When using higher concentration of ethane, the TiO_2 anatase phase is not strongly affected by the thermal treatment at 700°C. The lattice parameter increases with the carbon content, suggesting that the ratio C/Mo is also increasing and becomes close to the one of $MoC_{20E\text{-}700}/P25TiO_2$.

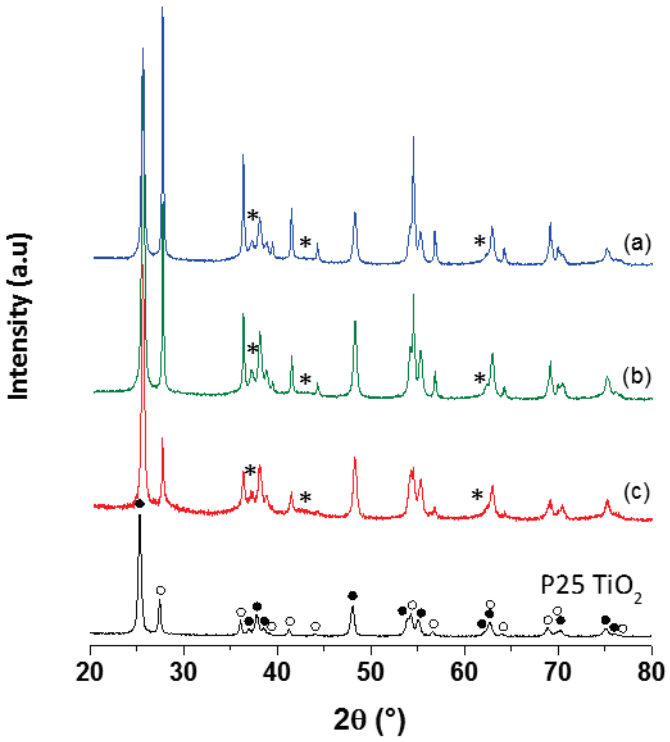

Figure 15 XRD diffraction patterns of the support P25 TiO_2 and the catalysts: a) $MoC_{5E\text{-}700}/P25TiO_2$, b) $MoC_{10E\text{-}700}/P25TiO_2$, and c) $MoC_{20E\text{-}700}/P25TiO_2$. Peaks associated with ● Anatase, ○ Rutile, * Cubic MoC phase.

The low concentrations of ethane (i.e. 5% and 10%) were not fully efficient for the carburization as the carbon content was less than the theoretical content (1.2 wt.% C for 10% wt. MoC/TiO_2) (Table 21). However, full carburization seems to occur with higher concentration of ethane (20% v/v). The carbon content of the catalysts seems similar to the content obtained with the same carbon weight % used in the case of methane (i.e. 20% v/v C_2H_6/H_2 is equivalent to 40% v/v CH_4/H_2).

Figure 16 presents TEM analysis for catalyst $MoC_{10E\text{-}700}/P25TiO_2$ and shows that the molybdenum carbide obtained has a cubic structure system with Fm-3m space group (Table 22). The particle has lattice parameters close to the ones of MoC with a = 4.281 Å (Table 21), as previously observed for the catalysts carburized by methane. The pictures of this catalyst present small particles < 5 nm, in agreement with the XRD

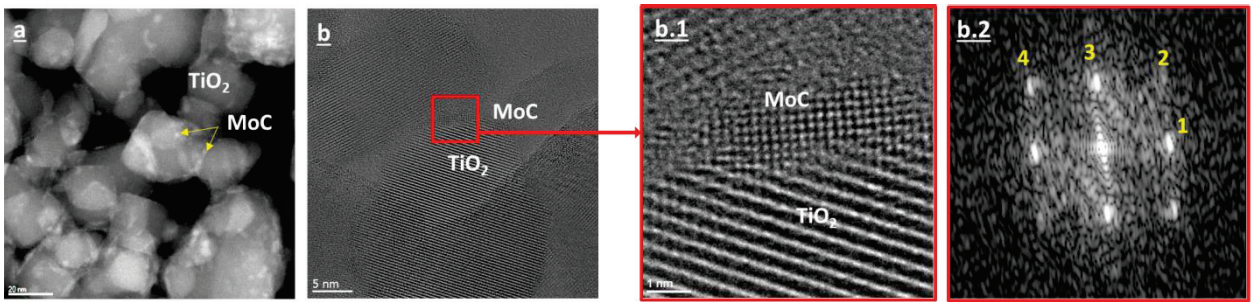

Figure 16 Representative STEM image (a), TEM image (b, b.1), and electron diffraction (b.2) of catalyst $MoC_{10E\text{-}700}/P25TiO_2$.

results.

Table 22 Example of lattice parameters obtained from TEM analysis.

Spot	h k l	α (°)		d (nm)	
		Exp.	Theo.*	Exp.	Theo.*
1	2 0 0	0.00	0.00	0.212	0.214
2	2 2 0	43.62	45.00	0.209	0.214
3	0 2 0	89.63	90.00	0.246	0.247
4	-2 2 0	133.70	135.00	0.147	0.151

* Theoretical values corresponding to cubic MoC, reference ICSD 197178

The XPS results of catalysts $MoC_{5E\text{-}700}/P25TiO_2$ and $MoC_{20E\text{-}700}/P25TiO_2$ are presented in Figure 17 and Table 23. The results show that more $Mo^{\delta+}$ related to molybdenum carbide is present for $MoC_{20E\text{-}700}/P25TiO_2$ than $MoC_{5E\text{-}700}/P25TiO_2$ with less amount of Mo^{4+} and Mo^{6+} related to molybdenum oxides. The C1s spectra show higher amount of graphitic carbon for $MoC_{20E\text{-}700}/P25TiO_2$ that can cover the surface preventing the detection of the actual molybdenum content, leading to less atomic concentration of Mo on the surface.

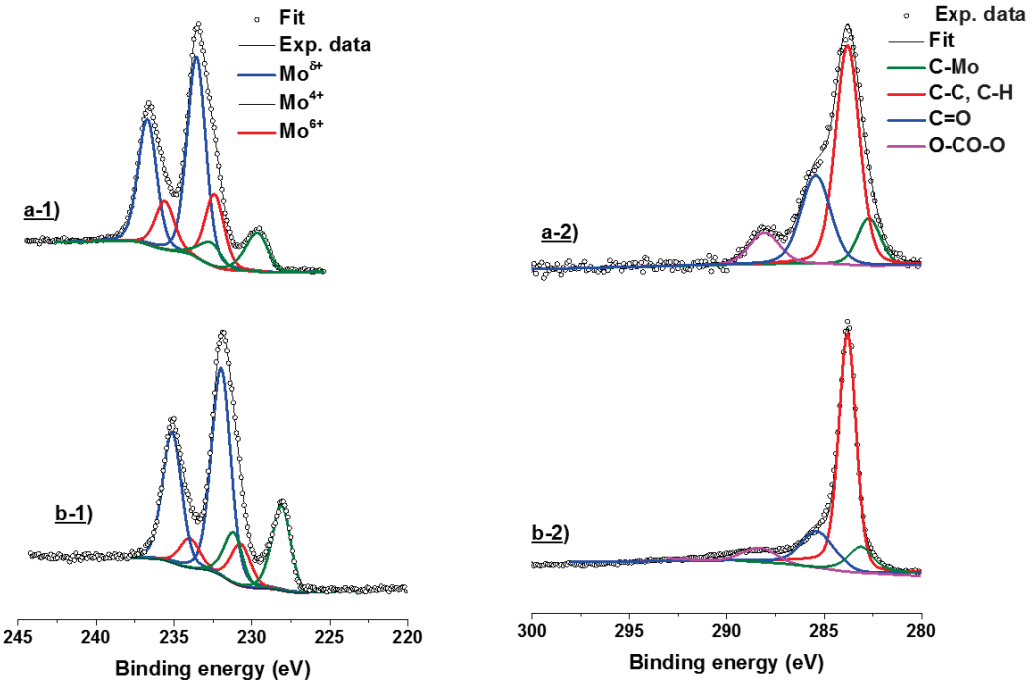

Figure 17 XPS spectra of catalysts a) $MoC_{5E\text{-}700}/P25TiO_2$ and b) $MoC_{20E\text{-}700}/P25TiO_2$ over 1) Mo 3d and 2) C 1s

Table 23 XPS analysis: atomic concentration of Mo and C, and the abundance of Mo and C species in catalysts $MoC_{5E\text{-}700}/P25TiO_2$ and $MoC_{20E\text{-}700}/P25TiO_2$.

	Atomic concentration %		**Mo species %**			**C species %**	
Catalyst	Mo	C	$Mo^{\delta+}$	Mo^{4+}	Mo^{6+}	Carbide	Graphite
$MoC_{5E\text{-}700}/P25TiO_2$	5.2	11.3	14	24	62	11	62
$MoC_{20E\text{-}700}/P25TiO_2$	3.0	33.0	37	14	49	6	80

Moreover, when comparing $MoC_{20E\text{-}700}/P25TiO_2$ with $MoC_{40M\text{-}700}/P25TiO_2$ (Figure 13 and Table 19), which has the same bulk carbon content, the distribution of Mo and C species show more amount of $Mo^{\delta+}$ related to molybdenum carbide and less amounts of Mo^{4+} related to MoO_2 when ethane was used as carbon source.

As the carburization was more efficient with the 20%v/v C_2H_6/H_2, this percentage was used when comparing the other parameters of preparation.

I.1.2.2. Effect of the maximum carburization temperature

Two other catalysts were prepared with 20% ethane and carburized at 600 °C and 800 °C to compare the effect of carburizing temperature.

Table 24 Characterizations of catalysts prepared at different carburizing temperatures.

Catalyst	% Mo[a]	% C[a]	% A/R[b]	Crystallite size[c] (nm)	a[d] (Å)
$MoC_{20E-600}/P25TiO_2$	9.7	0.8	75	3	n.a.
$MoC_{20E-700}/P25TiO_2$	9.4	1.2	74	3	4.256
$MoC_{20E-800}/P25TiO_2$	8.9	1.4	n.a.	n.a.	n.a.

[a] Weight percentage; [b] Anatase/Rutile composition (% Anatase); [c] For fcc MoC, determined by XRD ; [d] lattice parameter for fcc MoC; n.a.: not available.

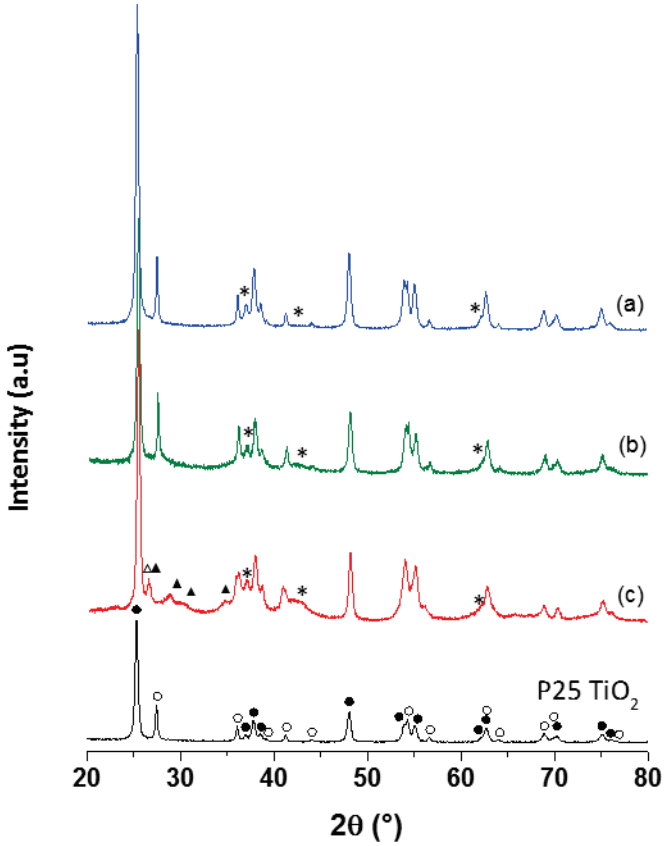

Figure 18 XRD diffraction patterns of the support P25 TiO_2 and the catalysts: a) $MoC_{20E-600}/P25TiO_2$, b) $MoC_{20E-700}/P25TiO_2$, and c) $MoC_{20E-800}/P25TiO_2$. Peaks associated with ● Anatase TiO_2, ○ Rutile TiO_2, ▲ Ti_5O_9, △ Ti_4O_7, * Cubic MoC phase.

The catalyst prepared at 600 °C has 0.8 % of carbon which is less than the theoretical amount for 10% w/w MoC/TiO_2 of ratio one. The XRD diffraction pattern (Figure 18-a) presents a really small peak associated with cubic MoC, which does not allow us to calculate the lattice parameters. With the detection of MoO_2 being difficult, it is hard to conclude if the reduction-carburization is complete under these conditions for this catalyst.

The catalysts prepared at 700°C and 800°C have similar carbon content (Table 24), and their diffraction patterns present the peak associated with cubic MoC. However, in catalyst $MoC_{20E\text{-}800}/P25TiO_2$ the TiO_2 is partially reduced to Ti_5O_9 and Ti_4O_7 (Figure 18-c). In this case the transformation is less prominent than in the case of methane as the anatase phase does not seem to be strongly affected. This could be due the presence of more carbon that retards the transformation [168].

As expected, for a defined temperature, higher carburization was achieved using ethane instead of methane, the difference is more pronounced when low carburization temperature was used (600 °C).

These results suggest that a treatment at 600°C using ethane carbion source is not efficient for the full carburization of molybdenum oxides in our conditions, as was observed for methane as carbon source; and that 800°C is higher than the desired temperature as the support starts to be altered. Accordingly we kept using 700°C as an optimum temperature for the TPRC process.

I.2. Effect of the Nature of the support

Besides P25 TiO_2, two other supports were used to investigate the effect of the support. DT51 TiO_2 consists only of the anatase phase and has higher surface area (92 m^2/g) than P25 TiO_2 (55 m^2/g). ZrO_2 of surface area 129 m^2/g was also tested as a support for comparison (only in case of ethane).

Table 25 characterizations of catalysts prepared with 20% v/v hydrocarbon at 700 °C on different supports

Catalyst	% Mo[a]	% C[a]	S[b] (m^2/g)	Crystallite size[c] (nm)	a[d] (Å)
$MoC_{20E\text{-}700}/P25TiO_2$	9.4	1.2	49	3	4.270
$MoC_{20E\text{-}700}/DT51TiO_2$	9.1	1.6	84	2	4.251
$MoC_{20E\text{-}700}/ZrO_2$	9.2	2.1	129	2	4.187
$MoC_{20M\text{-}700}/P25TiO_2$	9.5	0.6	n.d.	3	4.256
$MoC_{20M\text{-}700}/DT51TiO_2$	9.5	0.8	n.d.	2	4.237

[a] Weight percentage; [b] BET surface area, [c] For fcc MoC, determined by XRD ; [d] lattice parameter for fcc MoC, n.d.: not determined

The catalysts were prepared using 20 % C_2H_6 and 700 °C carburization temperature. The analysis of the diffraction pattern associated with catalysts supported on DT51TiO_2 is easier than the ones for the catalysts supported on P25 due to the absence of the peaks corresponding to rutile phase. The peak corresponding to cubic MoC at 2θ = 42.2° could be observed better as shown in Figure 19-d and e corresponding to catalysts $MoC_{20E\text{-}700}$/DT51TiO_2 and $MoC_{20M\text{-}700}$/DT51TiO_2 respectively. The lattice parameters obtained match the one associated with MoC (Table 25).

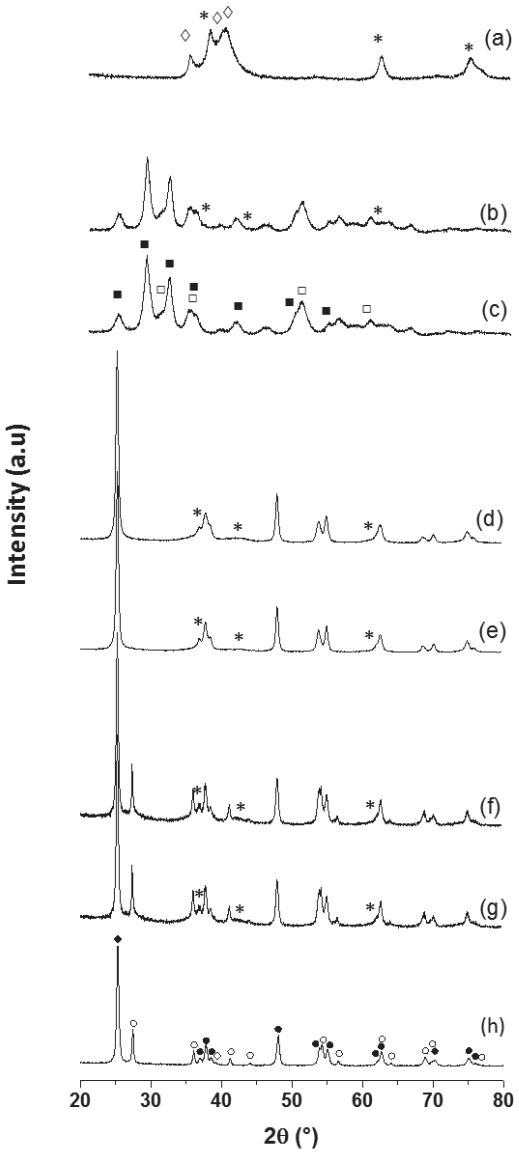

Figure 19 XRD diffractograms of a) Bulk MoC, b) $MoC_{20E\text{-}700}/ZrO_2$, c) ZrO_2, d) $MoC_{20E\text{-}700}$/DT51TiO_2, e) $MoC_{20M\text{-}700}$/DT51TiO_2 f) $MoC_{20E\text{-}700}$/P25TiO_2, g) $MoC_{20M\text{-}700}$/P25TiO_2, h) P25 TiO_2. Peaks associated with ● Anatase TiO_2, ○ Rutile TiO_2, ■ Monoclinic ZrO_2, □ Tetragonal ZrO_2 , * Fcc MoC, ◊Hexagonal Mo_2C.

For catalyst $MoC_{20E\text{-}700}/ZrO_2$, the XRD pattern (Figure 19-b) presents mainly the peaks associated with the ZrO_2 support (Figure 19-c). The most significant peaks of the monoclinic phase are at 28.2°, 31.5°, and 49.2°, and those of the tetragonal phase are at 30.2°, 50.1°, and 60.1°. The Rietveld analysis suggests that the catalyst possesses molybdenum carbide with a cubic structure. However the peaks again overlap with the ones from the support. The lattice parameter (a = 4.187 Å) is close to the one reported for $MoC_{0.5}$ and lower than all the ones obtained for MoC/TiO_2 (4.227-4.270 Å). This result suggests that the carburization is low, despite the high carbon content observed by elemental analysis (Table 25). This is in agreement with Adesina et al. where they reported that the carburization rate of supported cubic MoC_{1-x} was the highest on the TiO_2 support followed by SiO_2, ZrO_2, and Al_2O_3 [31], however the carbon content in the catalysts was not provided. The atomic numbers of Mo (42) and Zr (40) are too close to each other, hence the contrast was too low by microscopy and the STEM-TEM analysis was not possible for this sample.

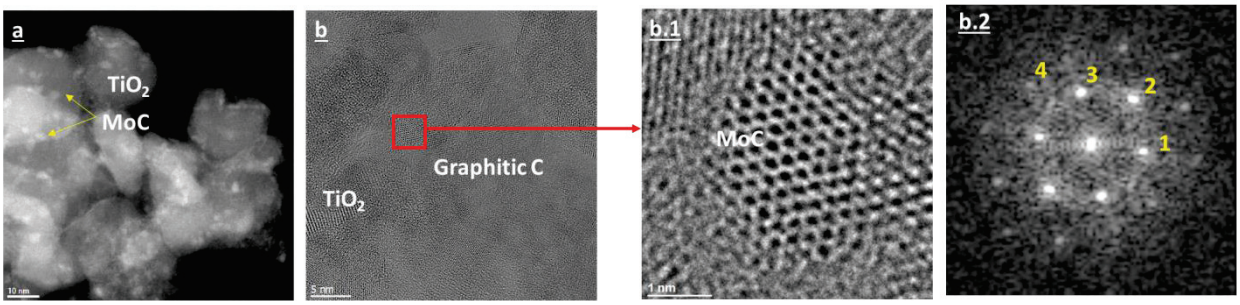

Figure 20 Representative STEM image (a), TEM image (b, b.1), and electron diffraction (b2) of catalyst $MoC_{20E\text{-}700}/DT51TiO_2$.

Table 26 Example of lattice parameters obtained from TEM analysis

Spot	h k l	α (°)		d (nm)	
		Exp.	Theo.*	Exp.	Theo.*
1	1 1 -1	0.00	0.00	0.248	0.247
2	2 0 0	54.89	54.74	0.213	0.214
3	1 -1 1	109.04	109.47	0.246	0.247
4	0 -2 2	144.49	144.74	0.151	0.151

* Theoretical values corresponding to cubic MoC, reference ICSD 197178

The STEM pictures of catalyst $MoC_{20E\text{-}700}/DT51TiO_2$ (Figure 20-a) show that the catalyst exhibits small particles dispersed on the surface of the support. As for the

catalysts supported on TiO_2 P25, molybdenum carbide exhibits cubic structure, confirmed by TEM analysis (Figure 20-b-2,Table 26), and the particles size was < 5 nm. The carbon content in this catalyst was in excess (1.6%) (Table 25) which is consistent with the graphitic carbon observed on the surface by TEM.

The BET surface area measured for the three catalysts is equivalent to, or slightly less than the surface area of the corresponding supports (Table 25).

An unsupported catalyst ($MoC_{20E-700}$) was prepared for comparison. It was synthesized via the same preparation procedure of TPRC, starting from ammonium molybdate tetrahydrate precursor. As shown in Figure 19-a, this catalyst possessed a mixture of hexagonal and cubic MoC. In a like manner, Christopheletti et al. obtained hexagonal molybdenum carbide by 20% v/v CH_4/H_2 at 10 °C/min till 700°C with 3 h holding time, whereas the same procedure for alumina-supported material gave cubic molybdenum carbide [58]. Thus, the presence of the support must affect the carburization process.

To summarize, a series of 15 catalysts were synthesized by impregnation followed by TPRC. The XRD and TEM analysis showed that supported MoC exhibits fcc structure. It was difficult to estimate the degree of carburization, i.e. Mo/C stoichiometry due to the possible presence of free carbon at the surface. However the determined lattice parameters suggest the formation of MoC. The degree of carburization increased with the temperature and hydrocarbon content. However at 800°C the support was drastically altered.

From this part, we conclude that as a carburizing gas, ethane was better than methane for the preparation of molybdenum carbides supported on P25 TiO_2 with 20% v/v; and 700°C maximum temperature was the best carburizing temperature (with 0.5°C/min heating ramp, and GHSV of 1091 h^{-1}). Furthermore, the presence of the support does affect the phase of the carbides obtained. Cubic carbides are obtained on the supported material, and mixture of cubic and hexagonal was obtained in the bulk one.

II. Catalytic testing: Aqueous phase hydrogenation of succinic acid

The different catalysts described in the previous part were tested for the hydrogenation of succinic acid in aqueous phase (Scheme 14). The reactions were carried out at 240 °C and under 150 bar, using 600 mg of catalyst and the products were analyzed over two days by GC and HPLC taking periodic liquid samples through the day.

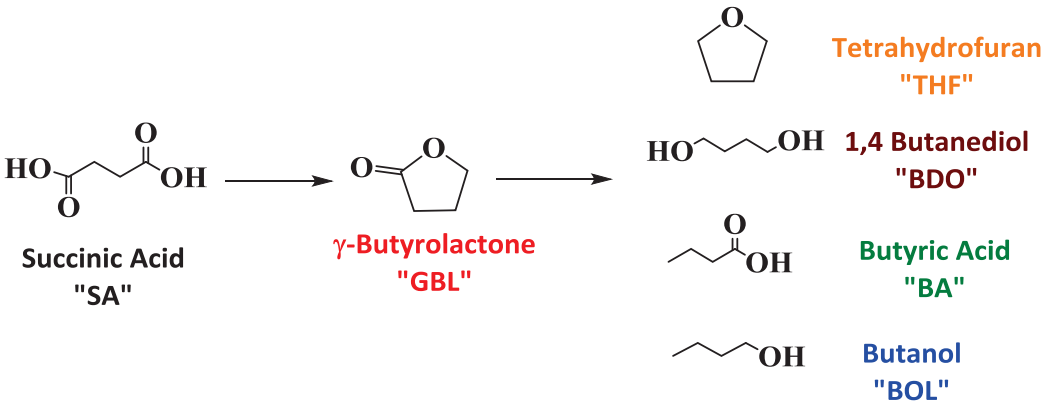

Scheme 14 General reaction scheme for the hydrogenation of succinic acid.

II.1. Catalysts prepared by methane

II.1.1. Testing the influence of methane concentration in the reductive-carburizing gas

Three reactions were done using the catalysts prepared with different methane concentrations: $MoC_{10M\text{-}700}/P25TiO_2$, $MoC_{20M\text{-}700}/P25TiO_2$, and $MoC_{40M\text{-}700}/P25TiO_2$ that are characterized before.

The results are shown by reporting the remaining amount of succinic acid as well as the selectivity to the main products obtained over time. The calculated carbon balance was also reported. Regardless the catalyst used, the carbon balance was c.a 100 % indicating that there is no loss of carbon in gas phase.

Figure 21 shows the conversion of succinic acid obtained over the three catalysts along with the corresponding products selectivities. After 46 hours, 38% of SA was converted using catalyst $MoC_{10M\text{-}700}/P25TiO_2$, whereas over catalyst $MoC_{20M\text{-}700}/P25TiO_2$, 70% of SA was converted, and 98% conversion was observed with $MoC_{40M\text{-}700}/P25TiO_2$ catalyst. The catalysts activity increased with the increase of methane

percentage in the gas mixture during their reduction-carburization. This was expected as the catalysts prepared with the higher concentrations were the ones with the higher degree of carburization, as discussed in the previous section. Moreover, constant reaction rate was observed with time regardless the catalyst, which indicates that there is no deactivation of the catalysts.

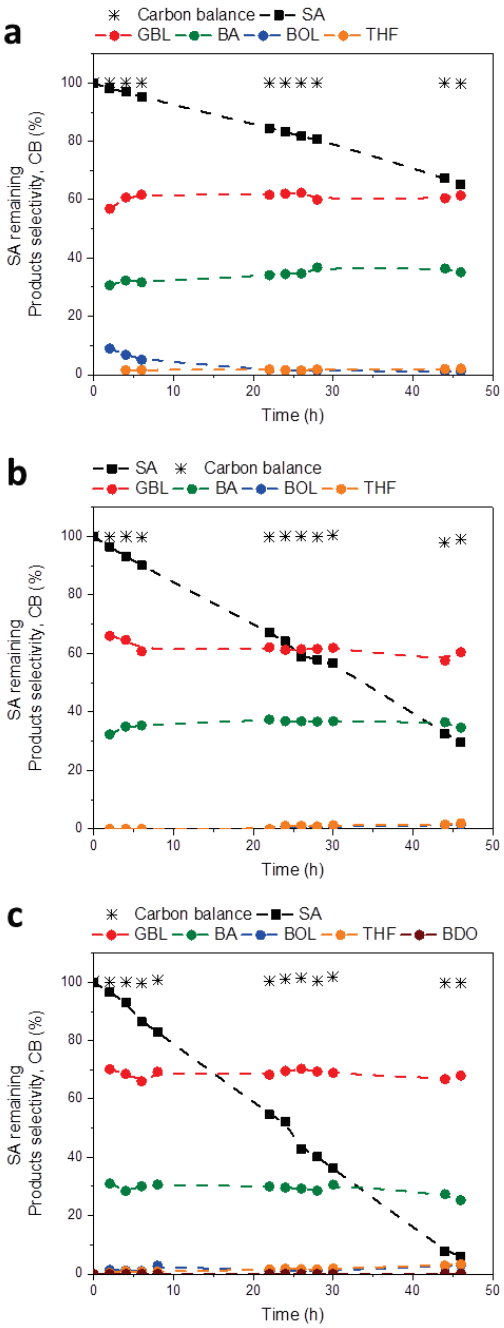

Figure 21 Hydrogenation of succinic acid over a) $MoC_{10M\text{-}700}/P25TiO_2$ b) $MoC_{20M\text{-}700}/P25TiO_2$ and c) $MoC_{40M\text{-}700}/P25TiO_2$ at 240 °C under 150 bar H_2: temporal evolution of the remaining concentrations of SA, the products selectivity and the carbon balance (CB). Aqueous solution of SA (0.12-0.13 M, 100 mL), 0.6 g of catalyst.

With the three catalysts, the products selectivity was distributed between GBL and unexpectedly BA. GBL was the major product (60-70% selectivity) and BA was the other main product (28-32% selectivity). Both products were formed simultaneously since the beginning of the reaction and constant selectivity (± 5 %) was observed over conversion. Low amounts of THF, BOL, and traces of BDO were obtained at the end of the reactions.

The selectivity to the products among the three catalysts was distinct from the results reported in literature for SA hydrogenation over precious metal catalysts. For example, at 160 °C and 150 bar over Pd/TiO_2, SA is converted to GBL with 94% selectivity [104]; under the same reaction conditions, introducing Re to this catalyst favoured the conversion of GBL to BDO with 83% selectivity [113]. On the other hand, using Re/C at 240 °C and under 80 bar of H_2 generated THF with 86% selectivity [111]. In the literature dealing with the hydrogenation of SA, BA is usually not observed unless as byproduct. A couple of studies report the formation of small amounts of BA (< 3%), e.g. over Au-Pt/TiO_2 [94], Pd-ReO_x/TiO_2 [105], FeO_x/C + Pd/C [109], and Pd/SiO_2-NH_2 [175]. A combined selectivity of 18% towards propionic acid and butyric acid (at 80% conversion) was reported during the hydrogenation of SA over Pd/alumina xerogel, in dioxane (P_{H2} = 60 bar, T = 240 °C) [176].

Butyric acid has many uses in different industries, and currently there is a great interest in using it as a precursor to biofuels [177]. In pharmaceutical industry, BA is known for its anticancer effects [177]. In the chemical industry, the primary application of butyric acid is in the manufacture of cellulose acetate butyrate plastics [178]. Furthermore, although butyric acid itself has an unpleasant odor, butyric acid esters such as methyl and ethyl butyrates are used as fragrant and flavoring agents [177]. Currently, BA is mainly produced by oxidation of butyraldehyde that is obtained from propylene derived from crude oil by oxosynthesis [179]. Nevertheless, as for all derivatives of crude oil, concerns arise concerning the increasing petroleum prices and availability along with the growing need for clean energy sources. The production of BA from renewable resources is receiving growing interest from the scientific community and the industry. Many attempts are reported to produce BA from renewable alternatives such as biomass through biological fermentation (e.g. glucose fermentation using bacteria) [179,180], however these processes are still relatively costly and the

chemical synthesis of BA still seems more viable [177].

In summary, after testing the three catalysts prepared by different methane concentrations, we showed that the conversions follow the order: $MoC_{40M\text{-}700}/P25TiO_2$ > $MoC_{20M\text{-}700}/P25TiO_2$ > $MoC_{10M\text{-}700}/P25TiO_2$. Therefore, increasing methane concentration produces better carburized catalyst and thus increases the catalytic activity in SA hydrogenation. The products selectivities seem to be not significantly affected with the change of methane concentration, for which the difference among the catalysts was within 10%.

The reaction pathway is further discussed in Chapter 4.

II.1.2. **Testing the influence of carburizing temperature**

The performance of $MoC_{20M\text{-}700}/P25TiO_2$ was compared with the two other catalysts prepared at lower (600°C) or higher temperature (800°C) of carburization.

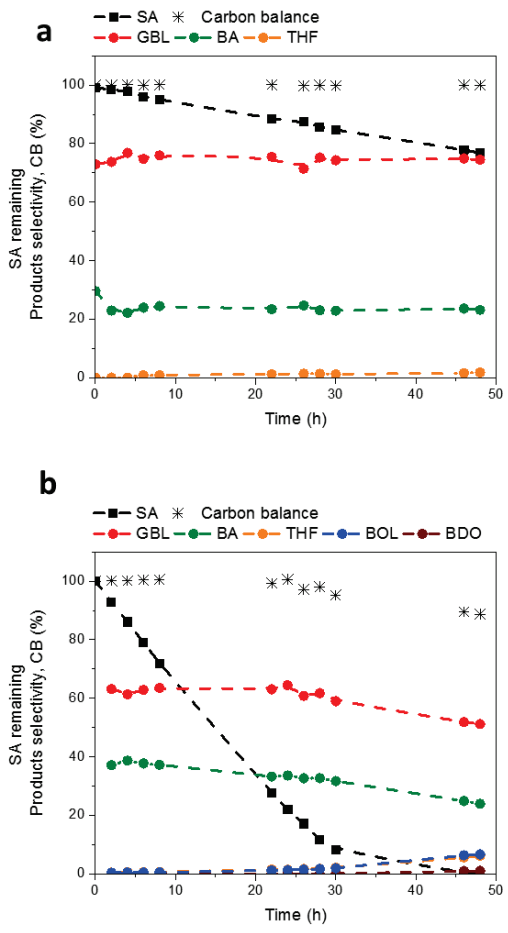

Figure 22 Hydrogenation of succinic acid over a) $MoC_{20M\text{-}600}/P25TiO_2$ and b) $MoC_{20M\text{-}800}/P25TiO_2$ at 240 °C and under 150 bar H_2: temporal evolution of the remaining concentrations of SA, the products selectivity and the carbon balance (CB). Aqueous solution of SA (0.12-0.13 M, 100 mL), 0.6 g of catalyst.

As expected, catalyst $MoC_{20M-600}/P25TiO_2$ was less active in the reaction probably because it is not well carburized. After 46 hours, only 23% of SA was converted with about 74% selectivity to GBL and 23% BA (Figure 22-a). On the other hand, catalyst $MoC_{20M-800}/P25TiO_2$ was more active than the two other catalysts prepared at lower temperatures, the conversion of SA was complete at 46 hours (Figure 22-b). For conversion under 95%, the products selectivity was around 60% and 40% for GBL and BA, respectively; this is similar to what was obtained over $MoC_{20M-700}/P25TiO_2$. However at the end of the reaction, GBL and BA started to be converted to BOL and THF. This was accompanied with a slight decrease in carbon balance when SA was fully converted. $MoC_{20M-700}/P25TiO_2$ and $MoC_{20M-800}/P25TiO_2$ possess similar carbon contents, but the significant modification of the TiO_2 support might modify the reactivity of the catalyst.

The conversions follow the order: $MoC_{20M-800}/P25TiO_2 > MoC_{20M-700}/P25TiO_2 > MoC_{20M-600}/P25TiO_2$ and the selectivity to BA decreases in favor to GBL in the same order. Increasing the maximum temperature during carburization gives more active catalyst in SA hydrogenation reaction which can be linked to an increase in the degree of carburization. Although the catalyst carburized at 800°C showed good conversion, undesired transformation of the support is observed. Moreover, as deep characterizations are not done in this study, it was hard to figure out the cause behind the better performance of this catalyst.

II.2. **Catalysts prepared by ethane**

II.2.1. **Testing the influence of ethane concentration in the reductive-carburizing gas**

The three catalysts prepared with different ethane concentrations were tested in SA hydrogenation reaction under the same conditions as before (Figure 23). After 46 hours, 42% of SA was converted using catalyst $MoC_{5E-700}/P25TiO_2$. With catalyst $MoC_{10E-700}/P25TiO_2$, 80% SA was converted after 46 hours, whereas full conversion was achieved with $MoC_{20E-700}/P25TiO_2$. As with the case of methane, the catalytic activity increases with the increase of ethane percentage used during carburization process. Moreover the catalysts synthesized with the same amount of carbon in the feed present similar conversion: 20% ethane and 40% methane (conversion ≈ 96%); 10% ethane and 20 % methane (conversion ≈ 75%); 5% ethane and 10% methane (conversion ≈ 40%).

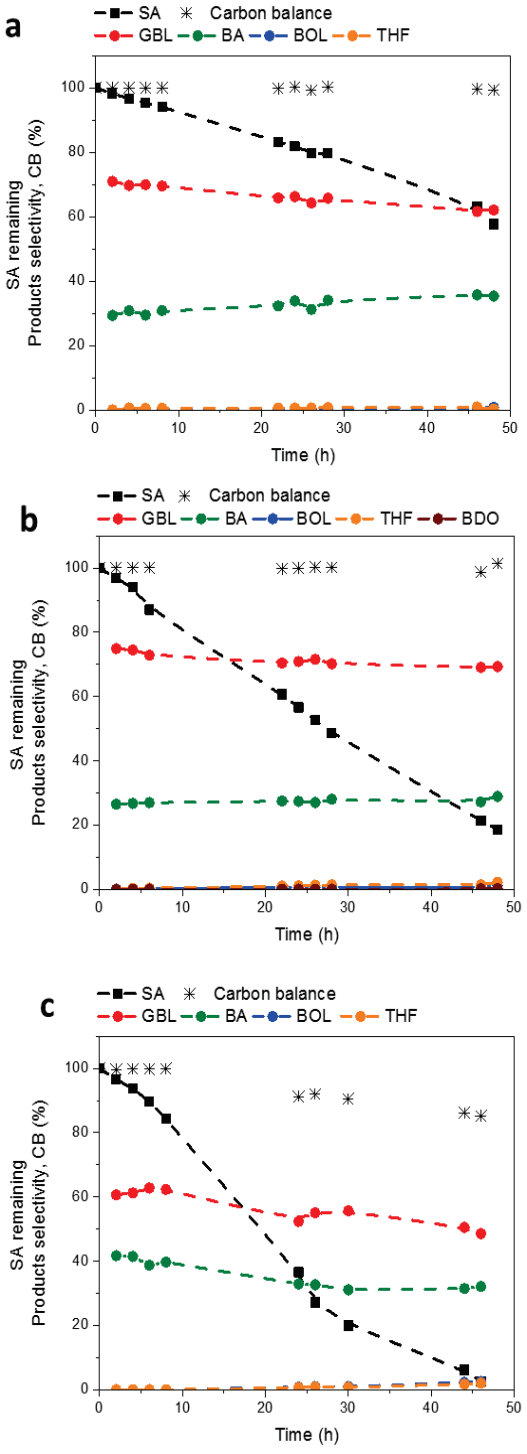

Figure 23 Hydrogenation of succinic acid over a)$MoC_{5E\text{-}700}/P25TiO_2$, b)$MoC_{10E\text{-}700}/P25TiO_2$ and b)$MoC_{20E\text{-}700}/P25TiO_2$ at 240 °C and under 150 bar H_2: temporal evolution of the remaining concentrations of SA, the products selectivity and the carbon balance (CB). Aqueous solution of SA (0.12-0.13, 100 mL), 0.6 g of catalyst.

The products distribution was mainly composed of GBL and BA for the three catalysts. GBL was the major product over $MoC_{5E\text{-}700}/P25TiO_2$ and $MoC_{10E\text{-}700}/P25TiO_2$ (62-69% selectivity) and BA was the second main product (35-29% selectivity). Few amounts of

THF, BOL, and traces of BDO were obtained at the end of the reactions. However for $MoC_{20E-700}/P25TiO_2$ lower GBL selectivity (still the major product) with higher BA selectivity was obtained (49% and 32% respectively) but this was associated with slight decrease in the carbon balance.

Increasing ethane concentration in the preparation of the catalyst led to more complete carburization as shown by elemental analysis, XRD and XPS, and accordingly higher conversions are obtained in SA hydrogenation.

II.2.2. **Testing the influence of carburization temperature**

The catalyst $MoC_{20E-600}/P25TiO_2$ prepared at 600°C was less carburized and it was less active in the reaction of hydrogenation of SA than $MoC_{20E-700}/P25TiO_2$. Around 30% of SA was converted after 46 hours of reaction. On the other hand, catalyst $MoC_{20E-800}/P25TiO_2$ prepared at 800°C gave full conversion after 46 hours (Figure 24). The

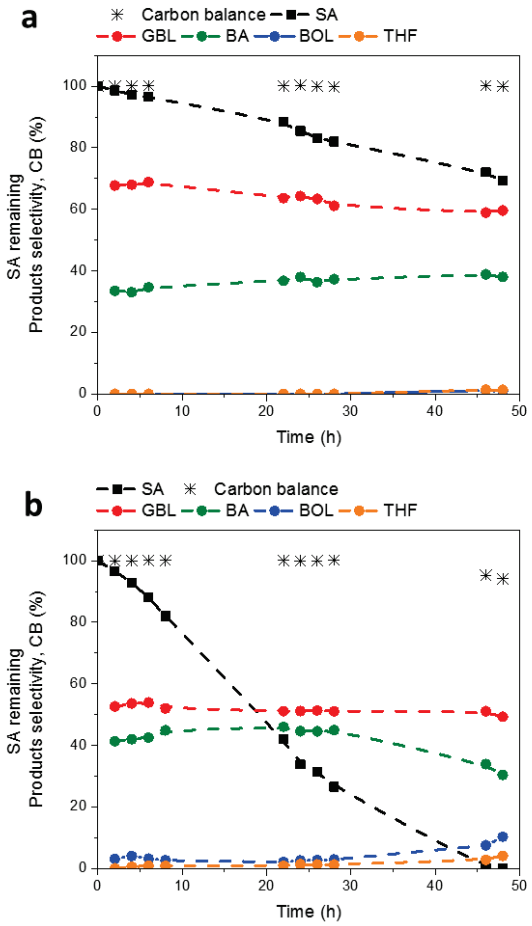

Figure 24 Hydrogenation of succinic acid over a)$MoC_{20E-600}/P25TiO_2$ and b)$MoC_{20E-800}/P25TiO_2$ at 240 °C and under 150 bar H_2: temporal evolution of the remaining concentrations of SA, the products selectivity and the carbon balance (CB). Aqueous solution of SA (0.12-0.13 M, 100 mL), 0.6 g of catalyst

conversions follow the same order as for methane where: $MoC_{20E\text{-}800}/P25TiO_2 > MoC_{20E\text{-}700}/P25TiO_2 > MoC_{20E\text{-}600}/P25TiO_2$.

Thus, regardless the nature of the gas, higher carburization temperature leads to higher degree of carburization as shown by elemental analysis, XRD and XPS analysis. Furthermore, the catalysts that are carburized at higher temperature were more active in SA hydrogenation reaction. A direct link between the degree of carburization and the activity of the catalyst in this reaction can be suggested.

With the three catalysts, GBL is the main product, but the level of selectivity is different. More GBL is produced with catalyst $MoC_{20E\text{-}600}/P25TiO_2$ (60% selectivity) compared to 49% for $MoC_{20E\text{-}700}/P25TiO_2$ and 45% with catalyst $MoC_{20E\text{-}800}/P25TiO_2$. In agreement with the trend shown by increasing the temperature using methane carbon source, the order suggest that the selectivity is related to the degree of carburization or carbon content, as more BA is produced when more carbon is present. Yet this cannot be fully confirmed at this stage especially with low conversions (with catalysts of very low carbon content) where selectivity becomes less accurate.

The higher temperature during carburization enhances the reactivity of the catalyst which is due to the possible reduction of the inactive MoO_2 and better carburization of the catalyst. However, as discussed in the characterization part, TiO_2 support undergoes modification at 800°C. This makes the analysis of the results obtained more difficult to analyze as these changes in the support may play a role in changing reactivity of the catalyst. This was not the focus of our study and thus it was better to avoid this high carburization temperature to narrow the factors that are playing a role in the conversion of SA and selectivity to the products.

II.3. **Testing the effect of the support**

The influence of parameters of synthesis of the supported carbide catalysts was studied over P25 TiO_2. In this section, two more supports were tested to investigate the effect of the nature of support on the performance of the catalysts. For comparison, bulk molybdenum carbide catalyst was also evaluated.

The previous characterization of the two catalysts $MoC_{20E\text{-}700}/P25TiO_2$ and $MoC_{20E\text{-}700}/DT51TiO_2$ showed that there is no modification of the crystallite phase of MoC under the conditions of preparation. The crystallite size was estimated around 3 nm in both catalysts, and the carbon content was higher in $MoC_{20E\text{-}700}/DT51TiO_2$ catalyst.

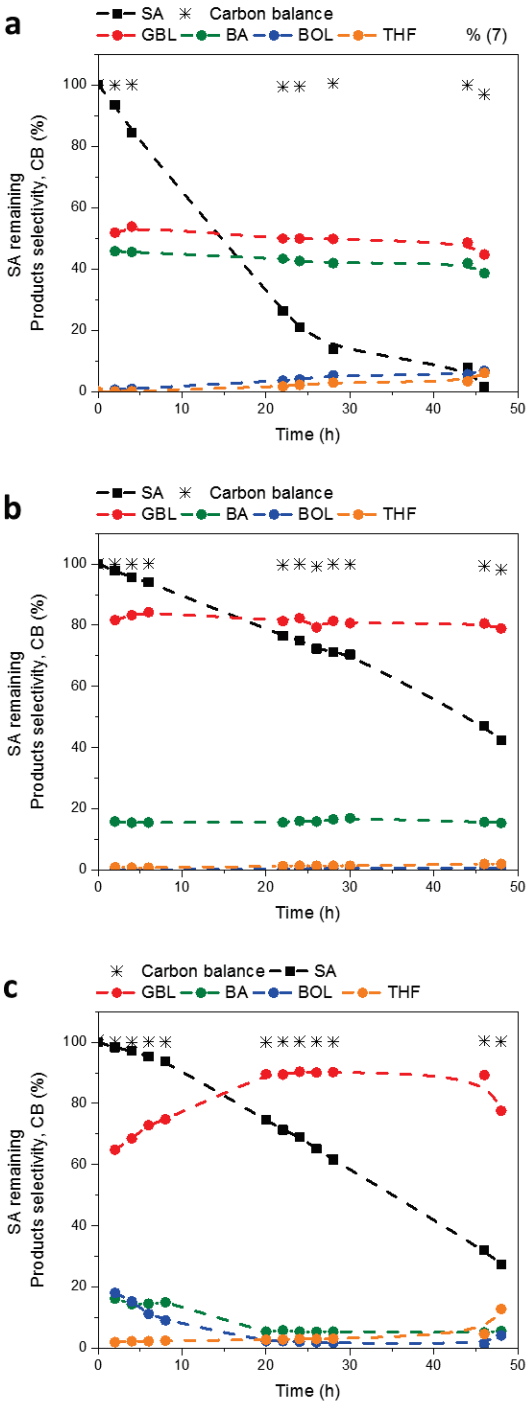

Figure 25 Hydrogenation of succinic acid over a)$MoC_{20E\text{-}700}/DT51TiO_2$, b)$MoC_{20E\text{-}700}/ZrO_2$, and c) $MoC_{20E\text{-}700}$ at 240 °C and under 150 bar H_2: temporal evolution of the remaining concentrations of SA, the products selectivity and the carbon balance (CB). Aqueous solution of SA (0.12-0.13 M, 100 mL), 0.6 g of catalyst (a and b), and 0.06 g of catalyst (c).

Figure 25-a shows the conversion of SA and selectivity to the products obtained over $MoC_{20E\text{-}700}/DT51TiO_2$ catalyst, which is to be compared with the result over $MoC_{20E\text{-}700}/P25TiO_2$ previously shown in Figure 23-c. Initially, the activity was higher with $MoC_{20E\text{-}700}/DT51TiO_2$ than $MoC_{20E\text{-}700}/P25TiO_2$ catalyst (conversion at 6h ≈ 20 % and 10 % respectively), but after 46 h reaction, similar conversions were achieved (> 97 %). Catalyst $MoC_{20E\text{-}700}/DT51TiO_2$ showed slightly higher selectivity to BA than catalyst $MoC_{20E\text{-}700}/P25TiO_2$ accompanied with slightly lower selectivity to GBL, giving close selectivity values for both products. Furthermore, with $MoC_{20E\text{-}700}/DT51TiO_2$ the amount of BOL and THF was higher but still < 7% (cf Table 27).

Alternatively, ZrO_2 support - also known as stable oxide support used for SA hydrogenation with supported noble metal catalysts - was evaluated. The characterizations of MoC/ZrO_2 catalyst showed more carbon amount but a lower degree of carburization when carburized under the same conditions as the two other catalysts supported on TiO_2.

Figure 25-b shows that this catalyst is much less efficient compared to $MoC_{20E\text{-}700}/DT51TiO_2$ and $MoC_{20E\text{-}700}/P25TiO_2$. After 46 h, SA conversion reached only 58 %. The more important difference is in the selectivity, this catalyst showed remarkable selectivity to GBL (80 %) with much less amount of BA.

Indeed, the selectivity observed with ZrO_2-supported catalyst is close to the one obtained with the unsupported MoC catalyst (Figure 25-c). For this latter one, the selectivity to GBL is even more pronounced and reached 89 % while BA selectivity is very low (< 5%). A reported work of Christofoletti comparing unsupported Mo_2C with the alumina supported catalyst showed that Mo_2C/Al_2O_3 was more active than the bulk catalyst in methane steam reforming. They suggested that the greater activity of the supported catalysts may be related to the higher activity of the cubic MoC species present in Mo_2C/Al_2O_3 samples, compared to the hexagonal Mo_2C species present in the unsupported material, or to the higher dispersion of the cubic MoC in the supported catalyst, knowing that the alumina support was not active in the reaction.

The above results show that for SA hydrogenation reaction the support does play a role in the activity and selectivity delivered by molybdenum carbide catalysts. Further

work is needed to characterize deeper the catalysts and establish the interactions between molybdenum carbide and the supports, and thus figure out what is the most important parameter influencing the catalytic behavior.

III. Conclusion

Screening for the best preparation conditions needed for the use of molybdenum carbide catalysts in SA hydrogenation showed that the catalytic response can be linked to the degree of carburization where catalysts reactivity increased with the increase in the degree of carburization.

Table 27 Catalytic results of succinic acid hydrogenation over molybdenum carbide catalysts prepared via different TPRC synthesis conditions and different supports.

	SA conversion		Products selectivity at 46 h			
Catalyst	**At 6 h**	**At 46 h**	**GBL**	**BA**	**BOL**	**THF**
$MoC_{10M\text{-}700}/P25TiO_2$	5	35	61	35	< 5	< 5
$MoC_{20M\text{-}700}/P25TiO_2$	10	70	60	36	< 5	< 5
$MoC_{40M\text{-}700}/P25TiO_2$	13	94	68	25	< 5	< 5
$MoC_{20M\text{-}600}/P25TiO_2$	4	23	74	23	7	6
$MoC_{20M\text{-}800}/P25TiO_2$	21	100	51	24	< 5	< 5
$MoC_{5E\text{-}700}/P25TiO_2$	5	42	62	35	< 5	< 5
$MoC_{10E\text{-}700}/P25TiO_2$	13	81	69	29	< 5	< 5
$MoC_{20E\text{-}700}/P25TiO_2$	10	97	49	32	< 5	< 5
$MoC_{20E\text{-}600}/P25TiO_2$	< 5	31	60	38	< 5	< 5
$MoC_{20E\text{-}800}/P25TiO_2$	12	100	50	30	10	< 5
$MoC_{20E\text{-}700}/DT51TiO_2$	20	99	45	39	7	6
$MoC_{20E\text{-}700}/ZrO_2$	6	58	80	15	< 5	< 5
$MoC_{20E\text{-}700}$	5	68	89	5	< 5	< 5

In general, ethane carbon source was more efficient than methane in preparing well carburized catalyst with MoC ratio close to one. Increasing the hydrocarbon percentage in the carburizing gas lead to more active catalyst regardless the hydrocarbon nature. Similarly, increasing the temperature of carburization increased the amount of carbon in the catalysts, and significant influence on the catalytic activity was observed. The catalysts prepared at lower carburization temperatures, whatever the hydrocarbon nature, were much less active than the two other catalysts prepared at higher temperatures. On the other hand, the high temperature lead to drastic modifications in the P25 TiO_2 support that was more significant when methane was the carbon source. The catalytic results obtained over the different catalysts are summarized in Table 27. For all the reactions the selectivity seems to be constant up to 95% conversion. Afterwards, THF and BOL are formed and the carbon balance starts decreasing.

The support seems playing significant role in the activity and selectivity of the catalyst, but still requires further investigations that were not done in our study, since only preliminary work was done on the DT51 TiO_2 and ZrO_2 supports for comparison.

As BA was observed in significant quantities for all the catalysts supported on titania, which was unexpected, we thus focus more in the following chapter on the reaction pathway. We also show the optimization of the reaction conditions, in addition to the recyclability of the catalyst. These are done with series of $MoC_{20E\text{-}700}/P25TiO_2$ catalyst for which GHSV is varied during the preparation.

CHAPTER 4.

TiO_2-supported molybdenum carbide catalyst for succinic acid hydrogenation: optimization of the catalyst and the reaction conditions

In this chapter, the TPRC was optimized by changing the gas hourly space velocity (GHSV) during the preparation and the catalytic activity of the material was evaluated for aqueous phase hydrogenation of succinic acid at 160-240 °C, and 90-150 bar of H_2 in batch reactor. The effects of reaction conditions, and some of the preparation parameters (GHSV and passivation), on the catalysts and their catalytic performance in terms of activity, and selectivity to the products were investigated. The reaction pathway is suggested according to the reactions conducted from each of the products obtained. And finally, the stability of the catalyst was studied under the harsh reaction conditions (240 °C, 150 bar H_2, in water).

I. Preparation of MoC/TiO_2 catalysts by TPRC

TiO_2-supported molybdenum carbides "MoC/TiO_2" were prepared by impregnation of Mo salt on P25 TiO_2 support, followed by temperature programmed reduction-carburization (TPRC) as previously described. In Chapter 3, the hydrocarbon, the composition of the gas mixture and the maximum temperature were optimized in order to obtain well carburized catalysts which exhibit good reactivity in SA hydrogenation. Thus the catalysts used in this chapter are according to the optimized conditions: 20%v/v C_2H_6/H_2 while heating the sample at 0.5 °C/min till 700°C using P25 TiO_2 support and 12% w/w Mo.

For this kind of catalysts the parameter of gas hourly space velocity -which is the quotient of the entering reactive gas to the catalyst bed volume- might have a remarkable

impact on the prepared material. Actually, the effect of GHSV has been studied for bulk molybdenum nitrides. It has been demonstrated that a decrease in space velocity during the preparation causes a drop in surface area. The use of high space velocities would facilitate the removal of H_2O from the vicinity of the solid surface, thus reducing the potential for hydrothermal sintering [181,182]. However, we could not find any report on the effect of GHSV on the synthesis of supported molybdenum carbides. In the case of carbides, the GHSV factor might also affect the carbon content of the catalyst which in turn might affect the catalytic performance.

I.1. The effect of the gas hourly space velocity (GHSV) in catalysts preparation

To evaluate this parameter, a series of TiO_2-supported molybdenum carbide catalysts were synthesized by changing the GHSV (1091 h^{-1}, 1527 h^{-1}, 2545 h^{-1}, and 7636 h^{-1}) denoted MoC-I/TiO_2, MoC-II/TiO_2, MoC-III/TiO_2 and MoC-IV/TiO_2 respectively (Table 28). The conditions used for MoC-I/TiO_2 catalyst are the same ones used in Chapter 3 (catalyst $MoC_{20E-700}$/P25TiO_2) but with 12% wt. Mo to be comparable to the catalysts of this chapter.

Table 28 Characterization of MoC/TiO_2 catalysts prepared by different GHSV during the TPRC.

Catalysts	Synthesis	Characterization				
	GHSV[a] (h^{-1})	% Mo[b]	% C[b]	S[c] (m^2/g)	Crystallite size[d] (nm)	a[e] (Å)
MoC-I/TiO_2	1091	11.0	1.4	47	3	4.249
MoC-II/TiO_2	1527	11.8	2.2	45	4	4.260
MoC-III/TiO_2	2545	12.0	3.7	47	4	4.273
MoC-IV/TiO_2	7636	11.9	5.3	46	4	4.268

[a] GHSV of 20% v/v C_2H_6/H_2 during the reduction-carburization process, [b] Weight percentage; [c] BET surface area ; [d] For fcc MoC, determined by XRD; [e]lattice parameter for fcc MoC.

The four catalysts exhibit similar BET surface area of 45-47 m^2/g, slightly lower than the support TiO_2 (55 m^2/g).

Rietveld refinement allowed us to identify the different crystalline phases present in the catalysts. Concerning the support, the main peaks corresponding to TiO_2 anatase and

rutile phases were observed (Figure 26). For the four catalysts, the composition anatase/rutile was the same as for the support P25 (75%/25%) and the lattice parameters of the anatase and rutile phases are similar as shown in (Table 29).

Table 29 Lattice parameters of anatase, rutile TiO_2, and cubic MoC of the support and catalysts.

Catalyst	Lattice parameters (Å)			
	Anatase TiO_2		Rutile TiO_2	
	a	c	a	c
TiO_2	3.784 (1)	9.503 (1)	4.592 (1)	2.957 (1)
MoC-I/TiO_2	3.784 (1)	9.494 (8)	4.591 (9)	2.958 (8)
MoC-II/TiO_2	3.787 (1)	9.507 (2)	4.596 (2)	2.960 (1)
MoC-III/TiO_2	3.787 (1)	9.506 (4)	4.596 (2)	2.961 (1)
MoC-IV/TiO_2	3.785 (1)	9.496 (2)	4.594 (2)	2.963 (2)

Regarding the molybdenum crystalline carbides, the main peaks attributed to cubic molybdenum carbide phase at 2θ = 36.4°, 42.2° and 61.3° were detected for all the catalysts (Figure 26). As already shown in the previous chapter, the peaks of cubic molybdenum carbide are broad and overlapped with the ones from the supports, which might alter the analysis. Rietveld refinement confirmed the presence of the cubic Mo

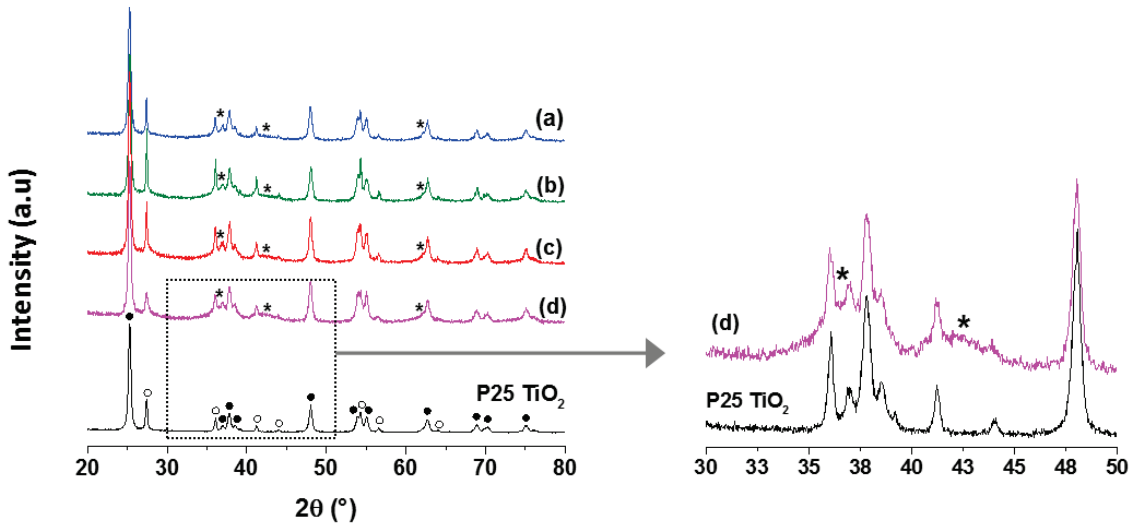

Figure 26 XRD diffraction patterns of the support P25 TiO_2 and the catalysts: a) MoC-I/TiO_2, b) MoC-II/TiO_2, c) MoC-III/TiO_2, and d) MoC-IV/TiO_2. Peaks associated with ● Anatase TiO_2, ○ Rutile TiO_2, * Cubic MoC.

carbide phase (> 10 %) with crystallite size below 5 nm (Table 28). The lattice parameters associated with MoC are similar for the four samples and consistent with fcc MoC. The presence of molybdenum oxides, such as MoO_2 or MoO_3, was not detected, which suggests full carburization.

Carbon elemental analysis was conducted to estimate the carbon content of the catalysts. The results in Table 28 show that the samples contained between 1.4 and 5.3 % wt. of carbon while the theoretical carbon content for MoC/TiO_2 with 12 % wt. of Mo should be 1.5 %. This reflects an excess of free carbon in the catalysts MoC-II/TiO_2, MoC-III/TiO_2, and MoC-IV/TiO_2 as observed on the TEM pictures that show the presence of graphitic carbon. The carbon content increased from 1.4% to 5.3% while increasing the GHSV during the preparation from 1091 to 7636 h^{-1} (Table 28). The presence of excess carbon at the surface of TMCs is well known. It is deposited on the surface during the synthesis, as ethane starts to decompose from 590 °C [57]. The temperature for complete formation of bulk molybdenum carbide is around 630 °C when using 10% v/v C_2H_6/H_2, however, supported catalysts often require more severe conditions [8,57]. Thus, the excess of carbon is not surprising after synthesis at 700 °C with high concentration of hydrocarbon (20% v/v C_2H_6/H_2) and high GHSV.

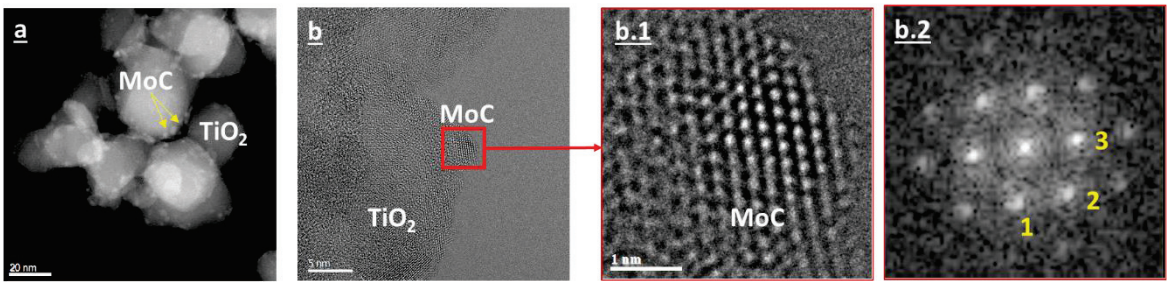

Figure 27 Representative STEM image (a), TEM (b, b.1), and electron diffraction (b.2) of MoC-II/TiO_2.

Table 30 Lattice parameters obtained from TEM analysis MoC-II/TiO_2.

Spot	h k l	α (°)		d (nm)	
		Exp.	Theo.*	Exp.	Theo.*
1	1 1 -1	0.00	0.00	0.243	0.246
2	2 0 0	54.04	54.74	0.213	0.213
3	1 -1 1	108.82	109.47	0.249	0.246

* Theoretical values corresponding to cubic MoC, reference ICSD 01-089-2868

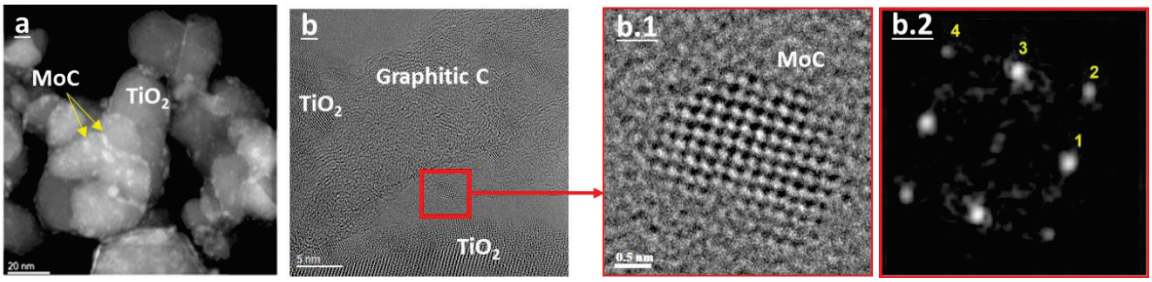

Figure 28 Representative STEM image (a), TEM (b, b.1), and electron diffraction (b.2) of MoC-IV/TiO_2.

Table 31 Lattice parameters obtained from TEM analysis of MoC-IV/TiO_2.

Spot	h k l	α (°)		d (nm)	
		Exp.	Theo.*	Exp.	Theo.*
1	2 0 0	0.00	0.00	0.212	0.213
2	2 2 0	44.37	45.00	0.150	0.150
3	0 2 0	89.40	90.00	0.214	0.213
4	-2 2 0	134.49	135.00	0.153	0.150

* Theoretical values corresponding to cubic MoC, reference ICSD 01-089-2868

Representative STEM and TEM images of catalysts MoC-II/TiO_2 and MoC-IV/TiO_2 are shown in Figure 27 and Figure 28 respectively. Small particles (< 5 nm) of MoC are obtained and are well dispersed on the TiO_2 support. Local EDX analyses and diffractogram patterns (Table 30, Table 31) revealed that these are particles of MoC with cubic phase, which is in agreement with XRD results. An excess of graphitic carbon was clearly seen in the TEM images.

I.2. The effect of passivation of the catalysts

Due to their pyrophoricity, TMCs are typically passivated prior to use in order to facilitate their handling and avoid oxidation in air. As described in Chapter 2, the prepared molybdenum carbide catalysts were passivated under 60 mL/min of 1% v/v O_2/N_2 for 4 h.

The passivation layer is supposed to be reduced at the very beginning of the reaction after which the catalyst becomes active. To verify the temperature at which passivation layer is removed in our catalysts a sample of MoC/TiO_2 was subjected to thermo gravimetric analysis/mass spectrometry under hydrogen flow (TGA-MS). Figure 29 shows the weight loss in the sample and the associated MS peaks corresponding to water

production. The first peak at 95°C corresponds to water which desorbs from the catalyst. The peak at 280°C refers to the reduction of the passivation layer in agreement with the literature [183].

However, it has been shown that the passivation treatment may affect the catalytic

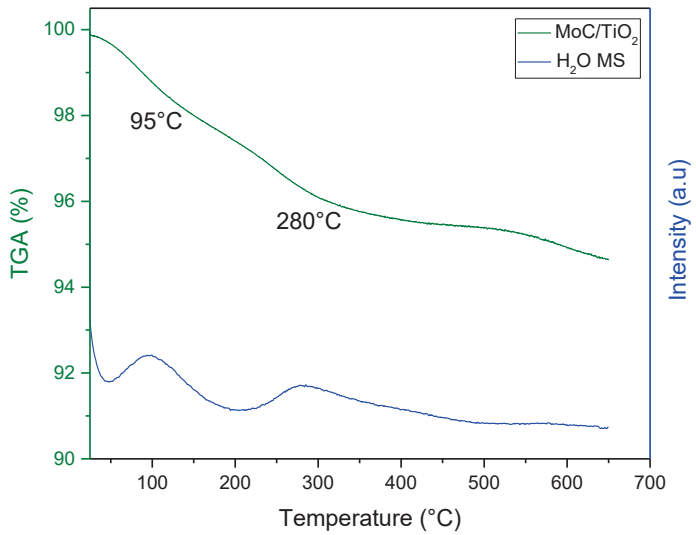

Figure 29 TGA-MS under H_2 for MoC/TiO_2 catalyst.

performance. For example, Nagai et al have shown that passivated molybdenum carbide catalysts supported on alumina were less active for CO_2 hydrogenation reaction than the non-passivated catalysts [163]. Similarly, Shou et al. found that, relative to a non-passivated molybdenum carbide, the activity for Fischer-Tropsch synthesis of the passivated sample was 37% lower [184]. On the contrary, Mehdad et al. showed that after the removal of the passivation layer of molybdenum carbide, the catalyst exhibited identical performance as the non-passivated one for toluene hydrogenation [185]. Therefore, two catalysts were synthesized without passivation (NP is added to the same catalysts labelling) to figure out whether this treatment affects the properties and performance of the catalyst in SA hydrogenation or not.

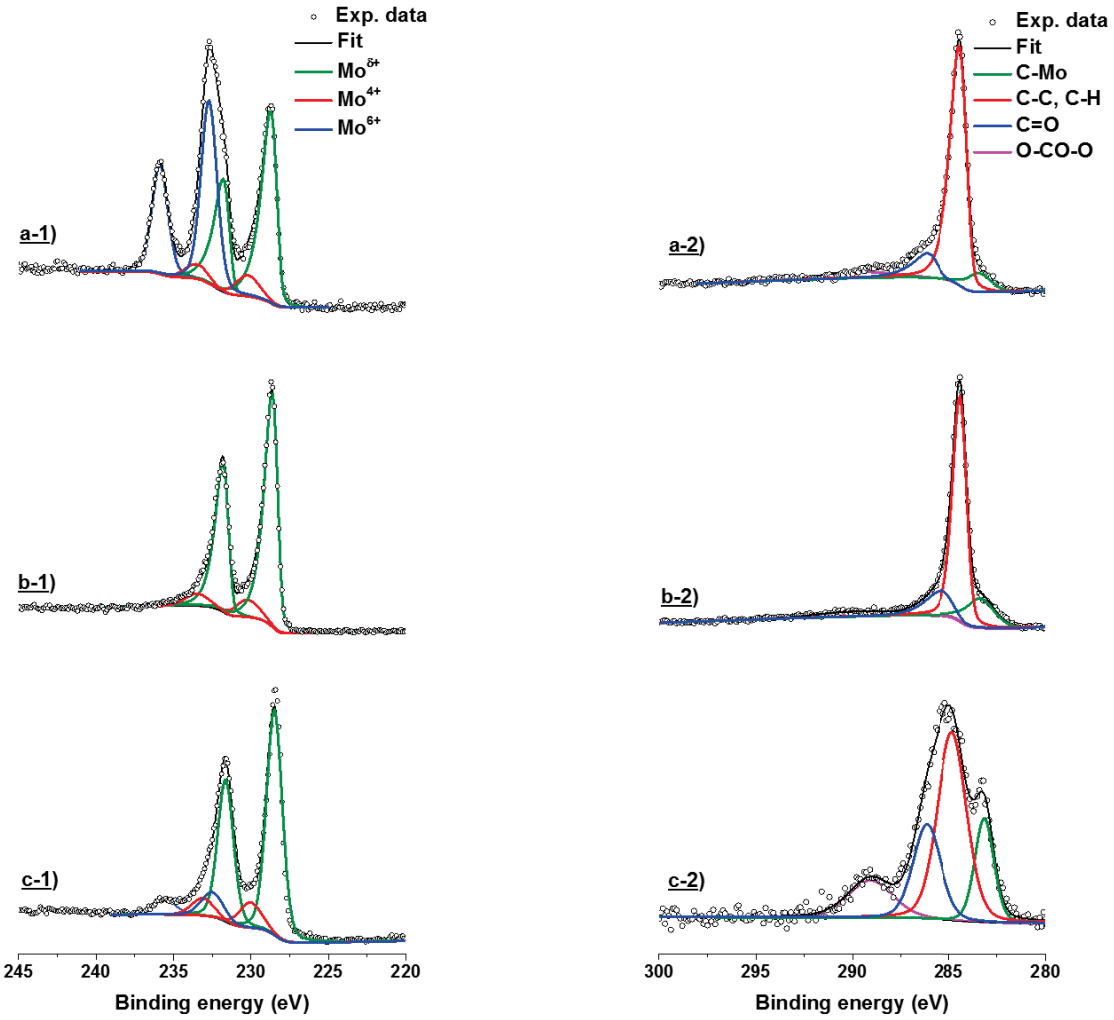

Figure 30 XPS spectra of catalysts a) MoC-IV /TiO_2, b) NP- MoC-IV/TiO_2, and c) NP- MoC-II/TiO_2 of 1) Mo 3d and 2) C 1s.

Table 32 XPS analysis: atomic concentration of Mo and C, and the abundance of Mo and C species.

	Atomic concentration %		**Mo species %**			**C species %**		**Ratio $C_{Carbide}/Mo^{\delta+}$**
Catalyst	Mo	C	$Mo^{\delta+}$	Mo^{4+}	Mo^{6+}	Carbide	Graphite	
MoC-IV/TiO_2	3.3	46.5	47	8	45	8	74	1.4
NP-MoC-IV/TiO_2	3.9	49.2	88	12	0	16	65	1.6
NP-MoC-II/TiO_2	4.8	22.4	76	13	12	17	47	0.7

Limited characterization could be performed on these non-passivated catalysts as they cannot be exposed to air, except for XPS analysis where the samples were transferred directly after synthesis to the XPS chamber via glovebox. XPS analyses was done for three

catalysts in order to assess the differences resulting from the passivation (MoC-IV/TiO_2 vs. NP-MoC-IV/TiO_2) and from variation of the GHSV (NP-MoC-II/TiO_2 vs. NP-MoC-IV/TiO_2).

The Mo 3d and C 1s spectra of the catalysts are presented in Figure 30. The chemical states of the catalyst components and their relative abundance are compiled in Table 32.

In Figure 30-a-1, the Mo 3d spectrum of MoC-IV/TiO_2 exhibits two peaks at BE = 228.7 eV and 231.9 eV which correspond to Mo $3d_{5/2}$ and Mo $3d_{3/2}$ peaks of $Mo^{\delta+}$. The former value falls within the range 227.6-228.9 eV which is attributed to carbidic Mo (Mo next to carbon) [170,171]. In addition, contributions assigned to Mo^{4+} (BE = 230.2 eV and 233.5 eV) and Mo^{6+} (BE = 232.7 eV and 235.8 eV) were also observed [172,173]. The difference between the passivated and non-passivated catalysts is clearly noticeable when comparing Mo 3d spectra of MoC-IV/TiO_2 and NP-MoC-IV/TiO_2 in Figure 30-a-1 and Figure 30-b-1, respectively. The absence of Mo^{6+} for the fresh sample (non-passivated), confirms that the presence of Mo^{6+} in the passivated sample is due to the passivation treatment. The absence of molybdenum bulk oxides phases (by XRD) suggest that the passivation treatment results in a thin layer of oxide on the surface. It is assumed that oxygen adsorbs on top of Mo atoms and hollow sites that are not occupied by C [185]. From the literature, it is expected to see a small amount of Mo^{4+}, even for the non-passivated sample [170]. Oxygen elemental analyses were also conducted and no difference was observed for the two catalysts. However the fact that the support is an oxide limits the efficiency of the analysis. As expected, MoC-IV/TiO_2 and NP-MoC-IV/TiO_2 present similar Mo and C atomic concentration knowing that the Mo theoretical atomic concentration of 12% w/w MoC/TiO_2 is 3.6 (Table 32). The C atomic concentration is in excess due to the presence of graphite on the surface. The C 1s spectrum of MoC-IV/TiO_2 displayed in Figure 30-a-2 exhibits a peak at BE = 283.4 eV which corresponds to the carbon in the carbidic form [171]. The broad peak at BE = 284.6 eV along with the peak at 289.5 eV refer to graphitic carbon. The additional peak at 286 eV can be attributed to carbon in C-O or C=O groups [171,174]. The ratios of carbidic C to Mo carbide are shown in Table 32 and are around 1.5 for the two samples. The Ti 2p spectrum of MoC-IV/TiO_2 is shown in Figure 31 as an example to confirm that the support is not reduced. The peaks at BE = 459.1 eV and 465

eV refer to Ti^{4+}, and no peaks corresponding to Ti^{3+} (BE = 457.5 eV) or other reduced forms were observed.

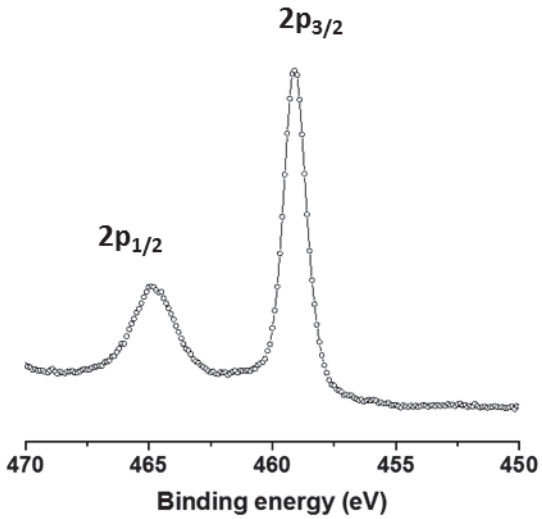

Figure 31 XPS spectra of MoC-IV/TiO_2 over Ti 2p.

The sample NP-MoC-II/TiO_2 synthesized at lower GHSV (Figure 30-c, Table 32) presents similar compositions as NP-MoC-IV/TiO_2. However, the presence of a small amount of Mo^{6+} suggests that a small fraction of molybdenum oxide was still not carburized. When looking at the atomic concentration determined by XPS, it is noticeable that the carbon content on the surface of the catalyst is lower (22% vs. 49%) when decreasing the GHSV. This result is in agreement with the carbon elemental analysis. Moreover the fraction of carbon graphite is slightly lower (from 65% to 47%) in favor of carbon as carbonyl/carbonate groups. The lower Mo % surface concentration on MoC-IV/TiO_2 might be related to the higher concentration of carbon in the sample. Indeed, the excess of carbon on the surface might be masking the Mo particles because only few nanometers are probed by XPS.

XPS analysis for the catalysts without passivation is more useful than the passivated ones, especially upon comparing the degree of carburization as our study in Chapter 3. However, it is quite demanding as synthesis of a second batch of the catalyst without passivation is required, and the transfer to the XPS chamber should be done through the glove box; accordingly it was done only occasionally and not handy to be routinely done on all catalysts.

II. Hydrogenation of succinic acid over MoC/TiO_2

The catalytic performance of MoC-III/TiO_2 catalyst was evaluated for the aqueous phase hydrogenation of succinic acid (SA) at 240 °C and 150 bar. A typical temporal evolution of the substrate and products in solution is presented in Figure 32. In the presence of the catalyst, SA was progressively converted with time and full conversion was achieved after 22 h. From the start of the reaction, parallel formation of γ-butyrolactone (GBL) and butyric acid (BA) were observed. After 8 h of reaction, 60% conversion was achieved with 38% yield of GBL and 26% yield of BA. Proceeding more in the reaction, the two intermediates started disappearing along with the formation of butanol (BOL), tetrahydrofuran (THF), and 1,4-butanediol (BDO). After 32 h, 22% of GBL, 6% of BA, 21% of BOL, 14% of THF, and 4% of BDO are present in solution. Traces of propionic acid were also observed, close to the detection limit (< 0.5%). The carbon balance (CB) started decreasing after 18 h and only 66% of the products were still present in liquid phase at the end of the reaction. This was confirmed by qualitative GC-MS analysis of the gas phase where butane as well as traces of propane were detected.

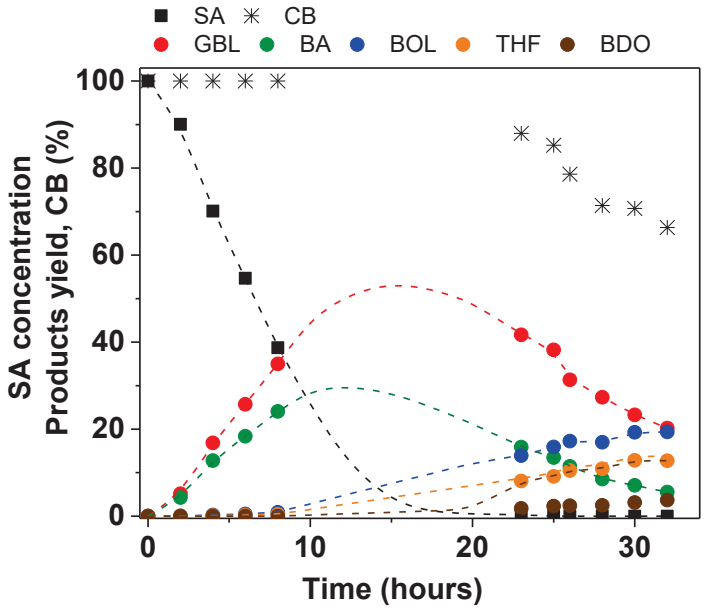

Figure 32 Hydrogenation of succinic acid over MoC-III/TiO_2 at 240 °C and under 150 bar H_2: temporal evolution of the concentrations of SA, the products yield and the carbon balance (CB). Aqueous solution of SA (0.12 M, 100 mL), 0.6 g of catalyst.

All the catalytic results were reproducible within similar conversion range and products selectivities (Figure 32 and Figure 33-a). The CB calculated based on GC and HPLC analysis

were close to the TOC measured, which means that all the products in liquid phase were identified and analyzed (Figure 33-b).

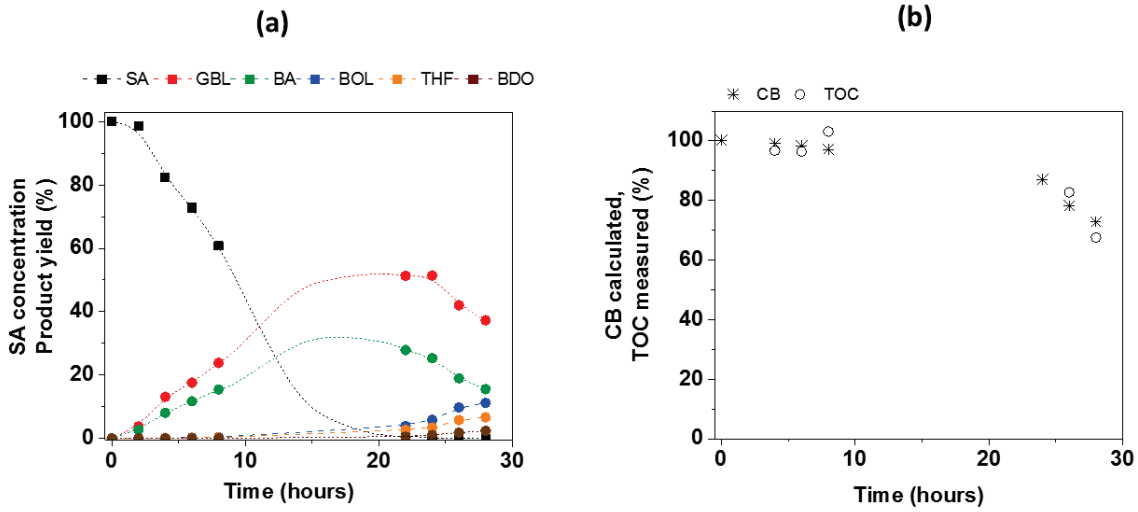

Figure 33 Typical hydrogenation of succinic acid at 240 °C and under 150 bar H_2. Temporal evolution of the concentrations of SA and the products yield (a), the carbon balance and TOC measured (b). Aqueous solution of SA (0.13 M, 100 mL), 0.6 g of MoC-III/TiO_2.

Besides BA, BOL is also not usually obtained in significant quantities in the hydrogenation of SA reported in literature. It can be produced from plant biomass by fermentation ‘‘biobutanol’’ or from fossil fuels ‘‘petrobutanol’’. Significant fraction of BOL is currently produced chemically from petroleum sources [186]. The research concerning biobutanol synthesis is continuously in progress due to the very high demand and that fermentation pathway remains insufficient and still undergoes optimizations. Previous research has also shown that butyric acid can be converted to butanol in a two steps fermentation process via bacteria, where sugars are converted to butyric acid in the first step and in the second step, butyric acid is converted to butanol [187].

Butanol is an important industrial solvent, and is a better fuel for replacing gasoline than ethanol [180]. It can be used for storing energy, as a chemical intermediate, a solvent for a wide variety of chemical and textile processes, and as a reactant in preparation of acrylic paint.

Since the products selectivity observed during the hydrogenation of SA over MoC/TiO_2 is distinct from the selectivity obtained over noble metals catalysts, the reaction pathway was investigated in more details.

II.1. Pathway of SA hydrogenation reaction over MoC/TiO_2

Hydrogenation reactions of GBL, BA, BDO, and THF were conducted under the same reaction conditions as those used for SA (150 bar H_2, 240°C). The temporal evolution of these reactions are shown in Figure 34.

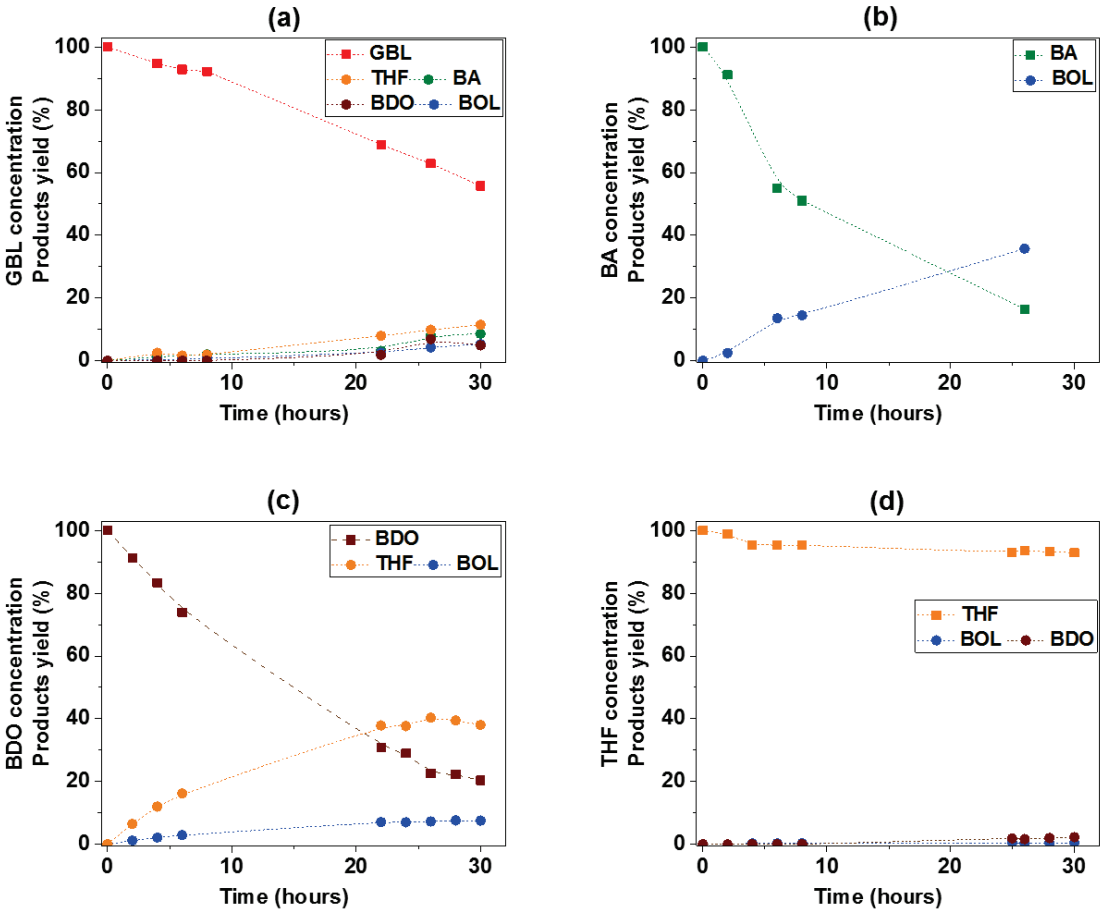

Figure 34 Hydrogenation of a) GBL, b) BA, c) BDO, and d) THF at 240 °C and under 150 bar H_2: temporal evolution of the concentrations of the substrates and products yield. Aqueous solution of substrates (0.12 M, 100 mL), 0.6 g of MoC-III/TiO_2.

After 30 h of reaction, 35 % of GBL was converted (Figure 34-a). THF was the main product with 31% selectivity, in addition to BOL (28%), BA (16%) and BDO (14%). BOL and BA were formed simultaneously which suggests that BOL can be formed directly from GBL. The hydrogenation of BA generated solely BOL in liquid phase (Figure 34-b), in agreement with literature [115]. Hydrogenation of BDO gave mainly THF (57% selectivity) in addition to BOL (10% selectivity) at 70 % conversion. Lastly, THF was stable in these reaction conditions where barely 7 % was converted to BDO after 30 h of reaction.

The hydrogenation of the intermediates suggests that BA can be formed mainly from SA as well as from GBL but at a lower level. Moreover gaseous products (i.e. butane) are mainly formed from BA. Figure 35 compares the product distributions at around 50-60% conversion and the initial rates of reaction (V_0) for the hydrogenation reactions of these intermediates and SA.

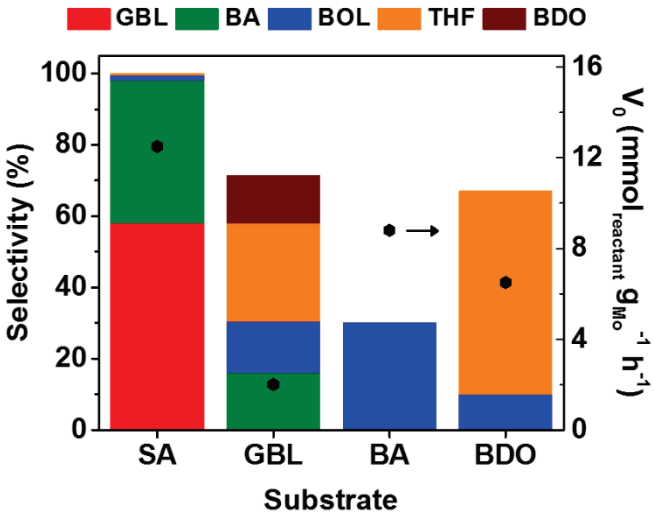

Figure 35 Selectivity to the products at 50-60% conversion and initial rate of reaction (V_0) for the hydrogenation reactions of SA, GBL, BA, and BDO, at 240 °C and 150 bar. Aqueous solution of reactant (0.12 M, 100 mL), 0.6 g of MoC-III/TiO_2 catalyst.

The rate of reaction follows the order: V_0 (SA) > V_0 (BA) > V_0 (BDO) > V_0 (GBL) >> V_0 (THF) (< 0.1 $mmol_{THF}$ g_{Mo}^{-1} h^{-1}). These reactions lead to the proposal of the reaction pathway shown in Scheme 15.

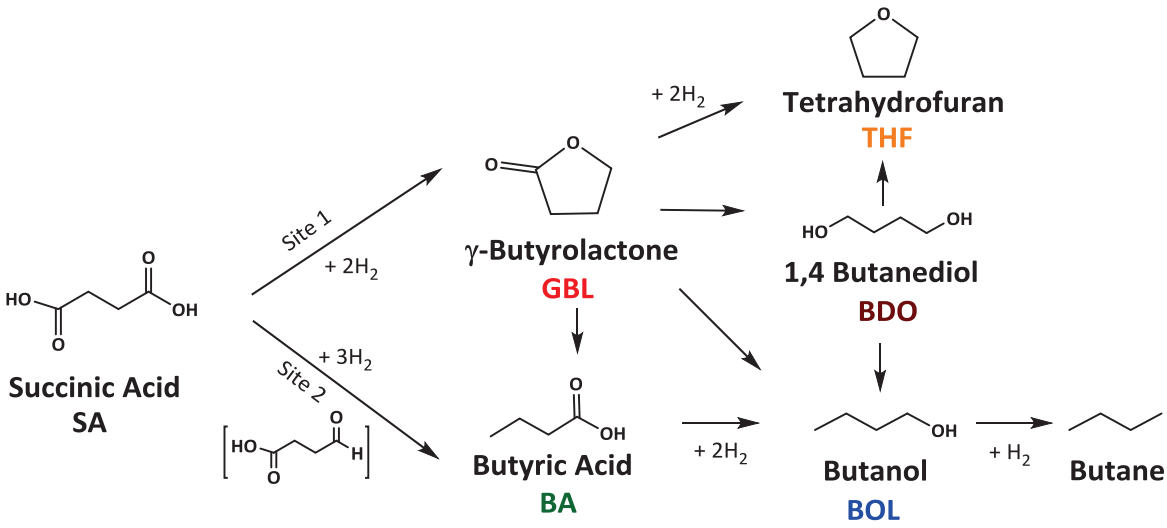

Scheme 15 Suggested reaction pathway for the aqueous phase hydrogenation of SA over MoC/TiO_2.

The selectivity to the products shows that the TiO_2 supported molybdenum carbide catalyst may possess two type of active sites, the first one being similar to the one of noble metal-based catalysts inducing the production of GBL from SA, whereas the second one is specific to the carbide catalyst producing BA as second major product.

Molybdenum carbide catalysts are known to be active for C=O hydrodeoxygenation reaction. In literature, it was proposed that the hydrogenation steps occur over metallic sites, while the dehydration occurs over Brønsted acid sites [188]. The hydrodeoxygenation of acrylic acid to propane has been studied in gas phase over Mo_2C [189]. The experimental and theoretical results suggested that the hydrogenation/dehydration of the carboxylic acid generates adsorbed aldehyde, which undergoes further hydrogenation/dehydration and forms propane.

Therefore, in our case, BA might be formed on "site 2" via successive hydrogenation / dehydration of SA, without desorption of the intermediate aldehyde (Scheme 15).

II.2. Optimization of the reaction conditions: effects of temperature and pressure.

In the literature, the conditions for aqueous phase hydrogenation of SA in the presence of noble metal catalysts are in the range of 80-150 bar of H_2 and 160-240 °C [104,110,111,115]. The effects of temperature and pressure were investigated over MoC-III/TiO_2, the reaction was conducted at different temperatures (160, 200, and 240 °C) and H_2 pressures (90, 110, 150 bar) for 22 h (Table 33).

Table 33 Effect of temperature and pressure on initial rate (V_0), SA conversion and product yields

T (°C)	P (bar)	V_0 ($mmol_{SA}\ g_{Mo}^{-1}\ h^{-1}$)	SA Conversion[a] (%)	Products yield (%)[a]				
				GBL	BA	BOL	THF	BDO
160	110	0.4	4	2	2	0	0	0
200	110	1.6	20	12	8	0	0	0
240	110	4.5	61	33	26	1	1	0
240	90	3.4	48	24	24	1	0	0
240	150	12.5	100	45	17	15	9	2

[a] after 22 h reaction : aqueous solution of SA (0.12 M, 100 mL), 0.6 g of MoC-III/TiO_2 catalyst.

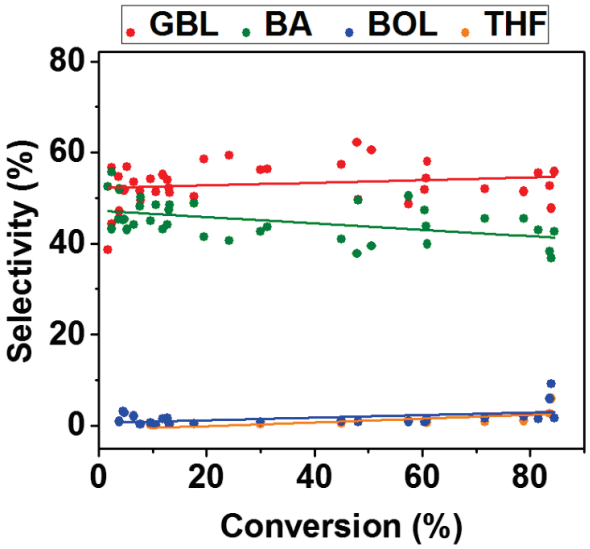

Figure 36 Selectivity to GBL, BA, BOL, and THF as function of SA conversion, for all reactions conducted over MoC-III/TiO_2 catalyst, at different pressure and temperature (see Table 33). Aqueous solution of SA (0.12 M, 100 mL), 0.6 g of MoC-III/TiO_2 catalyst.

At relatively low temperature (i.e. 160°C), the catalyst was not active and only 4% of SA was converted after 22 h. The initial rate of reaction (V_0) increased with temperature and pressure. According to the Arrhenius plots, the apparent activation energy is 55 kJ/mol for MoC-III/TiO_2. It is worth to mention that the effects of temperature and pressure were only limited on the activation of SA. Figure 36 represents the selectivity towards the products in function of conversion, for all the reactions conducted over MoC-III/TiO_2. The selectivity values were similar, independently of the reaction conditions, implying that the products distribution is not affected by the change of temperature and pressure. When going from 2 to 85% of conversion, the selectivity towards BA decreased slightly (from 52 to 43%). Above 90% SA conversion, GBL and BA started to be converted and the products BOL, BDO and THF appeared. It is well known that there is a competitive adsorption of SA and GBL. Indeed, on noble metal catalysts it is usually observed that GBL starts to be converted when SA has disappeared [105]. In the same manner, we observed that the conversion of BA to BOL occurred only when SA was almost fully converted. It is also worth noting that far less gaseous products were observed when working at 90 or 110 bar of H_2 (Figure 37). This was confirmed through the TOC measured and the carbon balance that remained close to the initial value. This is due to the fact that at low conversion, hardly any butanol, hence butane, were formed.

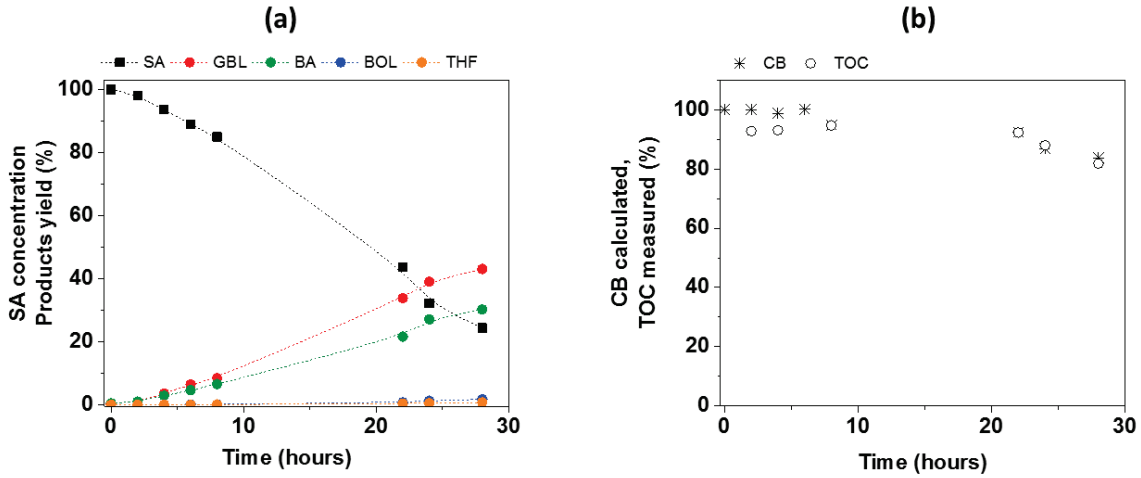

Figure 37 Typical hydrogenation of succinic acid at 240 °C and under 150 bar H_2. Temporal evolution of the concentrations of SA and the products yield (a), the carbon balance and TOC measured (b). Aqueous solution of SA (0.13 M, 100 mL), 0.6 g of MoC-III/TiO_2

II.3. Effect of variation of the GHSV during catalysts preparation on the corresponding catalytic performance in SA hydrogenation

The initial rate and products distribution of MoC-III/TiO_2 were compared to those of the catalysts prepared at different GHSV: MoC-I/TiO_2, MoC-II/TiO_2, and MoC-IV/TiO_2. All reactions were done at 240 °C and 110 bar of H_2, the results are included in Table 34. For these reactions the CB was always over 90%. By increasing GHSV of C_2H_6/H_2 during the carburization of the catalyst from 1091 h^{-1} (MoC-I/TiO_2) to 7636 h^{-1} (MoC-IV/TiO_2), V_0 increased from 1.3 to 7.8 $mmol_{SA}\ g_{Mo}^{-1}\ h^{-1}$ and the selectivity shifted towards BA. Indeed, when comparing the selectivity at 22-25 % conversion, MoC-IV/TiO_2 gave selectivity towards BA of 71% while 41, 44 and 49% were obtained over catalysts MoC-I/TiO_2 MoC-II/TiO_2 and MoC-III/TiO_2 respectively. In the catalyst characterization section it was shown that as the GHSV increases, the carbidic Mo and the free-carbon contents increase. Therefore the degree of carburization and/or the presence of free carbon must have a strong impact on activity and selectivity. A supported Mo oxide catalyst MoO_3/TiO_2 was also prepared and tested for comparison (Table 34). High selectivity to GBL was observed (95%). This shows that the carbon content has direct effect on shifting the selectivity towards BA as already observed in Chapter 3.

Table 34 Effect of GHSV during catalyst carburization on the initial rate and selectivity at 110 bar, 240 °C.

Catalyst	V_0 ($mmol_{SA}\ g_{Mo}^{-1}\ h^{-1}$)	Time[a] (h)	Selectivity[a] (%)			
			GBL	BA	BOL	THF
MoC-I/TiO_2	1.3	22	59	41	0	0
MoC-II/TiO_2	1.6	22	56	44	0	0
MoC-III/TiO_2	4.5	10	51	49	0	0
MoC-IV/TiO_2	7.8	6	29	71	0	0
MoO_3/TiO_2	4.1	10	95	1	0	0

[a] at 22-25 % conversion

In conclusion, the selectivity of SA hydrogenation is very sensitive to the modifications in the molybdenum carbide catalyst but independent of the reactions conditions (temperature and pressure).

II.4. Passivated versus non-passivated catalysts

The effect of the passivation treatment on the catalytic results was investigated under 110 bar of H_2. Figure 38-a presents the results obtained over MoC-IV/TiO_2, which was used directly after passivation. The non-passivated catalyst "NP-MoC-IV/TiO_2" (Figure 38-b) was transferred to the reactor in a glovebox, directly after synthesis, without passivation treatment. It is obvious that the two catalysts exhibited really similar catalytic response in terms of activity and selectivity. The conversion reached 87-92% after 24 h

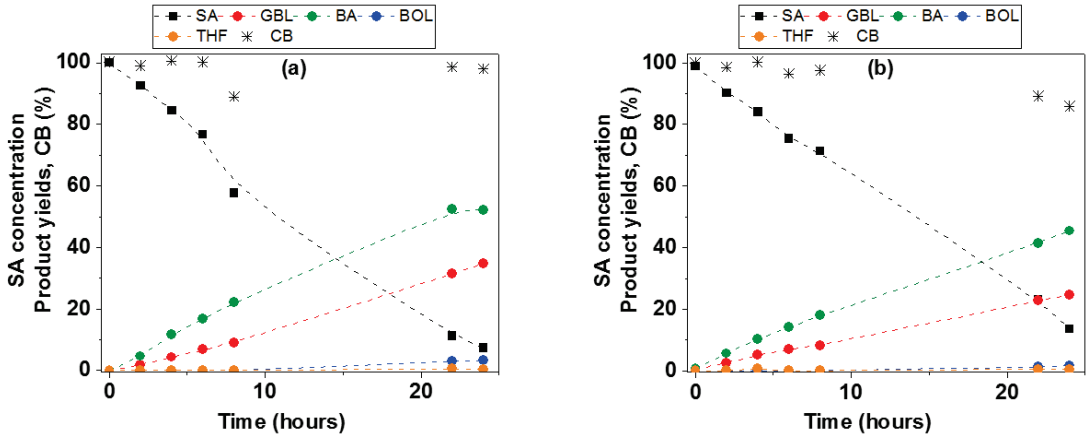

Figure 38 Hydrogenation of succinic acid over (a) MoC-IV/TiO_2 and (b) NP-MoC-IV/TiO_2 at 240 °C and under 110 bar of H_2: temporal evolution of the concentrations of SA, the product yields and the carbon balance (CB). Aqueous solution of SA (0.12 M, 100 mL), 0.6 g of catalyst.

reaction for both samples and the initial rates was of 7.6 ± 0.2 $mmol_{SA}\ g_{Mo}^{-1}\ h^{-1}$ (The difference in conversion is within experimental error ± 5%). The yield of GBL and BA reached around 30 % and 50%, respectively. Therefore the passivation layer does not affect the catalytic performance of the catalyst. As no pre-activation was conducted on the passivated sample, the reduction of the passivated sample must occur in situ, at the beginning of the reaction. The XPS results showed that no more Mo^{6+} and a lower amount of Mo^{4+} species were present in NP-MoC-IV/TiO_2 (Figure 30-b; Table 32). These results suggest that the oxides must be reduced at the beginning of the reaction and thus passivation does not affect the selectivity.

II.5. Stability of the catalysts

The stability tests were conducted with MoC-III/TiO_2 at 240 °C and 150 bar for 26 h, which are the harshest conditions used in this work. The results obtained during the first run over MoC-III/TiO_2 are shown in Table 35 and Figure 39. The catalyst was then filtered, washed with distilled water (under air) and dried at 80 °C; this catalyst is denoted R1-MoC-III/TiO_2. The percentage of Mo in the solution recovered after the first run was below 0.1 ppm, which means that no leaching occurred (< 0.1%).

Table 35 Initial rate (V_0) and product selectivity after recycling.

Catalyst	V_0 ($mmol_{SA}\ g_{Mo}^{-1}\ h^{-1}$)	Time[a] (h)	Products selectivity (%)[a]				
			GBL	BA	BOL	THF	BDO
MoC-III/TiO_2	11.2	6	60	40	0	0	0
R1- MoC-III/TiO_2	2.7	26	67	32	0	0	0
R2- MoC-III/TiO_2	8.5	6	34	60	5	1	0

[a] at 22-25 % conversion

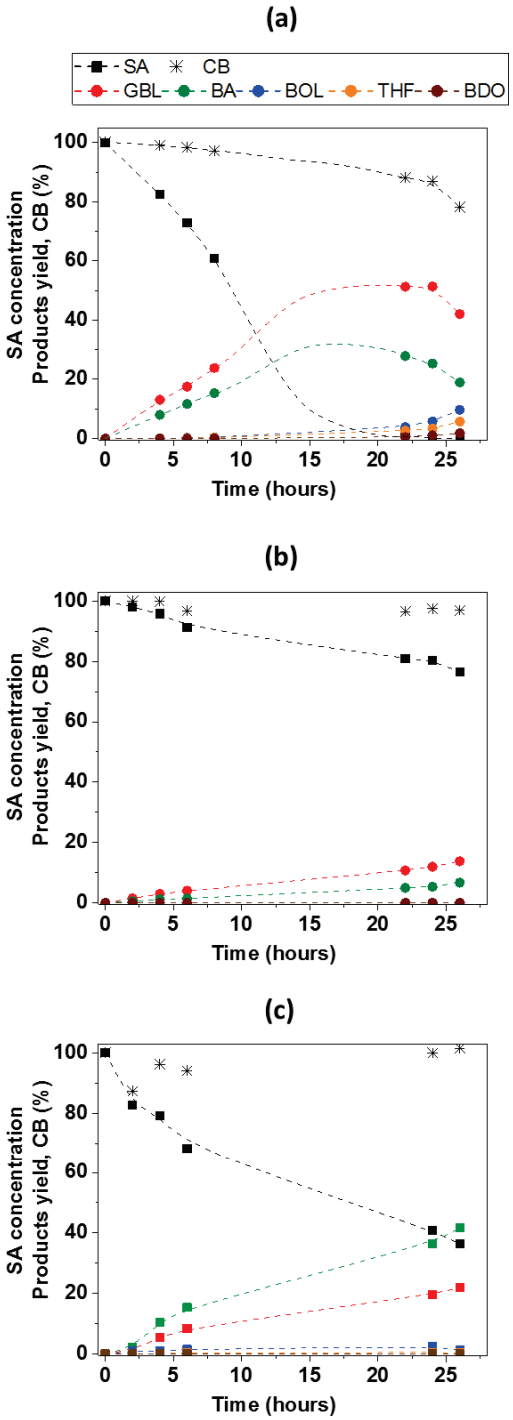

Figure 39 Hydrogenation of succinic acid over (a) MoC-III/TiO_2, (b) R1- MoC-III/TiO_2 and (c) $R2_{solid}$- MoC-III/TiO_2: temporal evolution of the concentrations of SA, products yield and carbon balance (CB). Aqueous solution of SA (0.13 M, 100 mL), 0.6 g of catalyst, 240°C and 150 bar of H_2.

Catalyst oxidation is a possible cause of deactivation for metal carbides catalysts [190]. The hydrothermal stability of Mo_2C in water at 250 °C for 48 h has been investigated in a previous study [191]. The formation of MoO_2 (by XRD) was observed and due to the oxidation by H_2O. In order to assess the presence of oxides in the solids (crystalline or

amorphous), Raman analysis were done for the catalyst before (MoC-III/TiO_2) and after reaction (R1-MoC-III/TiO_2). In Figure 40, the bands at 145, 196, 397, 517, and 637 cm^{-1} correspond to anatase phase of TiO_2 and the rutile phase is evidenced by two extra broad bands at 440 and 605 cm^{-1} [192]. The two bands at 1345 and 1597 cm^{-1} correspond to the disorder D and tangential G bands of graphitic carbon [45,193,194]. The presence of these two bands have previously been reported for molybdenum carbides synthesized under 10% C_2H_6/H_2 at 800 °C [45]. The weak bands at 2654, 2932, and 3209 cm^{-1} were attributed to second order features [195–197]. As the cubic MoC structure leads to no Raman active band, no bands were detected for MoC-III/TiO_2. Furthermore, the presence of the light absorbing carbon layer can hinder observation of underlying phase [198]. This result implies that the catalyst is covered with an excess of graphite during the synthesis, in agreement with the XPS, elemental analysis and TEM results. The absence of bands attributed to ν(Mo=O) vibrations around 950-1000 cm^{-1} [45,199,200] suggests that MoC-III/TiO_2 is fully carburized. In the spectra of R1- MoC-III/TiO_2, two additional ν(Mo=O) and ν(Mo-O-Mo) stretching bands located at 968 cm^{-1} and 832 cm^{-1}, respectively were observed and attributed to the presence of molecular polymolybdates [201,202]. The recovered catalyst (R1-MoC-III/TiO_2) was tested under the same reaction conditions (240 °C, 150 bar of H_2). After 26 hours, only 24% of SA is converted, with 14% yield of GBL and 7% yield of BA (Figure 39-b).

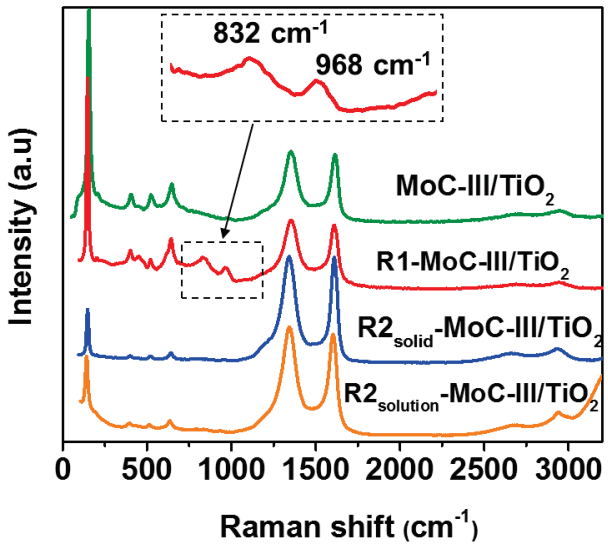

Figure 40 Raman spectra associated with MoC-III/TiO_2 (before reaction), R1- MoC-III/TiO_2 (recovered under air), $R2_{solid}$- MoC-III/TiO_2 (recovered under N_2) and $R2_{solution}$- MoC-III/TiO_2 (recovered in solution).

In a second stage, we aimed to assess when the oxidation of the catalyst was taking place. Indeed, the oxidation could occur during the reaction or during the recovery due to the exposure to air in the washing and filtration process. For that, another reaction was conducted with MoC-III/TiO_2 but the used catalyst denoted $R2_{solution}$-MoC-III/TiO_2 was recovered with the reaction solution. Raman spectra of the solid in solution did not show any peaks associated with molecular or crystalline molybdenum oxides (Figure 40), hence oxidation did not occur during the reaction. The presence of amorphous carbon might inhibit the oxidation of the particles, as observed for iron carbide [203]. In order to test the reusability of the catalyst, the reactor was transferred to a glove bag where the filtration was set up. The catalyst was recovered under inert atmosphere and without washing with water. Raman spectra associated with this solid, $R2_{solid}$-MoC-III/TiO_2, showed complete absence of molybdenum oxides. It was then concluded that the oxidation of the catalyst occurs during the recovery step, and not during the reaction. However, the relative intensity of the bands of graphitic carbon was higher after recovery suggesting that the quantity of such carbon was increased. $R2_{solid}$-MoC-III/TiO_2 was then tested for the hydrogenation of SA (Figure 39-c, Table 35). 64% conversion was achieved after 26 h. It is clear that the catalyst $R2_{solid}$-MoC-III/TiO_2 was more active than R1-MoC-III/TiO_2, however it was still less active than fresh MoC-III/TiO_2. The selectivity was also affected as more BA and less GBL were formed. The catalyst exhibited some deactivation, while the characterization of the bulk catalyst after the first run did not show any drastic changes, in terms of XRD, ICP and elemental analysis (C and O contents). Therefore XPS analysis of $R2_{solid}$-MoC-III/TiO_2 was conducted and the results are presented in Table 36 and Figure 41. It can be seen that the amounts of carbidic molybdenum and carbidic carbon have decreased in the recovered catalyst in comparison to the fresh one, i.e. from ca. 26 to 20% and from ca. 5 to 2% respectively. Moreover, despite the fact that the bulk carbon content (by elemental analysis) was constant, the surface carbon atomic concentration has increased. Therefore the partial oxidation of the catalysts on the surface, coupled with some coke formation, could be responsible for the deactivation. A regeneration of the catalyst under a flow of H_2/C_2H_6 at 700 °C might provide a recovery of the catalyst performance.

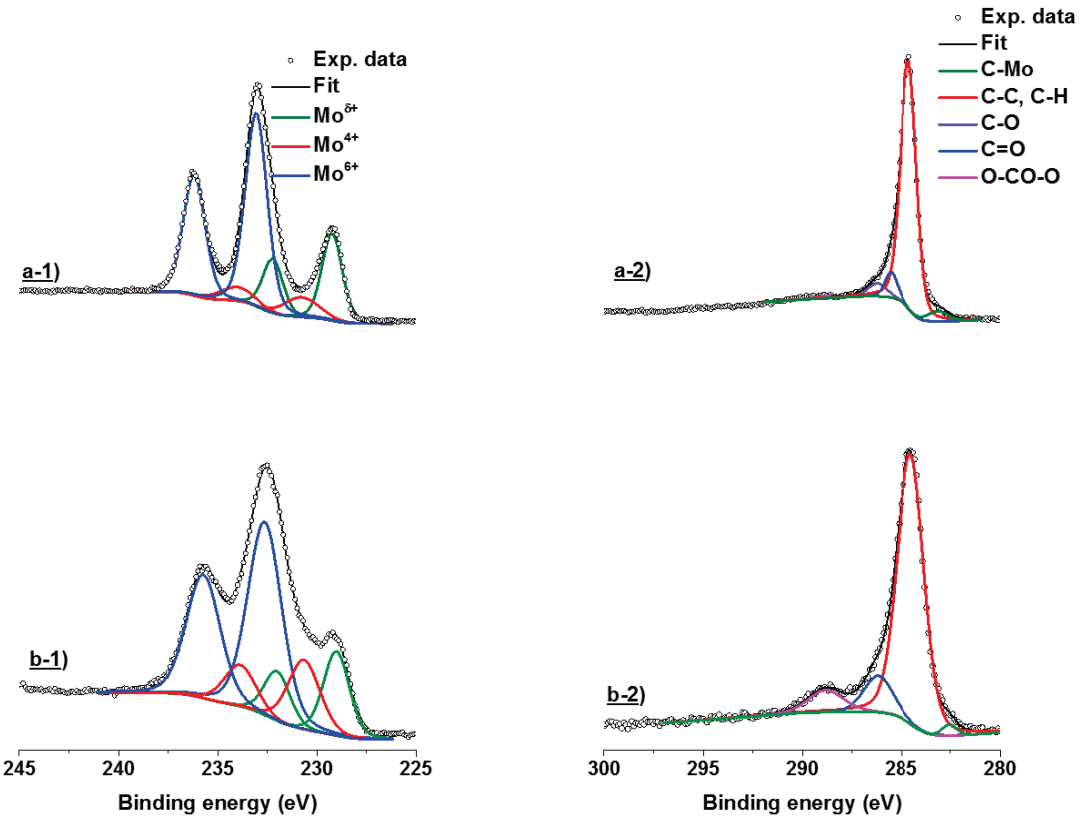

Figure 41 XPS spectra of catalysts a) MoC-II/TiO_2, and b) $R2_{solid}$-MoC-II/TiO_2 over 1) Mo 3d and 2) C 1s.

Table 36 XPS analysis: atomic concentration of Mo and C, and the abundance of Mo and C species.

	Atomic concentration %		Mo species %			C species %	
Catalyst	Mo	C	$Mo^{\delta+}$	Mo^{4+}	Mo^{6+}	Carbide	Graphite
MoC-III/TiO_2	3.6	33.9	26	11	63	5	89
$R2_{solid}$- MoC-III/TiO_2	4.7	49.3	20	20	60	2	80

III. Conclusion

In this part, we investigated the hydrogenation of succinic acid in aqueous phase using MoC/TiO_2 catalysts. The catalysts were synthesized by impregnation with $(NH_4)_6Mo_7O_{24}.4H_2O$ followed by hydrogenation/carburization under a flow of 20% v/v C_2H_6/H_2 at 700°C at different GHSV. XRD and TEM showed that well dispersed particles of cubic MoC phase were obtained, with size < 5 nm regardless the GHSV. The catalysts were active for the reaction and full conversion of SA was achieved. The main products after 24

hours are γ-butyrolactone, and more remarkably butyric acid. These intermediates are then converted to tetrahydrofuran, butanol, 1,4-butanediol and butane and the reaction pathway is suggested according to the reactions conducted from each of the products. The effects of H_2 pressure and temperature were investigated and the selectivity to the products was independent of conversion. The passivation treatment does not have a noticeable effect on the performance; in contrast, an increase in GHSV during the synthesis is associated with an increase in activity and a switch of selectivity towards BA. After recovering the catalyst under air, deactivation was observed, while keeping it under inert atmosphere limits the deactivation. Molybdenum does not leach during the reaction. The deactivation was mainly attributed to a decrease in the amounts of carbidic molybdenum and carbidic carbon, as demonstrated by XPS analysis.

In summary, Chapters 3 and 4 showed that performing SA hydrogenation over supported molybdenum carbides instead of the more conventional precious metal based catalysts is a promising reaction. However, the selectivity is different: the carbide catalyst seems to have two types of active sites that induce the hydrogenation of SA to GBL and BA simultaneously. The selectivity is sensitive to the catalyst properties produced by different synthesis conditions. Although the carbon content seems an essential factor, some exceptions do exist, and thus further work after this opening study are required to understand better the factors affecting the reactivity of these catalysts in this reaction.

CHAPTER 5.

Supported molybdenum carbide catalysts for carbon dioxide hydrogenation

The supported molybdenum carbide catalysts prepared in this work were tested in CO_2 hydrogenation reaction in a continuous gas flow reactor at 250 °C, 30 bar total pressure, and a total flow rate of 50 mL/min of H_2 / CO_2/ N_2 with a H_2:CO_2 ratio of 3:1. The reaction conditions (reactants flow rate and temperature) were optimized with the MoC/TiO_2-P25 catalyst. The performances of other catalysts were evaluated as function of the following parameters: support nature (P25 TiO_2, DT51 TiO_2, and ZrO_2), $GHSV_{preparation}$, carbon source (CH_4 or C_2H_6), concentration of the carburizing gas (% v/v Hydrocarbon/H_2), and maximum carburization temperature (600-800 °C).

The catalysts considered in this chapter are the ones presented in Chapters 3 and 4. The catalyst notations are kept the same to match the characterizations previously shown. This chapter starts directly with the catalytic results of molybdenum carbides in the hydrogenation of CO_2.

I. CO_2 hydrogenation over molybdenum carbide supported on P25 titanium dioxide

Prior to the tests of CO_2 hydrogenation over molybdenum carbide catalysts supported on titanium oxide, two blank tests were performed: blank with empty reactor, and blank with TiO_2 P25 support. In both cases no conversion was observed (< 0.1%).

For the first evaluation of the performance of TiO_2-supported molybdenum carbide, the conditions from reference [56] were employed. The reaction was done at 250 °C, with a pressure of 20 bar and a flow rate of 30 mL/min with a reaction mixture of 75% H_2/15% CO_2/10% N_2.

For this test, the catalyst supported on P25 TiO_2 synthesized using a flow of 20% C_2H_6/H_2

with a GHSV of 1527 h^{-1} at 700 °C was used (MoC-II/TiO_2 cf Chapter 4 section I.1 Table 28). To recall, the characterization of this catalyst showed that small particles (size < 4 nm) of cubic MoC were well dispersed on the surface of the support. The BET surface area was 45 m^2/g, and the molybdenum and carbon weight contents were 11.8% and 2.2% respectively, which means an excess of carbon present in this catalyst (the theoretical carbon content for 12 % wt. of Mo with Mo/C ratio of one is 1.5 %).

Figure 42-a shows the temporal evolution of CO_2 conversion and products yields. CO_2 conversion started around 190 °C and it increased with the temperature, and reached a maximum (3.5%) at 113 minutes corresponding to the overshooting of the temperature of the oven (260 °C). When the temperature stabilized at 250 °C after 150 min, the

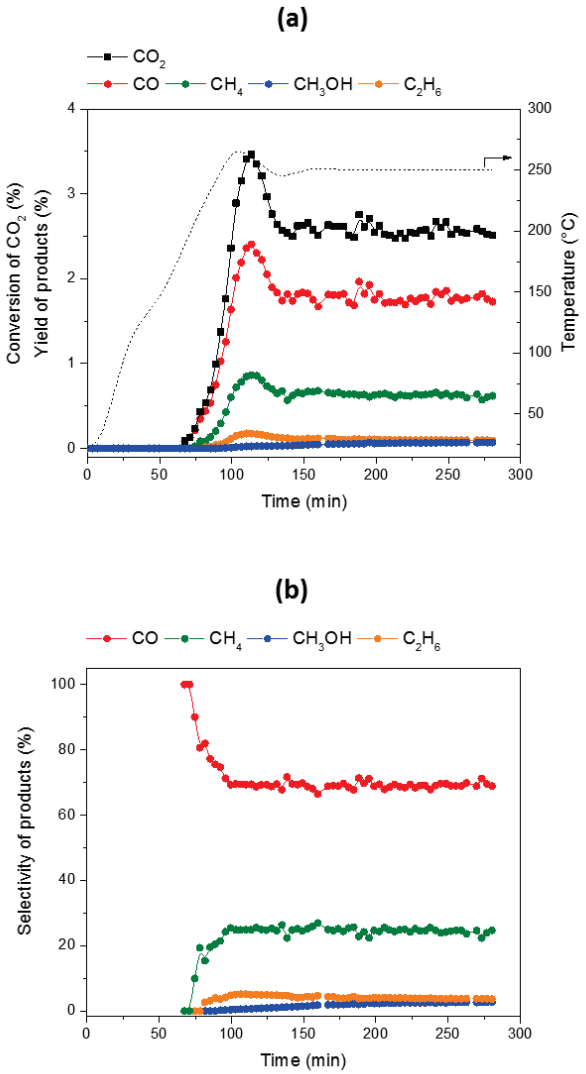

Figure 42 Temporal evolution of (a) CO_2 conversion and products yields, and (b) selectivity during the hydrogenation of CO_2 over 400 mg of MoC-II/TiO_2-P25 at 250 °C and 20 bar total pressure, with a total flow rate of 30 mL/min of H_2 / CO_2/ N_2 with a H_2:CO_2 ratio of 5:1.

conversion stabilized around 2.5%.

Four products were observed in this reaction, the major product being CO with a selectivity around 69% at quasi steady-state, followed by CH_4 (25%), C_2H_6 (< 4%), and CH_3OH (< 3%).

The evolution of the products selectivities, shown in Figure 42-b, reveals that at the beginning of the test (low temperature), only CO was produced, thus the main reaction occurring over MoC/TiO_2 was the reverse water-gas shift (RWGS) reaction ($CO_2 + H_2 \leftrightarrow CO + H_2O$). Afterwards, a decrease in CO selectivity was observed, associated with a corresponding increase in CH_4 which could be produced via the hydrogenation of CO [56]. CH_3OH, which is produced in small quantity, may be formed either by direct hydrogenation of CO_2 ($CO_2 + 3H_2 \leftrightarrow CH_3OH + H_2O$) or by subsequent hydrogenation of CO produced ($CO + 2H_2 \leftrightarrow CH_3OH$). C_2H_6 can be produced via the Fischer-Tropsch process from CO_2 ($2CO_2 + 7H_2 \leftrightarrow C_2H_6 + 4H_2O$) or from CO ($2CO + 5H_2 \leftrightarrow C_2H_6 + 2H_2O$). C_2H_6 and CH_3OH were formed in small quantities; however the yield of the latter was gradually increasing.

These results suggest that $MoC\text{-}II/TiO_2$ behaves primarily as a RWGS catalyst. According to the molybdenum content relative to the catalyst mass used, the conversion value obtained is in the range of the one reported in reference [56] over a cubic molybdenum carbide catalyst under the same conditions (11% conversion at 250 °C and 20 bar, with 30 mL/min total flow rate of H_2 / CO_2/ Ar with a H_2:CO_2 ratio 5:1). 200 mg of the bulk catalyst was used in the reference, compared to 400 mg from the supported catalyst (12% wt. MoC/TiO_2) that we used, the percentage of the metal relative to catalyst mass is around 8 folds more in the mentioned reference.

However, the selectivity distribution that we obtained is not consistent with this work; the present catalyst shows more selectivity to CO and CH_4 with less selectivity to methanol [56]. Indeed, the authors reported that molybdenum carbide catalyst of cubic phase was selective for CH_3OH production (23% CH_3OH and 16% CH_4 under the aforementioned conditions) whereas the catalyst of hexagonal molybdenum carbide phase gave higher CH_4 selectivity (37% CH_4 and 12% CH_3OH, the rest being CO mainly). They showed that the Mo centers bind well the CO_2 molecule, the cleavage of the first C–O bond is assisted by hydrogen (H + OCO → HOCO → HO + CO), and there is no rupture of the second C–O bond

[164]. However, the increase in the carbon content of the carbide moderates the reactivity [158,164]. In the MoC-II/TiO_2-P25 catalyst, graphitic carbon present on the surface may block the access of the reactants to the active surface of the material. Moreover, other parameters such as the support nature might play a role in modifying the selectivity, which will be shown later on in this chapter.

A high selectivity to CO (99.5% at 16% conversion) was measured by Illas and coworkers [162] over hexagonal polycrystalline Mo_2C under different reaction conditions (CO_2/H_2 = 1/1, 400 °C, and atmospheric pressure). They interpreted the complex experimental behavior from DFT-based calculations. The authors indicated that the formation of CO over Mo_2C can even occur at a quite low temperature (35 °C). However they also showed that C-terminated Mo_2C binds adsorbates too strongly preventing the easy removal of product, whereas a Mo-terminated surface exhibits more balanced properties. CO_2 dissociation occurs and a subsequent release of CO seems viable from a thermodynamic point of view.

I.1. Screening of the reaction conditions

The reaction conditions for CO_2 hydrogenation not only influence the conversion but also the selectivity to the products. The selectivity in this reaction is equally or even more important than conversion values in practical applications [129]. Accordingly, the conditions used in our work were not always those leading to the highest conversions, as the influence on the selectivity was also considered. After the above preliminary evaluation we moved to optimizing the reaction conditions over MoC-II/TiO_2-P25.

I.1.1. Mass of catalyst

400 mg of catalyst were introduced into the glass tube reactor of internal diameter 1.3 cm. First, the reproducibility was checked by conducting 2 reactions under the same conditions using two batches of MoC-II/TiO_2 synthesized in the same way (R1 and R2 in Table 37). The results were equivalent in terms of CO_2 conversion (ca. 2%) and products selectivity (within ± 1%).

When the mass of catalyst was doubled (R3), the weight hourly space velocity (WHSV) was divided by two, and the conversion was higher by a factor two, which suggests that

mass transfer limitations were avoided under the employed conditions. Moreover, the selectivities were fairly constant. This is in accordance with the work of Davis et al. on Rh/TiO_2, showing the increase in CO_2 conversion with the inverse of WHSV and without change in the selectivity [135].

For evaluating the other parameters, we then used 800 mg of catalyst, which enables better comparisons due to the higher conversion values.

Table 37 CO_2 hydrogenation results obtained over $MoC\text{-}II/TiO_2$ catalysts with different masses.

	Reaction conditions					**Catalytic results at 280 min**				
Reaction	**Catalyst mass (mg)**	**flow (mL/min)**	**T (°C)**	**P (bar)**	**H_2:CO_2 ratio**	**CO_2 conversion (%)**	**Products selectivity (%)**			
							CO	**CH_4**	**C_2H_6**	**CH_3OH**
R1	400	50	250	30	3:1	2	71	23	3	3
R2	400	50	250	30	3:1	2	71	22	3	3
R3	800	50	250	30	3:1	4	70	25	4	1

I.1.1. **Flow rate of reaction mixture**

The variation of CO_2 conversion and products selectivity with respect to the reactants flow rate was evaluated by changing the flow of H_2/ CO_2/ N_2 (with 3:1 H_2:CO_2 ratio) from 50 mL/min to 30 mL/min, and then down to 10 mL/min. The reactions were done at 250 °C and 30 bar, with the same heating ramp shown in Figure 42.

Decreasing the flow from 50 mL/min (Figure 43-a) to 10 mL/min (Figure 43-c) increases the conversion from 4% to 12% after 280 min which was expected since decreasing the flow rate increases the contact time and increases the conversion [144]. The selectivity to CO decreased from 70% to 61% in favor of CH_4 selectivity, which increased from 25% to 33%. The C_2H_6 selectivity increased from 4% to 6% and the CH_3OH one decreased from 1.3 to 0.4%. However, with the low flow rates the kinetics was not stabilized after 280 min on stream, which makes the comparison not reliable. Perhaps diffusion limitations or other issues are present in this case.

Thus, for studying the rest of reaction conditions, a flow of 50 mL/min was used.

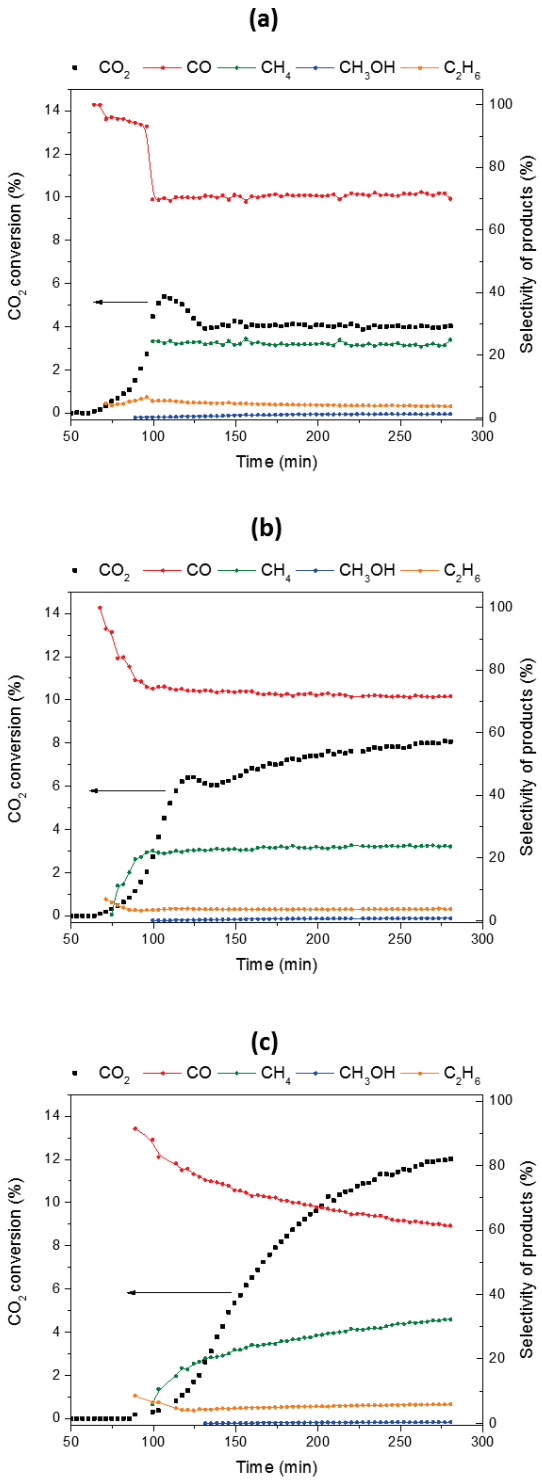

Figure 43 Evolution of CO_2 conversion and selectivities during the hydrogenation of CO_2 over 800 mg of MoC-II/TiO_2-P25 at 250 °C and 30 bar, with a) 50, b) 30, and c) 10 mL/min flow of H_2 / CO_2/ N_2 with H_2:CO_2 ratio 3:1.

I.1.2. **Temperature**

The effect of temperature on the reaction kinetics was investigated for temperatures of 200 °C, 250 °C and 300 °C. Figure 44 includes the reaction results obtained at 200 °C and

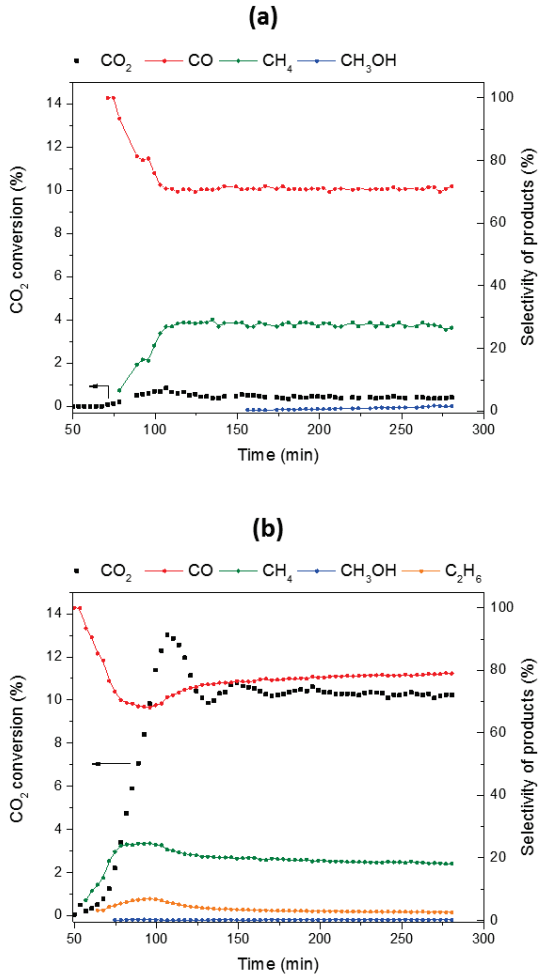

Figure 44 Effect of reaction temperature on CO_2 conversion and products selectivity at 200 °C (a) and 300 °C (b). Conditions: 800 mg of MoC-II/TiO_2 catalyst, 30 bar, 50mL/min, H_2:CO_2 = 3:1.

300 °C (the data for 250 °C are represented in Figure 43-a). The reactions were done at the same heating ramp.

When the temperature increased from 200 °C (Figure 44-a) to 300 °C (Figure 44-b), the quasi steady-state conversion increased from 0.5 to 11.4%. This increase in conversion was associated with a slight increase in selectivity towards CO (from 72% to 79%) and C_2H_6 (not detectable at the low temperature of 200 °C), along with a decrease in selectivity towards CH_4 (from 26% to 18%) and methanol (from 1.5 to 0.4%). Less methanol is expected when the temperature is increased according to Le Chatelier principle (cf Chapter 1 III.2.3). However, the increase in CO selectivity and decrease in CH_4 does not agree with literature [56] where the increase in the temperature over cubic MoC causes a decrease in CO selectivity and increase in CH_4, which thus requires further investigations.

As the catalyst was not active at 200 °C and the high temperature disfavors the methanol

selectivity, we kept 250 °C for studying the effects of the other parameters on this reaction. This allowed us to obtain significant conversion values with possibility of formation of methanol.

I.1.3. Effect of passivation

The influence of the passivation treatment on the catalytic performance of MoC/TiO_2 catalyst was evaluated by conducting another test with a fresh non-passivated catalyst transferred to the reactor through a glovebox.

The conversion of CO_2 and products selectivity obtained over the passivated and non-passivated catalysts are shown in Table 38. The non-passivated catalyst was more active than the passivated one: the CO_2 conversion increased from 4% to 7% while the products selectivity was not altered. This result is in agreement with the study of Omi and coworkers [163] who showed that passivation decreased the activity of molybdenum carbide catalysts supported on alumina in CO_2 hydrogenation at 300 °C and atmospheric pressure. However, the authors did not mention whether passivation has an influence on the selectivity.

Table 38 Effect of passivation on the performance of MoC-II/TiO_2-P25 in CO_2 hydrogenation. Reactions performed at 250 °C and 30 bar, with 50mL/min of H_2:CO_2 with 3:1 ratio.

	Catalytic results at 280 min				
Catalyst	**CO_2 conversion (%)**	**Products selectivity (%)**			
		CO	**CH_4**	**C_2H_6**	**CH_3OH**
Passivated MoC-II/TiO_2	4.0	70	25	3.7	1.3
Non-passivated MoC-II/TiO_2	7.2	73	23	2.9	1.1

Albeit these results, we did not use non-passivated catalysts in the rest of our work because of the complexity in their handling. It is clear from the above result that the comparison of conversion values with the literature makes more sense when both studies use passivated or non-passivated catalysts. The initial literature comparison that we made was with passivated catalyst in our case and non-passivated in reference [56]. Indeed, the authors prepared their catalysts in the same micro reactor used for the CO_2 hydrogenation tests. After the carburization, the samples were cooled down to the reaction temperature and directly exposed to the reaction mixture without any exposure to air to avoid the

formation of oxycarbides and possible deactivation.

After these preliminary evaluations of the performance of MoC/TiO_2-P25 in CO_2 hydrogenation, we assumed that the excess of carbon present in this catalyst might block the surface and thus alter the catalytic performance. Since this catalyst was prepared by carburization with 20%v/v C_2H_6/H_2 at 700 °C and a GHSV of 1527 h^{-1}, and contained excess carbon, we tested the catalysts presented in Chapter 3. As they were prepared under different conditions and did not exhibit any excess of carbon, they may show distinct catalytic performance in CO_2 hydrogenation.

II. Effect of the catalyst carburization conditions on the catalytic activity of molybdenum carbides supported on P25 titanium dioxide

The catalysts used in this part are the ones used in Chapter 3, and thus the characterization section is not shown here. A recall of the synthesis conditions and some of the characterization results is presented in Table 39.

Table 39 List of the catalysts with the corresponding preparation conditions and characterizations.

Catalyst	Characterizations			
	% Mo[a]	% C[a]	Crystallite size[b] (nm)	a[c] (Å)
$MoC_{5E\text{-}700}/P25\text{-}TiO_2$	9.6	0.8	3	4.234
$MoC_{10E\text{-}700}/P25\text{-}TiO_2$	9.6	0.8	3	4.246
$MoC_{20E\text{-}700}/P25\text{-}TiO_2$	9.4	1.2	3	4.270
$MoC_{20E\text{-}600}/P25\text{-}TiO_2$	9.7	0.8	3	n.a.
$MoC_{20E\text{-}800}/P25\text{-}TiO_2$	8.9	1.4	n.a.	n.a.
$MoC_{5M\text{-}700}/P25\text{-}TiO_2$	9.7	0.4	2	4.224
$MoC_{10M\text{-}700}/P25\text{-}TiO_2$	9.3	0.8	3	4.227
$MoC_{20M\text{-}700}/P25\text{-}TiO_2$	9.5	0.6	3	4.256
$MoC_{20M\text{-}600}/P25\text{-}TiO_2$	9.7	0.3	n.a.	n.a.
$MoC_{20M\text{-}800}/P25\text{-}TiO_2$	10.0	0.6	3	n.a.

[a] Weight percentage; [b] For cubic MoC determined by XRD; [c] lattice parameter for cubic MoC. n.a. not available.

Some literature work shows that for CO_2 hydrogenation, the metal loading and particle size can affect the selectivity and activity of the catalysts, as for Ni/SiO_2 [204] and Ir/CeO_2 [205] catalysts. However, in our case the XRD and TEM results suggested that all the catalysts exhibit similar particle size (≈ 3 nm) and the ICP analysis confirmed that the Mo loading is of ca. 9.5 wt. %. Thus these two parameters are not evaluated in this work.

It is evident from literature that the metal/carbon ratio in TMCs can have a strong effect in the reactivity of these materials towards CO_2 [56,164,165]. As shown in Chapter 3, the hydrocarbon concentration in the carburizing gas, and the final temperature of carburization affect the carbon content, the degree of carburization and the C/Mo ratio of MoC/TiO_2 catalysts. Thus, we evaluated the influence of these parameters by testing the catalysts prepared under different carburization conditions in CO_2 hydrogenation reaction.

II.1. **Effect of hydrocarbon concentration**

Concerning the hydrocarbons concentrations, the three catalysts prepared with different ethane concentrations (5%, 10%, and 20% v/v C_2H_6/H_2) that were characterized in Chapter 3 are used. However the catalyst prepared at 40% methane was not tested, as the series of catalysts prepared at the same hydrocarbons percentages (i.e. 5%, 10%, and 20% v/v HC/H_2) were used.

Low carbon content was obtained at low concentrations of hydrocarbon (5-10% ethane and 5-20% methane) and the C/Mo molar ratio was close to $MoC_{0.5}$; this ratio increases as the hydrocarbon concentration increases and becomes around one for $MoC_{20E\text{-}700}/P25\text{-}TiO_2$.

Figure 45-a shows the evolution of CO_2 conversion with time-on-stream for the six catalysts prepared at 700 °C with different methane or ethane concentrations. The general trend is that CO_2 conversion decreases slightly with the increase in carbon content (higher C/Mo ratio), which is in accordance literature [56,164]. Substantial increase in the selectivities towards CO and methanol were reported when moving from a C-rich surface to a Mo-rich surface. In our case of P25 TiO_2 supported catalysts, the products selectivities did not change significantly over the varied catalysts, as shown in Figure 45-b to e.

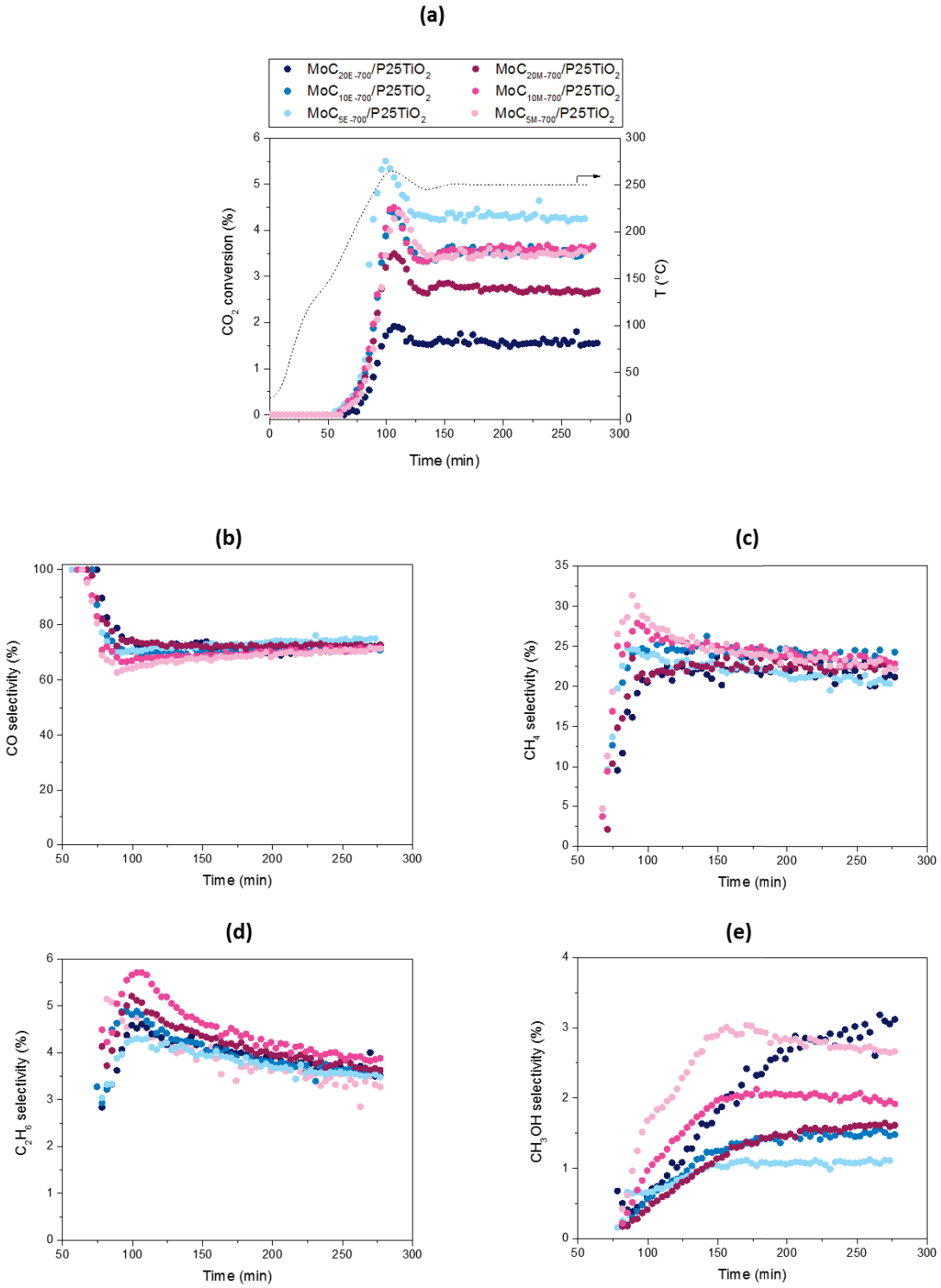

Figure 45 Evolution of CO_2 conversion (a) and selectivity towards (b) CO, (c) CH_4, (d) C_2H_6, and (e) CH_3OH. Conditions: 800 mg of catalyst, 30 bar, 50mL/min, H_2:CO_2 = 3:1.

Though, the slight differences can still lead us to conclude that preparing the carbide with methane at low concentration ($MoC_{5M\text{-}700}$/P25-TiO_2) is the best choice among the

tested catalysts in terms of conversion and methanol selectivity together. It provides one of the highest conversions compared to the rest of the catalysts (3.5 % after 280 min) with 2.6% selectivity to methanol. In contrast, although ethane at low concentration (MoC_{5E-700}/P25-TiO_2) provides the highest conversion (4.2 %) it does show the lowest methanol selectivity (1.0 %). Conversely, ethane at high concentration ($MoC_{20E-700}$/P25-TiO_2) provides the highest selectivity to methanol (3.0%), this catalyst had low overall activity (1.5% conversion after 280 min).

It is worth to mention that the selectivity to C_2H_6 and CH_3OH was not stabilized after 280 min. CH_3OH could be forming at the expense of C_2H_6, or presumably a change in the catalyst properties occurred so that it favors CH_3OH over C_2H_6. This issue requires post reaction analysis that may give more information about this behavior.

II.2. Effect of carburizing temperature

In Chapter 3 we showed that for both carbon sources the carburization was not complete at low temperature. A stoichiometry close to $MoC_{0.5}$ was obtained with methane carbon source at 700 and 800 °C maximum temperatures. A stoichiometry close to MoC was obtained when using ethane at 700 °C and 800 °C. However, the support underwent significant phase changes at the highest temperature (800 °C), especially in the case of the lowest carbon content (i.e. with methane carbon source).

The catalytic performances of the six catalysts prepared with methane or ethane at different carburization temperatures are shown in Figure 46. Considering the case of ethane (blue shades), the conversion decreases from 4.1 % to <0.1 % with the increase in the carburization temperature from 600 °C to 800 °C (Figure 46-a).

As the $MoC_{20E-800}$/P25-TiO_2 catalyst carburized at 800 °C was not active, the selectivity is not shown. The other two catalysts showed similar selectivities to the products. Similarly, in the case of methane (pink shades), the conversion decreases from 4.3 % to 0.5 % with the increase in the carburization temperature from 600 °C to 800 °C. The selectivities obtained at 0.5% conversion for $MoC_{20M-800}$/P25 TiO_2 are not shown.

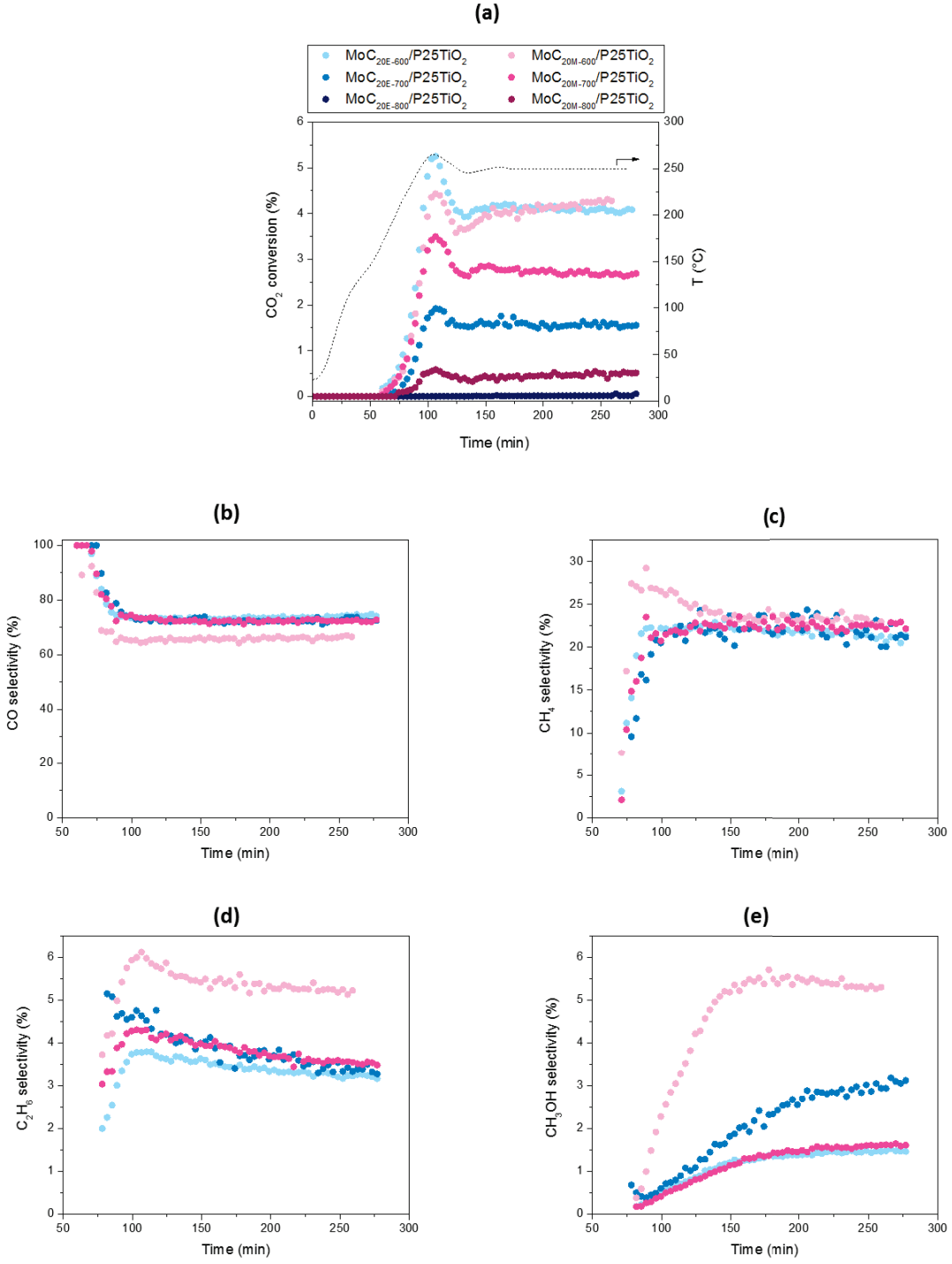

Figure 46 Evolution of CO_2 conversion (a) and selectivity towards (b) CO, (c) CH_4, (d) C_2H_6, and (e) CH_3OH. Conditions: 800 mg of catalyst, 30 bar, 50mL/min, H_2:CO_2 = 3:1.

Comparing the other two catalysts, the CO selectivity decreased from 72 % to 66 % by decreasing the carburization temperature, whereas the selectivities to C_2H_6 and CH_3OH increased by 2% and 4%, respectively, CH_3OH production seems to require an activation period of the catalyst on stream. Furthermore, as previously noticed, the conversion

decreases with higher carbon content.

Thus the best results in terms of highest conversion and highest methanol selectivity were obtained over the catalyst prepared by methane at lowest carburizing temperature ($MoC_{20M\text{-}600}/P25TiO_2$).

III. Effect of the nature of the support on the performance of molybdenum carbide catalysts in CO_2 hydrogenation

All the above results show that the selectivities over our catalysts differs from those of bulk molybdenum carbides, as investigated in the literature. In addition to possible carbide particle size effects, the presence of support may cause these differences. For example, Kim et al. have shown that the crystal structure of Ru/TiO_2 strongly affects its CO_2 hydrogenation performance (at atmospheric pressure and 200 °C under 20 mL/min of $CO_2/H_2/He$ of 4:1 ratio of $H_2:CO_2$) [206]. Moreover $PtCo/ZrO_2$ and $PtCo/TiO_2$ were reported to exhibit distinct selectivities in CO_2 hydrogenation through experimental and DFT calculations [207], where the former catalyst showed a higher selectivity to CH_4. In both studies the differences of behaviors were attributed to the distinct metal-support interaction in the catalysts which can be a way to tune the selectivity.

Table 40 List of the catalysts with the corresponding preparation conditions and characterization results.

Catalyst	Characterization			
	% Mo[a]	% C[a]	Crystallite size[b] (nm)	a[c] (Å)
$MoC_{20E\text{-}700}/P25\text{-}TiO_2$	9.4	1.2	3	4.270
$MoC_{20E\text{-}700}/DT51\text{-}TiO_2$	9.1	1.6	2	4.251
$MoC_{20E\text{-}700}/ZrO_2$	9.2	2.1	2	4.187
$MoC_{20M\text{-}700}/P25\text{-}TiO_2$	9.5	0.6	3	4.256
$MoC_{20M\text{-}700}/DT51\text{-}TiO_2$	9.5	0.8	2	4.237

[a] Weight percentage; [b] For cubic MoC determined by XRD; [c] lattice parameter for cubic MoC.

In this section, the effect of the nature of the support was evaluated by comparing three catalysts supported on P25 TiO_2, DT51 TiO_2, and ZrO_2. A summary of the catalysts preparation conditions and characterization results is shown in Table 40.

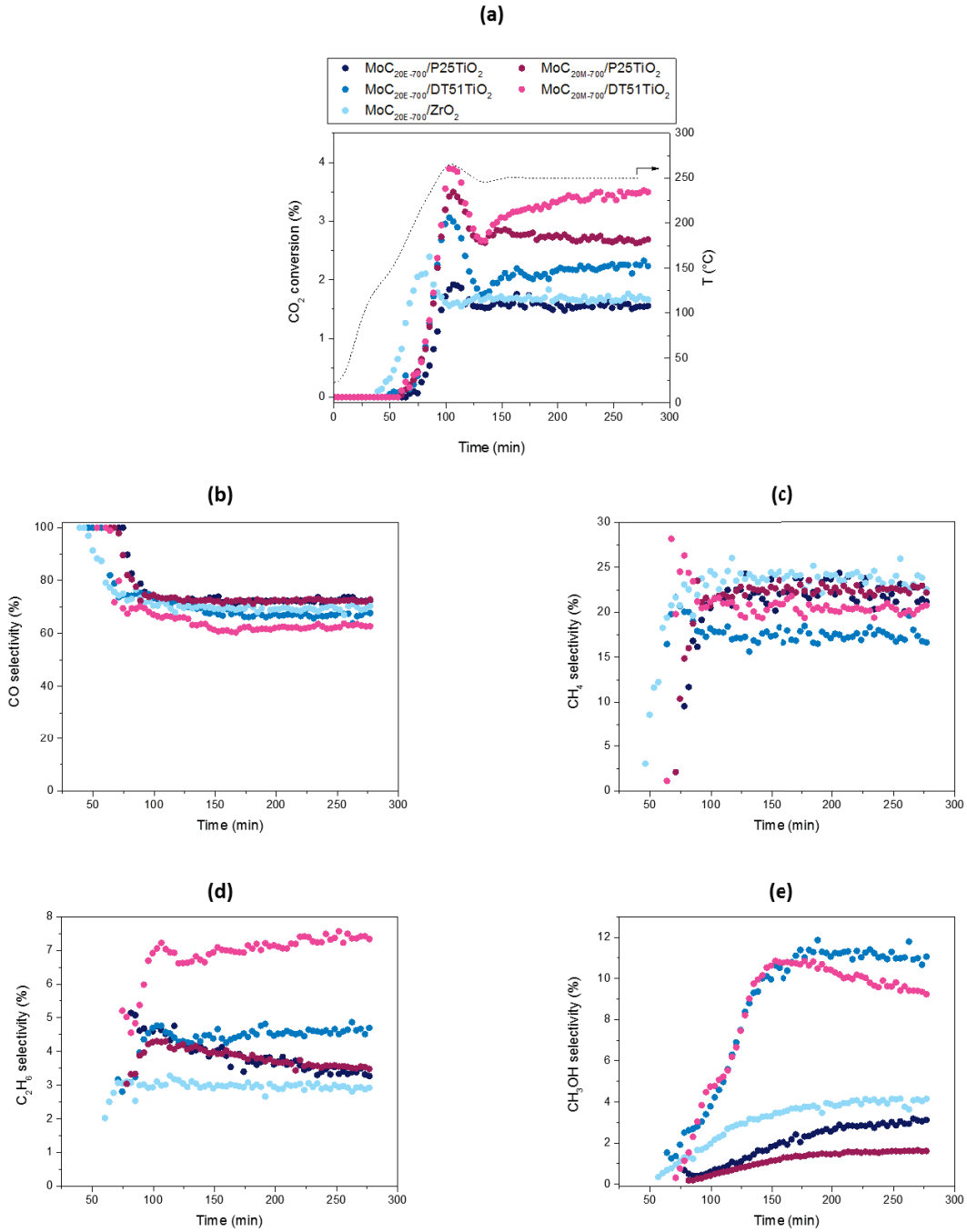

Figure 47 Evolution of CO_2 conversion (a) and selectivity towards (b) CO, (c) CH_4, (d) C_2H_6, and (e) CH_3OH. Conditions: 800 mg of catalyst, 30 bar, 50mL/min, H_2:CO_2 = 3:1.

Before testing the supported catalysts, blank reactions with supports only were done: the conversion was < 0.2% in all cases.

As we already showed that better results are obtained by methane as carbon source, we also tested a catalyst prepared by methane on DT51 support ($MoC_{20M\text{-}700}$/DT51-TiO_2).

Figure 47 shows the temporal evolution of the catalytic performances of molybdenum carbides prepared using 20% HC/H_2, 700 °C carburization temperature, and supported on the two types of TiO_2 and on ZrO_2 (we used only ethane as carbon source with ZrO_2). When comparing the catalysts prepared with the same carbon source, the catalysts supported on DT51 TiO_2 show higher conversions than those supported on P25 TiO_2 and ZrO_2 (Figure 47-a). Moreover, similar to the case of P25 TiO_2, $MoC_{20M\text{-}700}$/DT51 TiO_2 is slightly more active than $MoC_{20E\text{-}700}$/DT51-TiO_2. A significant difference is observed in the products selectivity, which is affected by the nature of the support more than by the C/Mo ratio or carbon content. The selectivity to CH_3OH over the catalysts supported on DT51 is superior by ≈ 8% compared to the ones supported on P25 TiO_2 regardless the carburizing gas nature and carbon content. These catalysts also show lower CO and CH_4 selectivities, and higher C_2H_6 selectivity, however after 280 min it seems that the conversion was still not stabilized. The selectivity of $MoC_{20E\text{-}700}/ZrO_2$ is similar to that of $MoC_{20E\text{-}700}$/P25 TiO_2.

These results make the use of DT51 TiO_2 preferable over the other supports as CO_2 conversion and methanol selectivity decrease in the order: MoC supported on DT51 TiO_2 > P25 TiO_2 ≈ ZrO_2. However, it is difficult to understand the effect of titania nature on the selectivity to methanol, at least from fresh catalyst characterization data.

IV. **Conclusion**

The catalytic results obtained over the different catalysts are summarized in

Table 41.

Screening for the best preparation conditions obtained among molybdenum carbides in this work for CO_2 hydrogenation showed that the use of methane as carbon source (5%) and 600 °C carburizing temperature with DT51 TiO_2 support are the optimal parameters in terms of CO_2 conversion and selectivity to methanol.

Table 41 Catalytic results of CO_2 hydrogenation over molybdenum carbide catalysts prepared via different TPRC synthesis conditions and different supports. Conditions: 800 mg of catalyst, 30 bar, 50mL/min, H_2:CO_2 = 3:1.

	CO_2 conversion	Products selectivities			
Catalyst		**CO**	**CH_4**	**C_2H_6**	**CH_3OH**
$MoC_{5M\text{-}700}/P25TiO_2$	3.5	71	22	3.8	2.6
$MoC_{10M\text{-}700}/P25TiO_2$	3.6	71	23	3.7	1.9
$MoC_{20M\text{-}700}/P25TiO_2$	2.7	72	23	3.4	1.6
$MoC_{20M\text{-}600}/P25TiO_2$	4.3	66	23	5.2	5.3
$MoC_{20M\text{-}800}/P25TiO_2$	0.5	-	-	-	-
$MoC_{20M\text{-}700}/DT51TiO_2$	3.5	63	20	7.4	9.3
$MoC_{5E\text{-}700}/P25TiO_2$	4.2	75	20	3.6	1.1
$MoC_{10E\text{-}700}/P25TiO_2$	3.5	72	23	3.5	1.5
$MoC_{20E\text{-}700}/P25TiO_2$	1.5	71	22	3.4	2.9
$MoC_{20E\text{-}600}/P25TiO_2$	4.1	74	21	3.1	1.5
$MoC_{20E\text{-}800}/P25TiO_2$	< 0.1	-	-	-	-
$MoC_{20E\text{-}700}/DT51TiO_2$	2.2	68	16	4.7	11.1
$MoC_{20E\text{-}700}/ZrO_2$	1.7	69	24	2.9	4.1

Indeed, the degree of carburization and the support nature seem playing a role in the catalytic response but it is not fully clear as sometimes catalysts with similar characteristics did not behave in the same manner. This work was a preliminary evaluation of supported molybdenum carbide in CO_2 hydrogenation and requires further investigations, especially concerning the selectivity towards the products in relation to the actual structure of the catalysts activated on stream. Further characterizations of the catalysts after the reaction are also necessary to compare their state before and after test, given that some catalysts were much more interesting for methanol synthesis at the end of the test, with an absence of deactivation.

General conclusion and perspectives

The main objective of this work was to evaluate the proficiency of supported molybdenum carbide catalysts in the aqueous phase hydrogenation of succinic acid and gas phase hydrogenation of carbon dioxide, and assess the possibility of replacing precious and scarce metals used in these reactions by supported molybdenum carbide catalysts.

For the first time, supported Mo carbides were proved to be active for the aqueous phase hydrogenation of SA. The reaction conditions were optimized with the molybdenum carbide catalyst supported on P25 TiO_2. The catalyst was efficient at 240 °C and H_2 pressure above 90 bar. The main products were γ-butyrolactone and butyric acid that were produced simultaneously from succinic acid. The products distribution was not affected by the change of temperature and pressure during the reaction. In contrast, changing the catalyst preparation conditions directly influenced its reactivity in terms of substrate conversion and products selectivity. Increasing the hydrocarbon percentage in the reductive-carburizing gas mixture as well as increasing the carburization temperature lead to catalysts with higher C to Mo ratios that were more active in converting succinic acid without significant difference in the products selectivity. However, increasing GHSV of the reactive gas lead to pronounced increase in the carbon content above the theoretical amount of MoC. This increase was advantageous for the reaction where succinic acid conversion increased, and the selectivity of the products switched more toward butyric acid. Leaving the reaction for longer time lead to the conversion of γ-butyrolactone and butyric acid to tetrahydrofuran and butanol respectively, as revealed by the overview of the reaction pathway. Passivation treatment for the catalysts did not have a noticeable effect on the performance.

After evaluating the activity of the catalyst, its stability in the challenging severe reaction conditions was verified under the harshest conditions used in this work (240 °C, and 150 bar). The catalyst underwent considerable deactivation when recovered under air, however the recovery under inert atmosphere lead to less significant deactivation.

XPS analysis of the recovered catalyst revealed a decrease in the amount of carbibic carbon and molybdenum species related to the carbide phase which could be the cause of deactivation.

Comparing three types of oxide supports showed that succinic acid conversion follow the order of: MoC supported on ZrO_2 < P25 TiO_2 < DT51 TiO_2. The same order was observed for the increase in butyric acid selectivity with a corresponding decrease in butyrolactone selectivity. The support seems to play a significant role which is to be further investigated.

Performing the aqueous phase hydrogenation of succinic acid in the absence of noble metals is a step towards the development of a sustainable economy, since molybdenum carbides are more abundant and less expensive than precious metals based catalysts that are usually used.

A part of the thesis project was dedicated to evaluating the performance of molybdenum carbide catalysts for the hydrogenation of carbon dioxide that is an appealing subject in the field of valorization of sustainable resources and reduction of greenhouse gases. The reaction conditions were optimized using MoC/TiO_2 catalyst such that measurable conversion values were maintained. For similar molybdenum weight percentage, the conversion of the catalyst was comparable to results in the literature but the selectivity to carbon monoxide was higher. The catalysts mainly functioned as water gas shift catalyst, where the other products were methane, ethane, and methanol. The decrease in the C to Mo ratio lead to more active catalysts, without considerable impact on the selectivity, contrary to the results obtained in the hydrogenation of succinic acid. This shows that carbon dioxide hydrogenation is more favored on catalysts with surfaces richer in molybdenum. Interestingly, modifying the catalyst support affected the catalytic performance in terms of activity and selectivity where CO_2 conversion and methanol selectivity followed the order: MoC supported on DT51 TiO_2 > P25 TiO_2 ≈ ZrO_2.

The two parts of the work show that there is a direct link between the degree of carburization of supported molybdenum carbides and the catalytic reactivity. The support itself plays a role in the catalytic response which is to be further investigated.

As this work was a primary study for the use of supported molybdenum carbide catalysts

in the hydrogenation of succinic acid, many further perspectives are envisioned. In terms of products selectivity a major focus on one desired products can be done by optimizing the catalyst preparation conditions that can either lead to favored formation of GBL (e.g. a low GHSV, with ZrO_2 support) or butyric acid (e.g. high GHSV and DT51 P25 support). Further recyclability tests would also be interesting, especially testing the re-activation of the catalyst by a supplementary reduction-carburization step.

Since these catalysts were active for succinic acid hydrogenation they could also be evaluated for the hydrogenation of levulinic acid which is an easier reaction that requires milder conditions. Primary results showed that the conversion of levulinic acid over 12% w/w MoC/TiO_2, under the reaction conditions used in the case of succinic acid, led to full levulinic acid conversion after 7 hours. The major product was γ-valerolactone, which is in agreement with the results reported in literature over noble metals based catalyst and 20% w/w molybdenum carbide catalyst supported on carbon nanotubes [41,72,118]. After the complete conversion of levulinic acid, γ-valerolactone starts to be converted to pentanoic acid, and after 24 h pentanol appears. It seems to be produced from further hydrogenation of pentanoic acid. Though, it would be interesting to compare MoC/TiO_2 catalyst with the data in the literature by using similar reaction conditions in order to better evaluate the catalytic performance.

An interesting pathway for one pot esterification of γ-valerolactone to valeric esters through pentanoic acid is reported in literature over Cu based catalysts [208]. We thus verified the possibility of an analogous pathway through the esterification of butyric acid as it was obtained in considerable quantities in all the reactions of succinic acid hydrogenation over MoC/TiO_2 catalysts, and thus its further valorization might also be interesting. A preliminary esterification test of butyric acid with butanol at 120 °C and atmospheric pressure was done to verify the feasibility of this pathway over 12% w/w MoC/TiO_2. After 28 h, around 30 % of butyric acid was converted to butyl butyrate. Optimization of the reaction conditions of this test to increase the conversion, and later on the one-pot esterification of succinic acid are also opened perspectives.

For CO_2 hydrogenation on supported molybdenum carbides many additional optimizations can improve the conversion and switch the selectivity toward the desired product. Reducing the catalysts prior to the reactions might improve the performance by

removing the passivation layer which was proved to alter the catalytic activity. Combining the best preparation conditions from our study, i.e. lower methane concentration and lower carburization temperature with DT51 TiO_2 support and without passivation, should enhance the conversion and increase the selectivity to methanol. In contrast, using higher reaction temperature obviously favors the selectivity to CO.

Deep catalyst characterizations after the reaction are necessary to understand more their catalytic performance. Furthermore, testing other oxidation states of molybdenum, especially molybdenum metal (Mo^0) would also be interesting in order to understand more the relation between molybdenum oxidation states and the reactivity in CO_2 hydrogenation.

Testing molybdenum carbide catalysts was done within the framework of a study where we compared molybdenum carbides and molybdenum nitrides in CO_2 hydrogenation. The nitrides part is not included in this thesis, preliminary evaluations showed promising results over these catalysts. A comparison of the current carbide results with the performance of nitrides will be done later in our group.

References

[1] S.T. Oyama, The Chemistry of Transition Metal Carbides and Nitrides, Blackie Academic, London, 1996.

[2] S.T. Oyama, Encycl. Chem. Technol. 4 (2015) 476–482.

[3] A.H. Cottrell, Mater. Sci. Technol. 11 (1995) 329–333.

[4] S. Ramanathan, S.T. Oyama, J. Phys. Chem. 99 (1995) 16365–16372.

[5] W.-F. Chen, J.T. Muckerman, E. Fujita, Chem. Commun. 49 (2013) 8896–8909.

[6] C. Chan-Thaw, A. Villa, Appl. Sci. 8 (2018) 259–277.

[7] G. Ertl, H. Knozinger, J. Weitkamp, Preparation of Solid Catalysts, Wiley-VCH, 1999.

[8] S.T. Oyama, Catal. Today 15 (1992) 179–200.

[9] Y. Zhong, X. Xia, F. Shi, J. Zhan, J. Tu, H.J. Fan, Adv. Sci. 3 (2016) 1500286.

[10] V. Lazic, D. Milosavljevic, S. Aleksandrovic, P. Marinkovic, G. Bogdanovic, B. Nedeljkovic, Tribol. Ind. 32 (2010) 11–20.

[11] D. Ham, J. Lee, Energies 2 (2009) 873–899.

[12] Y. Liu, T.G. Kelly, J.G. Chen, W.E. Mustain, ACS Catal. 3 (2013) 1184–1194.

[13] Q. Zeng, J. Peng, A.R. Oganov, Q. Zhu, C. Xie, X. Zhang, D. Dong, L. Zhang, L. Cheng, Phys. Rev. B 88 (2013) 214107.

[14] S. Kim, I. Szlufarska, D. Morgan, J. Appl. Phys. 107 (2010) 053521.

[15] X.-X. Yu, C.R. Weinberger, G.B. Thompson, Comput. Mater. Sci. 112 (2016) 318–326.

[16] T. Meng, M. Cao, Chem. - Eur. J. 24 (2018) 16716–16736.

[17] D.J. Brugh, T.J. Ronningen, M.D. Morse, J. Chem. Phys. 109 (1998) 7851–7862.

[18] J.G. Chen, J. Eng Jr, S.P. Kelty, Catal. Today 43 (1998) 147–158.

[19] J.G. Chen, Chem. Rev. 96 (1996) 1477–1498.

[20] R.B. Levy, M. Boudart, Science 181 (1973) 547–549.

[21] G.M. Dolce, P.E. Savage, L.T. Thompson, Energy Fuels 11 (1997) 668–675.

[22] D.V.N. Vo, A.A. Adesina, Appl. Catal. Gen. 399 (2011) 221–232.

[23] A. Goguet, S. Shekhtman, F. Cavallaro, C. Hardacre, F.C. Meunier, Appl. Catal. Gen. 344 (2008) 30–35.

[24] J. Patt, D.J. Moon, C. Phillips, L. Thompson, Catal. Lett. 65 (2000) 193–195.

[25] E. Furimsky, Appl. Catal. Gen. 240 (2003) 1–28.

[26] P.A. Aegerter, W.W.C. Quigley, G.J. Simpson, D.D. Ziegler, J.W. Logan, K.R. McCrea, S. Glazier, M.E. Bussell, J. Catal. 164 (1996) 109–121.

[27] B. Dhandapani, S. Ramanathan, C.C. Yu, B. Frühberger, J.G. Chen, S.T. Oyama, J. Catal.

176 (1998) 61–67.

[28] T. Xiao, A.P.E. York, V.C. Williams, H. Al-Megren, A. Hanif, X. Zhou, M.L.H. Green, Chem. Mater. 12 (2000) 3896–3905.

[29] C. Sayag, M. Benkhaled, S. Suppan, J. Trawczynski, G. Djéga-Mariadassou, Appl. Catal. Gen. 275 (2004) 15–24.

[30] T. Li, M. Virginie, A.Y. Khodakov, Appl. Catal. Gen. 542 (2017) 154–162.

[31] D.V.N. Vo, A.A. Adesina, Fuel Process. Technol. 92 (2011) 1249–1260.

[32] A.C. Lausche, J.A. Schaidle, N. Schweitzer, L.T. Thompson, in: Compr. Inorg. Chem. II, Elsevier, 2013, pp. 371–404.

[33] J.S. Lee, M. Boudart, Appl. Catal. 19 (1985) 207–210.

[34] J.C. Schlatter, S.T. Oyama, J.E. Metcalfe, J.M. Lambert, Ind. Eng. Chem. Res. 27 (1988) 1648–1653.

[35] J. Han, J. Duan, P. Chen, H. Lou, X. Zheng, Adv. Synth. Catal. 353 (2011) 2577–2583.

[36] H. Guo, Y. Song, P. Chen, H. Lou, X. Zheng, Catal. Sci. Technol. 8 (2018) 4199–4208.

[37] S.A.W. Hollak, R.W. Gosselink, D.S. van Es, J.H. Bitter, ACS Catal. 3 (2013) 2837–2844.

[38] E. Ochoa, D. Torres, R. Moreira, J.L. Pinilla, I. Suelves, Appl. Catal. B Environ. 239 (2018) 463–474.

[39] J. Engelhardt, P. Lyu, P. Nachtigall, F. Schüth, Á.M. García, ChemCatChem 9 (2017) 1985–1991.

[40] Y. Zhang, A. Wang, T. Zhang, Chem Commun 46 (2010) 862–864.

[41] E.F. Mai, M.A. Machado, T.E. Davies, J.A. Lopez-Sanchez, V. Teixeira da Silva, Green Chem 16 (2014) 4092–4097.

[42] P.M. Mortensen, H.W.P. de Carvalho, J.-D. Grunwaldt, P.A. Jensen, A.D. Jensen, J. Catal. 328 (2015) 208–215.

[43] W.-S. Lee, Z. Wang, W. Zheng, D.G. Vlachos, A. Bhan, Catal. Sci. Technol. 4 (2014) 2340–2352.

[44] J.B. Claridge, A.P.E. York, A.J. Brungs, C. Marquez-Alvarez, J. Sloan, S.C. Tsang, M.L.H. Green, J. Catal. 180 (1998) 85–100.

[45] T. Mo, J. Xu, Y. Yang, Y. Li, Catal. Today 261 (2016) 101–115.

[46] J.S. Lee, Encycl. Catal. Horváth Ed (2010).

[47] J.S. Lee, S.T. Oyama, M. Boudart, J. Catal. 106 (1987) 125–133.

[48] J.S. Lee, L. Volpe, F.H. Ribeiro, M. Boudart, J. Catal. 112 (1988) 44–53.

[49] G.S. Ranhotra, A.T. Bell, J.A. Reimer, J. Catal. 108 (1987) 40–49.

[50] P. Ren, Z. Zhao, Catal. Commun. 119 (2019) 71–75.

[51] L. He, Y. Qin, H. Lou, P. Chen, RSC Adv. 5 (2015) 43141–43147.

[52] C. Wan, N.A. Knight, B.M. Leonard, Chem. Commun. 49 (2013) 10409–10411.

[53] J. Pielaszek, B. Mierzwa, G. Medjahdi, J.F. Marêché, S. Puricelli, A. Celzard, G. Furdin, Appl. Catal. Gen. 296 (2005) 232–237.

[54] A. Hanif, T. Xiao, A.P.E. York, J. Sloan, M.L.H. Green, Chem. Mater. 14 (2002) 1009–1015.

[55] C. Bouchy, S.B. Derouane-Abd Hamid, E.G. Derouane, Chem. Commun. (2000) 125–126.

[56] W. Xu, P.J. Ramirez, D. Stacchiola, J.A. Rodriguez, Catal. Lett. 144 (2014) 1418–1424.

[57] T. Xiao, A.P. York, K.S. Coleman, J.B. Claridge, J. Sloan, J. Charnock, M.L. Green, J. Mater. Chem. 11 (2001) 3094–3098.

[58] T. Christofoletti, J.M. Assaf, E.M. Assaf, Chem. Eng. J. 106 (2005) 97–103.

[59] B. Frank, K. Friedel, F. Girgsdies, X. Huang, R. Schlögl, A. Trunschke, ChemCatChem 5 (2013) 2296–2305.

[60] H. Li, W. Hong, Y. Cui, S. Fan, L. Zhu, J. Alloys Compd. 569 (2013) 45–51.

[61] H.J. Guzmán, W. Xu, D. Stacchiola, G. Vitale, C.E. Scott, J.A. Rodríguez, P. Pereira-Almao, Can. J. Chem. 91 (2013) 573–582.

[62] Q. Bkour, C.M. Cuba-Torres, O.G. Marin-Flores, S. Tripathi, N. Ravishankar, M.G. Norton, S. Ha, J. Mater. Sci. 53 (2018) 12816–12827.

[63] S. Li, W.B. Kim, J.S. Lee, Chem. Mater. 10 (1998) 1853–1862.

[64] X.-H. Wang, H.-L. Hao, M.-H. Zhang, W. Li, K.-Y. Tao, J. Solid State Chem. 179 (2006) 538–543.

[65] G. Ertl, K. Helmuth, S. Ferdi, W. Jens, eds., Handbook of Heterogeneous Catalysis: 8 Volumes, 2nd ed., WILEY-VCH, 2008.

[66] G. Busca, Heterogeneous Catalytic Materials: Solid State Chemistry, Surface Chemistry and Catalytic Behaviour, Elsevier, 2014.

[67] M. Kosmulski, J. Colloid Interface Sci. 337 (2009) 439–448.

[68] P. Forzatti, L. Lietti, E. Tronconi, in: P. Barbaro, C. Bianchini (Eds.), Catal. Sustain. Energy Prod., Wiley-VCH Verlag GmbH & Co. KGaA, 2009, pp. 393–438.

[69] D.A.H. Hanaor, C.C. Sorrell, J. Mater. Sci. 46 (2011) 855–874.

[70] B. Ohtani, O.O. Prieto-Mahaney, D. Li, R. Abe, J. Photochem. Photobiol. Chem. 216 (2010) 179–182.

[71] J. Regalbuto, ed., Catalyst Preparation: Science and Engineering, Taylor & Francis Group, 2007.

[72] J. Ftouni, A. Muñoz-Murillo, A. Goryachev, J.P. Hofmann, E.J.M. Hensen, L. Lu, C.J. Kiely, P.C.A. Bruijnincx, B.M. Weckhuysen, ACS Catal. 6 (2016) 5462–5472.

[73] J.F. Le Page, ed., Applied Heterogeneous Catalysis: Design, Manufacture, Use of Solid Catalysts, Éditions Technip, Institut français du pétrole publications, 1987.

[74] P. Munnik, P.E. de Jongh, K.P. de Jong, Chem. Rev. 115 (2015) 6687–6718.

[75] J. Moreau, O. Delpoux, E. Devers, M. Digne, S. Loridant, J. Phys. Chem. A 116 (2012)

263–270.

[76] P. Célestin Bakala, E. Briot, J.-Y. Piquemal, J.-M. Brégeault, P. Beaunier, Catal. Commun. 8 (2007) 1447–1451.

[77] D.S. Kim, D. Hardcastle, J. Catal. 120 (1989) 325–336.

[78] T. Miyao, I. Shishikura, M. Matsuoka, M. Nagai, S.T. Oyama, Appl. Catal. Gen. 165 (1997) 419–428.

[79] L.A. Sousa, J.L. Zotin, V. Teixeira da Silva, Appl. Catal. Gen. 449 (2012) 105–111.

[80] C. Kunkel, F. Viñes, P.J. Ramírez, J.A. Rodriguez, F. Illas, J. Phys. Chem. C (2018) 7567–7576.

[81] P. Delporte, F. Meunier, C. Pham-Huu, P. Vennegues, M.J. Ledoux, J. Guille, Catal. Today 23 (1995) 251–267.

[82] J.J. Bozell, G.R. Petersen, Green Chem. 12 (2010) 539–554.

[83] S.K. Brar, S.J. Sarma, K. Pakshirajan, Platform Chemical Biorefinery, Elsevier, 2016.

[84] T. Werpy, G. Petersen, A. Aden, J. Bozell, J. Holladay, J. White, A. Manheim, Top Value Added Chemicals from Biomass. Volume 1-Results of Screening for Potential Candidates from Sugars and Synthesis Gas, US Department of Energy Washington DC, 2004.

[85] N. Nghiem, S. Kleff, S. Schwegmann, Fermentation 3 (2017) 26–39.

[86] J.M. Pinazo, M.E. Domine, V. Parvulescu, F. Petru, Catal. Today 239 (2015) 17–24.

[87] A. Mazière, P. Prinsen, A. García, R. Luque, C. Len, Biofuels Bioprod. Biorefining 11 (2017) 908–931.

[88] J. Akhtar, A. Idris, R. Abd. Aziz, Appl. Microbiol. Biotechnol. 98 (2014) 987–1000.

[89] A. H. Tullo, Chem. Eng. News 95 (2017) 22–23.

[90] S. Vaswani, Process Econ. Program Rev. (2010).

[91] H. Song, S.Y. Lee, Enzyme Microb. Technol. 39 (2006) 352–361.

[92] J.B. McKinlay, C. Vieille, J.G. Zeikus, Appl. Microbiol. Biotechnol. 76 (2007) 727–740.

[93] O. Dinhill, Formule Verte (2018).

[94] G. Budroni, A. Corma, J. Catal. 257 (2008) 403–408.

[95] M.J. Biddy, C. Scarlata, C. Kinchin, Chemicals from Biomass: A Market Assessment of Bioproducts with near-Term Potential, National Renewable Energy Laboratory (NREL), Golden, CO (United States), 2016.

[96] J.M. Keels, X. Chen, S. Karakalos, C. Liang, J.R. Monnier, J.R. Regalbuto, ACS Catal. 8 (2018) 6486–6494.

[97] P.N. Rylander, Hydrogenation Methods, Academic Press, London, 1985.

[98] R.M. Deshpande, V.V. Buwa, C.V. Rode, R.V. Chaudhari, P.. Mills, Catal. Commun. 3 (2002) 269–274.

[99] S.M. Jung, E. Godard, S.Y. Jung, K.-C. Park, J.U. Choi, J. Mol. Catal. Chem. 198 (2003)

297–302.

[100] C. Zhang, L. Chen, H. Cheng, X. Zhu, Z. Qi, Catal. Today 276 (2016) 55–61.

[101] K.H. Kang, U.G. Hong, Y. Bang, J.H. Choi, J.K. Kim, J.K. Lee, S.J. Han, I.K. Song, Appl. Catal. Gen. 490 (2015) 153–162.

[102] U.G. Hong, J.K. Kim, J. Lee, J.K. Lee, J.H. Song, J. Yi, I.K. Song, J. Ind. Eng. Chem. 20 (2014) 3834–3840.

[103] U.G. Hong, J. Lee, S. Hwang, I.K. Song, Catal. Lett. 141 (2011) 332–338.

[104] B. Tapin, F. Epron, C. Especel, B.K. Ly, C. Pinel, M. Besson, ACS Catal. 3 (2013) 2327–2335.

[105] B.K. Ly, D.P. Minh, C. Pinel, M. Besson, B. Tapin, F. Epron, C. Especel, Top. Catal. 55 (2012) 466–473.

[106] C. Zhang, W. Cao, H. Cheng, L. Chen, Z. Qi, Catalysts 6 (2016) 100.

[107] T. Werpy, J. Frye, Y. Wang, A. Zacher, Textured Catalysts Comprising Catalyst Metal and Metal Oxide on Carbon Support, Methods of Making Textured Catalysts, and Use in Hydrogenation Reactions Conducted in Hydrothermal Conditions, WO2002102511A1, 2002.

[108] D.P. Minh, M. Besson, C. Pinel, P. Fuertes, C. Petitjean, Top. Catal. 53 (2010) 1270–1273.

[109] X. Liu, X. Wang, G. Xu, Q. Liu, X. Mu, H. Liu, J. Mater. Chem. A 3 (2015) 23560–23569.

[110] D.R. Vardon, A.E. Settle, V. Vorotnikov, M.J. Menart, T.R. Eaton, K.A. Unocic, K.X. Steirer, K.N. Wood, N.S. Cleveland, K.E. Moyer, W.E. Michener, G.T. Beckham, ACS Catal. 7 (2017) 6207–6219.

[111] Z. Shao, C. Li, X. Di, Z. Xiao, C. Liang, Ind. Eng. Chem. Res. 53 (2014) 9638–9645.

[112] B. Tapin, F. Epron, C. Especel, B.K. Ly, C. Pinel, M. Besson, Catal. Today 235 (2014) 127–133.

[113] B.K. Ly, B. Tapin, M. Aouine, P. Delichere, F. Epron, C. Pinel, C. Especel, M. Besson, ChemCatChem 7 (2015) 2161–2178.

[114] X. Di, C. Li, G. Lafaye, C. Especel, F. Epron, C. Liang, Catal. Sci. Technol. 7 (2017) 5212–5223.

[115] X. Di, C. Li, B. Zhang, J. Qi, W. Li, D. Su, C. Liang, Ind. Eng. Chem. Res. 56 (2017) 4672–4683.

[116] Z. Huang, K.J. Barnett, J.P. Chada, Z.J. Brentzel, Z. Xu, J.A. Dumesic, G.W. Huber, ACS Catal. 7 (2017) 8429–8440.

[117] X. Di, Z. Shao, C. Li, W. Li, C. Liang, Catal. Sci. Technol. 5 (2015) 2441–2448.

[118] J. Quiroz, E.F. Mai, V. Teixeira da Silva, Top. Catal. 59 (2016) 148–158.

[119] W. Wang, S. Wang, X. Ma, J. Gong, Chem. Soc. Rev. 40 (2011) 3703–3727.

[120] S. Saeidi, N.A.S. Amin, M.R. Rahimpour, J. CO2 Util. 5 (2014) 66–81.

[121] H. Michael, Transformation and Utilization of Carbon Dioxide, Springer, Heidelberg ; New York, 2014.

[122] T. Sakakura, J.-C. Choi, H. Yasuda, Chem. Rev. 107 (2007) 2365–2387.

[123] M. Mikkelsen, M. Jørgensen, F.C. Krebs, Energy Env. Sci 3 (2010) 43–81.

[124] J. Artz, T.E. Müller, K. Thenert, J. Kleinekorte, R. Meys, A. Sternberg, A. Bardow, W. Leitner, Chem. Rev. 118 (2018) 434–504.

[125] E.T. Kho, T.H. Tan, E. Lovell, R.J. Wong, J. Scott, R. Amal, Green Energy Environ. 2 (2017) 204–217.

[126] G. Zhao, X. Huang, X. Wang, X. Wang, J Mater Chem A 5 (2017) 21625–21649.

[127] M. Peters, B. Köhler, W. Kuckshinrichs, W. Leitner, P. Markewitz, T.E. Müller, ChemSusChem 4 (2011) 1216–1240.

[128] Y.A. Daza, J.N. Kuhn, RSC Adv. 6 (2016) 49675–49691.

[129] S. Kattel, P. Liu, J.G. Chen, J. Am. Chem. Soc. 139 (2017) 9739–9754.

[130] A.Y. Khodakov, W. Chu, P. Fongarland, Chem. Rev. 107 (2007) 1692–1744.

[131] Y. Liu, D. Liu, Int. J. Hydrog. Energy 24 (1999) 351–354.

[132] L. Wang, H. Liu, Y. Liu, Y. Chen, S. Yang, J. Rare Earths 31 (2013) 969–974.

[133] J.-N. Park, E.W. McFarland, J. Catal. 266 (2009) 92–97.

[134] S. Kattel, B. Yan, J.G. Chen, P. Liu, J. Catal. 343 (2016) 115–126.

[135] M.R. Gogate, R.J. Davis, Catal. Commun. 11 (2010) 901–906.

[136] A.G. Kharaji, A. Shariati, M. Ostadi, J. Nanosci. Nanotechnol. 14 (2014) 6841–6847.

[137] W. Wei, G. Jinlong, Front. Chem. Sci. Eng. 5 (2011) 2–10.

[138] S. Schiebahn, T. Grube, M. Robinius, V. Tietze, B. Kumar, D. Stolten, Int. J. Hydrog. Energy 40 (2015) 4285–4294.

[139] K. Stangeland, D. Kalai, H. Li, Z. Yu, Energy Procedia 105 (2017) 2022–2027.

[140] S. Danaci, L. Protasova, J. Lefevere, L. Bedel, R. Guilet, P. Marty, Catal. Today 273 (2016) 234–243.

[141] S. Tada, T. Shimizu, H. Kameyama, T. Haneda, R. Kikuchi, Int. J. Hydrog. Energy 37 (2012) 5527–5531.

[142] A. Beuls, C. Swalus, M. Jacquemin, G. Heyen, A. Karelovic, P. Ruiz, Appl. Catal. B Environ. 113–114 (2012) 2–10.

[143] S. Tada, O.J. Ochieng, R. Kikuchi, T. Haneda, H. Kameyama, Int. J. Hydrog. Energy 39 (2014) 10090–10100.

[144] H. Arakawa, J.-L. Dubois, K. Sayama, Energy Convers Mgmt 33 (1992) 521–528.

[145] M. Aresta, Carbon Dioxide Recovery and Utilization, Kluwer Academic Publishers, Dordrecht, 2010.

[146] T. Lunkenbein, J. Schumann, M. Behrens, R. Schlögl, M.G. Willinger, Angew. Chem. Int. Ed. 54 (2015) 4544–4548.

[147] A. Goeppert, M. Czaun, J.-P. Jones, G.K. Surya Prakash, G.A. Olah, Chem Soc Rev 43 (2014) 7995–8048.

[148] M. Behrens, F. Studt, I. Kasatkin, S. Kühl, M. Hävecker, F. Abild-Pedersen, S. Zander, F. Girgsdies, P. Kurr, B.-L. Kniep, M. Tovar, R.W. Fischer, J.K. Nørskov, R. Schlögl, Science 336 (2012) 893–897.

[149] M. Bertau, H. Offermanns, L. Plass, F. Schmidt, H.-J. Wernicke, eds., Methanol: The Basic Chemical and Energy Feedstock of the Future, Springer Berlin Heidelberg, Berlin, Heidelberg, 2014.

[150] H. Lei, R. Nie, G. Wu, Z. Hou, Fuel 154 (2015) 161–166.

[151] J. Słoczyński, R. Grabowski, A. Kozłowska, P. Olszewski, J. Stoch, J. Skrzypek, M. Lachowska, Appl. Catal. Gen. 278 (2004) 11–23.

[152] C. Li, X. Yuan, K. Fujimoto, Appl. Catal. Gen. 469 (2014) 306–311.

[153] X.-L. Liang, X. Dong, G.-D. Lin, H.-B. Zhang, Appl. Catal. B Environ. 88 (2009) 315–322.

[154] X. Zhou, J. Qu, F. Xu, J. Hu, J.S. Foord, Z. Zeng, X. Hong, S.C. Edman Tsang, Chem. Commun. 49 (2013) 1747–1749.

[155] H. Bahruji, M. Bowker, G. Hutchings, N. Dimitratos, P. Wells, E. Gibson, W. Jones, C. Brookes, D. Morgan, G. Lalev, J. Catal. 343 (2016) 133–146.

[156] C. Kunkel, F. Viñes, F. Illas, Energy Environ. Sci. 9 (2016) 141–144.

[157] Y. Chen, S. Choi, L.T. Thompson, J. Catal. 343 (2016) 147–156.

[158] S. Posada-Pérez, F. Viñes, J.A. Rodriguez, F. Illas, Top. Catal. 58 (2015) 159–173.

[159] J. Gao, Y. Wu, C. Jia, Z. Zhong, F. Gao, Y. Yang, B. Liu, Catal. Commun. 84 (2016) 147–150.

[160] M.D. Porosoff, X. Yang, J.A. Boscoboinik, J.G. Chen, Angew. Chem. 126 (2014) 6823–6827.

[161] S. Posada-Pérez, P.J. Ramírez, R.A. Gutiérrez, D.J. Stacchiola, F. Viñes, P. Liu, F. Illas, J.A. Rodriguez, Catal. Sci. Technol. 6 (2016) 6766–6777.

[162] X. Liu, C.R. Kunkel, N. Homs, F. Viñes, F. Illas, ACS Catal. (2017) 4323–4335.

[163] M. Nagai, K. Oshikawa, T. Kurakami, T. Miyao, S. Omi, J. Catal. 180 (1998) 14–23.

[164] S. Posada-Pérez, F. Viñes, P.J. Ramirez, A.B. Vidal, J.A. Rodriguez, F. Illas, Phys Chem Chem Phys 16 (2014) 14912–14921.

[165] S. Posada-Pérez, P.J. Ramírez, J. Evans, F. Viñes, P. Liu, F. Illas, J.A. Rodriguez, J. Am. Chem. Soc. 138 (2016) 8269–8278.

[166] C. Kunkel, F. Viñes, F. Illas, ACS Appl. Energy Mater. 1 (2018) 43–47.

[167] R.B. Quincy, M. Houalla, A. Proctor, D.M. Hercules, J. Phys. Chem. 94 (1990) 1520–1526.

[168] O. Ostrovski, G. Zhang, AIChE J. 52 (2006) 300–310.

[169] G. Zhang, O. Ostrovski, Metall. Mater. Trans. B 31 (2000) 129–139.

[170] K. Oshikawa, M. Nagai, S. Omi, J. Phys. Chem. B 105 (2001) 9124–9131.

[171] A.A. Smirnov, Z. Geng, S.A. Khromova, S.G. Zavarukhin, O.A. Bulavchenko, A.A. Saraev, V.V. Kaichev, D.Y. Ermakov, V.A. Yakovlev, J. Catal. 354 (2017) 61–77.

[172] N. Perret, X. Wang, L. Delannoy, C. Potvin, C. Louis, M.A. Keane, J. Catal. 286 (2012) 172–183.

[173] R.A. Mir, P. Sharma, O.P. Pandey, Sci. Rep. 7 (2017) 3518–3529.

[174] A.C. Lausche, J.A. Schaidle, L.T. Thompson, Appl. Catal. Gen. 401 (2011) 29–36.

[175] C. You, C. Zhang, L. Chen, Z. Qi, Appl. Organomet. Chem. 29 (2015) 653–660.

[176] U.G. Hong, S. Hwang, J.G. Seo, J. Lee, I.K. Song, J. Ind. Eng. Chem. 17 (2011) 316–320.

[177] M. Dwidar, J.-Y. Park, R.J. Mitchell, B.-I. Sang, Sci. World J. 2012 (2012) 1–10.

[178] Y. Cao, H. Li, J. Zhang, Ind. Eng. Chem. Res. 50 (2011) 7808–7814.

[179] G.N. Baroi, H.N. Gavala, P. Westermann, I.V. Skiadas, Ind. Crops Prod. 104 (2017) 68–80.

[180] D.E. Ramey, S.-T. Yang, The Ohio State Univ., Columbus, OH (United States), Production of Butyric Acid and Butanol from Biomass, 2005.

[181] J.-G. Choi, R.L. Curl, L.T. Thompson, J. Catal. 146 (1994) 218–227.

[182] E.J. Markel, J.W. Van Zee, J. Catal. 126 (1990) 643–657.

[183] S. Boullosa-Eiras, R. Lødeng, H. Bergem, M. Stöcker, L. Hannevold, E.A. Blekkan, Catal. Today 223 (2014) 44–53.

[184] H. Shou, D. Ferrari, D.G. Barton, C.W. Jones, R.J. Davis, ACS Catal. 2 (2012) 1408–1416.

[185] A. Mehdad, R.E. Jentoft, F.C. Jentoft, J. Catal. 347 (2017) 89–101.

[186] A.B. van der Merwe, H. Cheng, J.F. Görgens, J.H. Knoetze, Fuel 105 (2013) 451–458.

[187] D.E. Ramey, Continuous Two Stage, Dual Path Anaerobic Fermentation of Butanol and Other Organic Solvents Using Two Different Strains of Bacteria, 5753474, 1998.

[188] M.M. Sullivan, A. Bhan, ACS Catal. 6 (2016) 1145–1152.

[189] A.S. Rocha, L.A. Souza, R.R. Oliveira, A.B. Rocha, V. Teixeira da Silva, Appl. Catal. Gen. 531 (2017) 69–78.

[190] L. Souza Macedo, D.R. Stellwagen, V. Teixeira da Silva, J.H. Bitter, ChemCatChem 7 (2015) 2816–2823.

[191] J.-S. Choi, V. Schwartz, E. Santillan-Jimenez, M. Crocker, S. Lewis, M. Lance, H. Meyer, K. More, Catalysts 5 (2015) 406–423.

[192] P. Kitsiou, N. Lagopati, E.-P. Tsilibary, P. Falaras, P. Papazafiri, E.P. Pavlatou, E. Kotsopoulou, Int. J. Nanomedicine 9 (2014) 3219–3230.

[193] A.C. Ferrari, J. Robertson, Philos. Trans. R. Soc. Math. Phys. Eng. Sci. 362 (2004) 2477–2512.

[194] M.A. Pimenta, G. Dresselhaus, M.S. Dresselhaus, L.G. Cançado, A. Jorio, R. Saito, Phys Chem Chem Phys 9 (2007) 1276–1290.

[195] J. Jehlička, O. Urban, J. Pokorný, Spectrochim. Acta. A. Mol. Biomol. Spectrosc. 59 (2003) 2341–2352.

[196] S. Vollebregt, R. Ishihara, F.D. Tichelaar, Y. Hou, C.I.M. Beenakker, Carbon 50 (2012) 3542–3554.

[197] Y.-J. Lee, J. Nucl. Mater. 325 (2004) 174–179.

[198] S. Loridant, I.C. Marcu, G. Bergeret, J.M.M. Millet, Phys. Chem. Chem. Phys. 5 (2003) 4384–4389.

[199] R. Radhakrishnan, C. Reed, S.T. Oyama, M. Seman, J.N. Kondo, K. Domen, Y. Ohminami, K. Asakura, J. Phys. Chem. B 105 (2001) 8519–8530.

[200] E. de B. Santos, F.A. Sigoli, I.O. Mazali, Mater. Res. Bull. 60 (2014) 242–246.

[201] M. Dieterle, G. Mestl, Phys. Chem. Chem. Phys. 4 (2002) 822–826.

[202] L. Kumari, Y.-R. Ma, C.-C. Tsai, Y.-W. Lin, S.Y. Wu, K.-W. Cheng, Y. Liou, Nanotechnology 18 (2007) 115717–115724.

[203] X.Q. Zhao, Y. Liang, Z.Q. Hu, B.X. Liu, J. Appl. Phys. 80 (1996) 5857–5860.

[204] H.C. Wu, Y.C. Chang, J.H. Wu, J.H. Lin, I.K. Lin, C.S. Chen, Catal. Sci. Technol. 5 (2015) 4154–4163.

[205] S. Li, Y. Xu, Y. Chen, W. Li, L. Lin, M. Li, Y. Deng, X. Wang, B. Ge, C. Yang, S. Yao, J. Xie, Y. Li, X. Liu, D. Ma, Angew. Chem. Int. Ed. 56 (2017) 10761–10765.

[206] A. Kim, D.P. Debecker, F. Devred, V. Dubois, C. Sanchez, C. Sassoye, Appl. Catal. B Environ. 220 (2018) 615–625.

[207] S. Kattel, W. Yu, X. Yang, B. Yan, Y. Huang, W. Wan, P. Liu, J.G. Chen, Angew. Chem. Int. Ed. 55 (2016) 7968–7973.

[208] C.E. Chan-Thaw, M. Marelli, R. Psaro, N. Ravasio, F. Zaccheria, RSC Adv 3 (2013) 1302–1306.

Scientific contribution

Publications:

- **TiO_2-supported molybdenum carbide: an active catalyst for the aqueous phase hydrogenation of succinic acid.**

  M.Abou Hamdan, S. Loridant, M. Jahjah, C.Pinel, N.Perret, Applied Catalysis A, General 571 (2019) 71-81

- **Influence of TPRC preparation parameters on the performance of supported molybdenum carbide catalysts in succinic acid hydrogenation.**
  Manuscript under preparation

- **Supported molybdenum carbide and nitride catalysts for CO_2 hydrogenation.**
  Manuscript under preparation

Conferences:

- **Poster in the 12th International Symposium on the Scientific Bases for the Preparation of Heterogeneous Catalysts (PREPA12).**

  July 8-12, 2018, Louvain-La-Neuve – Belgium.

- **Poster in Journée de l'école Doctorale de Chimie de Lyon.**

  April 24, 2018, Lyon – France.

- **Poster in the 4th International Congress on Catalysis for Biorefineries (CatBior).**

  Dec. 11-15, 2017, Lyon – France.

- **Poster in the 13th European Congress on Catalysis (EUROPACAT 2017).**

  Aug. 27-31, 2017, Florence – Italy. “Best poster award”

- **Oral presentation in Journée de Printemps 2017 de la SCF Rhône Alpes.**

  June 15, 2017, Chambéry - France.